In vitro Antibacterial and Cytotoxic Studies of Engineered Copper Nanoparticles

A Thesis submitted in fulfillment of the requirement

for the award of the degree of

DOCTOR OF PHILOSOPHY

IN

BIOTECHNOLOGY

PURNIMA SHARMA

(Registration No.: 901300011)

Under the Supervision of

Dr. Dinesh Goyal
(Professor)

Dr. B.N. Chudasama
(Associate Professor)

Department of Biotechnology
Thapar Institute of Engineering & Technology Patiala,
Punjab
INDIA

January 2021

DEDICATION

This thesis is dedicated to my beloved Grandmother

Whose support and love helped me in achieving my goals

Whose encouragement was my best supporter through the entire journey of my PhD

CERTIFICATE

Certified that the thesis entitled **"*In vitro* Antibacterial and Cytotoxic Studies of Engineered Copper Nanoparticles"**, which is being submitted by Ms. Purnima Sharma, in fulfilment of the requirement for the award of the degree of **Doctor of Philosophy** in Biotechnology, Thapar Institute of Engineering & Technology, Patiala, India is a record of candidate's own independent and original research work carried out by her under our supervision and guidance. The matter embodied in this thesis has not been submitted in part or full to any other University or Institute for the award of any degree.

(Dr. Dinesh Goyal)
Supervisor
Professor
Department of Biotechnology
Thapar Institute of Engineering & Technology, Patiala-147004,
Punjab, India

(Dr. B. N. Chudasama)
Supervisor
Associate Professor
School of Physics and Materials Science
Thapar Institute of Engineering & Technology, Patiala-147004,
Punjab, India

Place: Patiala
Date: January 12, 2021

DECLARATION

I hereby declare that the work which is being presented in this thesis **"*In vitro* Antibacterial and Cytotoxic Studies of Engineered Copper Nanoparticles"** submitted by me for the award of the degree of **Doctor of Philosophy** in the Department of Biotechnology, Thapar Institute of Engineering & Technology, Patiala, India, is true and original record of my own independent and original research work carried out under the supervision of Dr. Dinesh Goyal, Professor, Department of Biotechnology and Dr. B.N. Chudasama, Associate Professor, School of Physics and Materials Science, Thapar Institute of Engineering & Technology, Patiala, India. The matter embodied in this thesis has not been submitted in part or full to any other University or Institute for the award of any degree in India or abroad.

Purnima Sharma

(Purnima Sharma)

Place: Patiala
Date: January 12, 2021

ACKNOWLEDGEMENT

An acknowledgement in my thesis is just a small gesture and doesn't truly represent how much I appreciate the influence that many people have had on my life. It is a pleasant task to express my thanks to all those who contributed in many ways to my doctoral work and made it an unforgettable journey for me.

My joy knows no boundaries as I take this opportunity to express my deepest and sincere gratitude to my supervisor Dr. Dinesh Goyal, Professor, Department of Biotechnology (DBT), Thapar Institute of Engineering & Technology (TIET), Patiala, who has provided me unwavering support and mentorship throughout this endeavor. With deep regards and profound respect, I also thank my co-supervisor Dr. B.N. Chudasama, Associate Professor, School of Physics and Materials Science (SPMS), Thapar Institute of Engineering & Technology (TIET), Patiala. Both of them have always poured me with the exquisite knowledge they hold with them in their respective fields of research and they have always motivated me with constructive remarks. I really feel privileged to be associated with them during my life. Their association with this endeavor of mine will remain a beacon of light to me throughout my life.

I would like to thank the members of my Doctoral committee Dr. N. Das, Dr. Sanjay Saxena and Dr. Amjad Ali for examining the progress reports and encouraging me to make my work better. I express my sincere thanks to Dr. M. S. Reddy, Head, Department of Biotechnology, TIET, Patiala, for support and encouragement. I am also grateful to Dr. Rafat Siddique, Senior Professor and Dean, Research and Sponsored Projects, TIET.

Sincere thanks to Dr. Manoj Baranwal, Associate Professor, Department of Biotechnology (DBT), Thapar Institute of Engineering & Technology (TIET), for the support in laboratory and experimental work. I am also thankful to SAIF, IIT Bombay and Dr. Diptiman Chuudhury, Assistant Professor, School of Chemistry and Biochemistry (SCBC), Thapar Institute of Engineering & Technology (TIET), for extending characterization facilities.

I am indebted to Dr. OP Pandey, Professor and Head, School of Physics and Materials Science (SPMS), Thapar Institute of Engineering & Technology (TIET), for his invaluable support and encouragement. Words fail me to express my appreciation to Dr. Chandni Khurana for her moral support and motivation, whenever I was low. She always encourage me and guidance me throughout my research work. I owe my deepest gratitude to Dr. Chandni Khurana for her continuous support in infinite number of ways every time and any time.

I would like to offer my gratitude to colleagues of Research Lab-3 and Nanomedicine Lab for their help and support in the completion of this work. I am

thankful to Lab assistants (Mr. Ram Newal, Surinder Pal, Lalan ji and Phoolchand ji) for their support.

I am extremely thankful to my friends Amandeep Kaur, Gurpreet Saggu, Kiranjeet Kaur, Neha Bhardwaj, Neha Srivastva, Noorpreet Kaur, Pooja Singla, Harleen Kaur, Vanshita Goyal, Sonal Singh and Tamanna for always being there with big smiles on their faces and I am thankful for the advices they gave me along my journey of this achievement.

I am filled with immense joy as I thank my brother-like friend Hemant, who has always proved to be a shoulder to lean on whenever stressful situations invaded during the course of this work and his companionship will be acknowledged till the last breath. The support, encouragement and comfort that came from the gems of my life Mozam, Khushboo, Pankaj, Rahul, Harman Kang, Radha, Manmeet, Neelmani and Amiteshwar Kaur is gratefully acknowledged.

The smiling face of my little brother Moksh Sharma and the unconditional love he offered has always been a stress buster for me throughout this work. There have been a lot of people who walked alongside this journey, helped me and guided me, knowingly and unknowingly. I offer heartfelt thanks to all of them.

I may be short of words to pay the debt of recognition towards the lady who have always been a source of strength for me, my grandmother, Late Smt. Krishna Devi. I, in whole of my lifetime, will not be able to compensate her love, which nourished me and accompanied me through every step of my life. A distinctive thanks to my grandfather Late Sri. Raghunandan Das, for always leading from behind and it was because of him only that I was courageous enough to dream big. Thanks to my brother Er. Abhishek Sharma for his support. My parents are also entitled to be a source of encouragement for me and deserve a vote of thanks. In the last, I would love to pay my profound obligation to all those people who have been a part of this momentous achievement.

Last but not the least; I would like to pay high regards to almighty God for giving me skills, wisdom, knowledge and ability to work hard to reach where I am today. Moreover, I thank God for the blessings and support He has showered on me through my family, friends, professors and colleagues. Without His blessings and support, this thesis would have never been possible.

(Purnima Sharma)

List of Publications

1. **Purnima Sharma**, Dinesh Goyal and Bhupendra Chudasama, Role of hydrodynamic size in colloidal and optical stability of plasmonic Copper nanoparticles, Micro and Nano Letters, 2019, 14, 1388 (IF=0.97).
2. **Purnima Sharma**, Dinesh Goyal, Manoj Baranwal and Bhupendra Chudasama, ROS-induced cytotoxicity of colloidal copper nanoparticles in MCF-7 human breast cancer cell line: an in vitro study, Journal of Nanoparticle Research, 2020, 22, 244 (IF=2.132).
3. **Purnima Sharma**, Dinesh Goyal and Bhupendra Chudasama, Ecotoxicity of as-synthesized Copper Nanoparticles on Soil Bacteria. **Accepted** in IET Nanobiotechnology (IF-1.859).
4. **Purnima Sharma**, Dinesh Goyal and Bhupendra Chudasama, Effect of reaction parameters on the synthesis of colloidal copper nanoparticles by chemical reduction method. **Accepted** in Colloid Journal (IF-0.8).
5. **Purnima Sharma**, Dinesh Goyal, Manoj Baranwal and Bhupendra Chudasama, Oxidative stress induced cytotoxicity of colloidal copper nanoparticles on RAW 264.7 macrophage cell line. **Accepted** in Journal of Nanoscience and Nanotechnology (IF-1.3).

Communicated

1. **Purnima Sharma**, Dinesh Goyal and Bhupendra Chudasama, Antibacterial Activity of colloidal copper nanoparticles against Gram-negative (*Escherichia coli* and *Proteus vulgaris*) Bacteria. **Under Review** in Frontiers in Molecular Biosciences (IF-4.1).

Conference Presentations

1. Poster presentation in Internal Conferences on Condensed Matter Physics (ICCMP 2014), HP University, India entitled, "Antibacterial Activity of Silver Nanoparticles against Gram negative and Gram positive Bacteria" Purnima Sharma, Dinesh Goyal and Bhupendra Chudasama (2014).
2. Participation in National Conference on Advances in Engineering Materials (NAEM-2015) DIT University, Dehradun, Punjab, India (2015).
3. Poster presentation in Internal Conferences on Biopharma drug discovery, Thapar Institute of Engineering and Technology, Patiala, Punjab entitled "Antibacterial studies of engineered copper nanoparticles against Gram positive and Gram negative bacteria" Purnima Sharma, Dinesh Goyal and Bhupendra Chudasama (2018).
4. Poster presentation in NANOBIOTECK-2019, 4th Annual Conference of Indian Society of Nanomedicine (2019), New Delhi, India entitled "Copper nanoparticle induced cell death and oxidative stress in RAW 264.7 Macrophage cell line" Purnima Sharma, Dinesh Goyal and Bhupendra Chudasama (2019).

PREFACE

The term infectivity attributes to the ability of microorganisms (bacteria, parasites, virus and fungi) to enter and multiply in the body of host causing infections. Globally, infectious diseases cause 9 million deaths annually, which accounts for 41 % of the global disease burden measured in terms of Disability-Adjusted Life Years (DALYS). Infections with most pathogens trigger the immune response inside the host, which inactivates or kill the disease causing pathogen as first line of defense. However, if the host is unable to do so, then external help in the form of antibiotics is required to treat the infectious disease.

Antibiotics are chemical compounds that kill or inhibit the growth of microorganisms. Based on target group, they are classified as antibacterial, antifungal and antiviral agents. For decades, antibiotics have been used to treat infectious diseases. They are also used in medical procedures like organ transplants and chemotherapy. Antibiotics are either bactericidal (lethal to bacteria) or bacteriostatic (prevents growth of bacteria). Excessive and uncontrolled use of antibiotics has resulted into development of Antimicrobial Resistance (AMR) in both intra-hospital and non-hospital strains. Development of antibiotic resistant strains poses a serious global threat to the disease management. Disease Control and Prevention (CDC), World Economic Forum, Infectious Diseases Society of America and the World Health Organization (WHO) have jointly declared Antimicrobial Resistance (AMR) as one of the 'biggest threats to public health globally'.

Many intra-hospital pathogens have developed resistance against multiple antibiotics resulting in decrease in the efficiency of treatments. Decline in the effectiveness of existing antibiotics has caused higher morbidity and mortality in patients which are infected with multidrug-resistant (MDR) strains. Therefore, development of new and unconventional antibiotics is the need of the hour to overcome the threats put up by the multiple drug resistance. Metal nanoparticles owing to their high surface-to-volume ratio exhibits enhanced chemical and biological activities. Target sites of metal nanoparticles in pathogens are random and because of this it is highly unlikely that microorganisms will develop drug resistance against metal nanoparticles. Among metals, gold, silver and copper are known for their antiseptic properties since ancient times. However, because of economic constraints associated with gold and silver, it is unlikely to develop an effective and economical antibiotic drug system associated with these metals.

In recent years there has been growing interest in synthesis of copper nanoparticles (CuNPs) because of their potential applications in nanomedicine. CuNPs and their complexes are now used as antibacterial, antiviral, anti-fungal and anti-fouling agents. The United States Environmental Protection Agency has registered copper as antimicrobial agents.

Despite copper being essential trace element which plays vital role in metabolic and physiological processes in animals and plants, it can cause acute toxicity at higher

concentrations. Compare to the bulk, copper at nano-scale possess higher antibacterial activities and greater toxicity. Because of high sensitivity towards aggregation and oxidation, scale-up of CuNPs per batch yield remains a challenge, which dramatically alters their antibacterial and toxicological properties. Therefore, development of synthesis protocols leading to a successful scale-up of nanoparticle per batch yield without altering their antibacterial and toxicological activities remain a subject of great interest to the researchers. Further, the correlation between per batch yield of CuNPs and their antibacterial activities and cytotoxicity was completely missing in literature. The major objective of this thesis is to development the synthesis protocols for the preparation of CuNPs that are stable against aggregation and oxidation. Developed protocols were further optimized for the scale-up of nanoparticles per batch yield (from 0.2 g to 0.4 g). This thesis makes an attempt to understand the effect of CuNPs' per batch yield on their antibacterial and cytotoxic activities.

Chapter 1 provides an insight into various infectious diseases and summarizes the limitations of conventional treatment methods. The concept and mechanism of multiple drug resistance (MDR) in bacterial strains is introduced. The need for the development of the new antibacterial agents, which can overcome the threats of drug resistance is also highlighted. The potential of nanoparticles as antibacterial agents is explored. The possible mechanisms of nanoparticles' antibacterial activities, which make them invulnerable from development of drug resistance, are summarized in this chapter.

Chapter 2 begins with detailed literature survey on antibacterial activities of conventional antibiotics, their mode of actions and development of multiple drug resistance. Following this a brief review is presented on the antibacterial activities of metal nanoparticles and explored possibility of copper nanoparticles as an alternate to conventional narrow targeting antibiotics. Existing protocols for the synthesis of CuNPs found in literature was explored along with their physical and chemical properties. Literature on antibacterial activities of CuNPs and their synergy with conventional antibiotics against pathogenic and environmental strains was also reviewed. An overview on the cytotoxicity of CuNPs was also summarized in this chapter.

Chapter 3 provides details of experimental protocols followed for the synthesis of CuNPs and their characterization by UV-visible absorption spectroscopy, photon correction spectroscopy, transmission electron microscopy (TEM) and inductively coupled plasma atomic emission spectroscopy (ICP-AES). Synthesis of CuNPs was carried out by chemical reduction method. Variables of the study were: (i) copper precursor, (ii) reaction time and (iii) reaction temperature. Highest nanoparticle yield, smallest hydrodynamic size and stable plasmon resonance corresponding to Cu^0 was used as criteria for the process optimization. From this, optimized conditions for the chemical reduction reaction were established. $CuCl_2$ as copper precursor, 80 °C as reaction temperature and 5 min as reaction time were the optimized reaction parameters. Under optimized conditions, three set of CuNPs were synthesize with per batch yield 0.2 g, 0.3 g and 0.4 g. Irrespective of per batch yield,

synthesized CuNPs possess a single plasmon resonance band centred at 570-580 nm with monomodal size distribution, indicting the formation of symmetrical (spherical) nanoparticles whose hydrodynamic size ranges between 11-14 nm, demonstrating the successful process scale-up. In the last part effect of aging on the colloidal stability of synthesized CuNPs was evaluated. Irrespective of per batch yield, synthesized CuNPs were stable up to 180 days, beyond which they aggregate and lose their colloidal stability.

In Chapter 4, an *in-vitro* study on antibacterial activities of three sets of CuNPs with per batch yield 0.2 g, 0.3 g and 0.4 g was presented. Antibacterial activities of CuNPs were studied on two pathogenic bacteria [*Escherichia coli* (MTCC No. 739) and *Proteus vulgaris* (MTCC No. 426)] and two soil bacteria [*Bacillus subtilis* (MTCC No. 441) and *Pseudomonas fluorescens* (MTCC No. 1749)]. Minimum inhibitory concentration (MIC) and the minimum bactericidal concentration (MBC) of CuNPs were measured by micro-dilution method and disk diffusion assay, respectively. It was observed that tested CuNPs even at low concentrations were toxic to pathogenic and soil bacteria. CuNPs with smaller hydrodynamic size exhibits greater antibacterial effects on the tested bacteria. An insight into nanoparticle-bacteria interaction and their possible underlying mechanism of antibacterial activities were provided by estimating the cytoplasmic (protein and sugar) leakage and reactive oxygen species (ROS) generation. Leakage of cytoplasmic components and generation of extracellular oxidative stress by reactive oxygen species (ROS) causes cell death in tested bacteria. Chapter 3 ends with a study on synergistic effect of antibacterial activities of CuNPs with antibiotics tetracycline, kanamycin, ampicillin and streptomycin. Irrespective of per batch yield, strong synergy was observed between the synthesized CuNPs and tested antibiotics. From this study, it was concluded that the scale-up protocols presented in this work did not impact antibacterial activities of CuNPs negatively and makes them a potential candidate for an alternate to the conventional antibiotics.

In Chapter 5, *in-vitro* cytotoxicity of three sets of colloidal CuNPs synthesized with per batch yield 0.2 g, 0.3 g and 0.4 g was evaluated on MCF-7 human breast cancer cell line and RAW 264.7 macrophage cell line. Dose-dependent cytotoxicity was evaluated by MTT, colorimetric and reactive oxygen species (ROS) assays. No significant difference was observed in the cytotoxicity of CuNPs having different per batch nanoparticle yield. This suggests that the cytotoxicity of CuNPs was independent of nanoparticle yield and it only depends on nanoparticles' dose. Oxidative stress produced by generation of extracellular ROS in the cells treated with CuNPs might have damaged membrane lipids causing cell shrinkage and fragmentation leading to the cell death. Against MCF-7, the IC_{50} values of CuNPs were in the range of 0.3 to 0.7 μg/mL, whereas against RAW 264.7, the IC_{50} values were in the range of 4.37 to 5.04 μg/mL. The shift in IC_{50} values viz-a-viz to the tested dose (0 – 100 μg/mL) was minimal, suggesting that the scale-up of CuNPs' yield did not significantly alter the cytotoxicity of nanoparticles. The ability to scale-up the nanoparticle yield with strong dose-dependent cytotoxicity makes CuNPs the potential candidate for the development of anticancer drugs.

Chapter 6, summaries important findings of present work and propose the scope for future work on antimicrobial and cytotoxic properties of metal nanoparticles that could lead to the development of nanoparticle based therapeutics, which will be immune from the development of drug resistance.

TABLE OF CONTENTS

LIST OF FIGURES

LIST OF TABLES

LIST OF ABBREVIATIONS

AMR	Antimicrobial resistance
BSA	Bovine serum albumin
CDC	Center for Disease Control and Prevention
CFU	Colony forming units
$Cu(NO_3)_2$	Copper nitrate
$Cu(OAc)_2$	Copper acetate
$CuCl_2.2H_2O$	Copper chloride
CuNPs	Copper nanoparticles
$CuSO_4$	Copper sulphate
DCFH	2, 7-dicholrofluorescin diacetate
D_H	Hydrodynamic particle size
DMEM	Dulbecco's modified eagle's medium
DMSO	Dimethyl sulfoxide
DNA	Deoxyribonucleic acid
DNS	3, 5-dintrosalicyclic acid
DOX	Doxorubicin hydrochloride
EDTA	Ethylenediamine tetraacetic acid
et al.	And others
etc.	And other things
eV	Electron volt
FBS	Fetal Bovine serum
g	Gram
h	Hour
H_2O_2	Hydrogen peroxide
HIV	Human immunodeficiency virus
HNO_3	Nitric acid
IC	Inhibitory concentration
ICP-AES	Inductively coupled plasma atomic emission spectroscopy
MBC	Minimum bactericidal concentration
MDR	Multiple drug resistance

MIC	Minimum inhibitory concentration
min	Minutes
MTCC	Microbial type culture collection
MTT	(3-(4,5-dimethylthiazol-2-yl)-2,5-diphenyltetrazolium bromide)
mV	Millivolts
$NaBH_4$	Sodium borohydride
NCCS	National Centre for Cell Culture
nm	nanometer
OD	Optical density
PALS	phase angle light scattering
PBS	Phosphate buffer saline
PCS	Photon correlation spectroscopy
PVP	Polyvinylpyrrolidone
ROS	Reactive oxygen species
rpm	Revolution per minute
SPR	Surface plasmon resonance
TEM	Transmission electron microscopy
WHO	World Health Organization
ZIH	Zone of Inhibition
μg/mL	Microgram per milliliter
μL	Microliter
μM	Mircomolar

CHAPTER 1

Introduction

Antibiotics are extensively used in preventive and curative health care. They have become part of civilization and it is impossible to envision world without antibiotics. Uncontrolled usage of antibiotics causes several side-effects with symptoms such as nausea, diarrhea, headache, stomach pains, fever, body and muscle aches, vomiting, skin rashes accompanied by itching and peeling [Laseni et al., 2016; Kapoor et al., 2017]. Excessive usage of antibiotics has led to the development of resistance to conventional antibiotics in microorganisms, which is of a serious concern in modern day medicine [Pelgrift and Friedman, 2013; Ventola, 2015; Candelas et al., 2017]. ESKAPE (*Enterococcus faecium*, *Staphylococcus aureus*, *Klebsiella pneumoniae*, *Acinetobacter baumannii*, *Pseudomonas aeruginosa* and *Enterobacter species*) pathogens inside the hospitals have acquired resistance against antibiotics [Pendleton et al., 2013].

Pathogens develop antibiotic resistance against multiple antibiotics and acquire multiple drug resistance (MDR). In turn, these superbugs cause high morbidity and increase mortality [Allahverdiyev et al., 2011; Kumar and Singh, 2013]. Vancomycin-resistant *Enterococcus* (VRE), methicillin-resistant *Staphylococcus aureus* (MRSA), carbapenem-resistant *Enterobacteriaceae* (CRE) and multi-drug-resistant *Mycobacterium tuberculosis* (MDR-TB) are few examples of superbugs, which have acquired resistance against most of the current antibiotics [Kumar and Singh, 2013]. Besides MDR in pathogenic bacteria many soil bacteria such as *Pseudomonas aeruginosa* and *Acinetobacter baumannii* have also acquired resistance against multiple antibiotics, mainly through horizontal gene transfer from pathogenic bacteria [Aslam et al., 2018]. Development of drug resistance in environmental microbes is also become a matter of great concern.

Increase in number of pathogenic microbes developing MDR, has necessitated the search for non-conventional antimicrobials that are immune from developing resistance in microorganisms. Metals have been widely used for the treatment of infectious diseases from the ancient times [Vimbela et al., 2017]. There are several reports on antibacterial activities of metals [Feng et al., 2002; Nomiya et al., 2004; Vimbela et al., 2017; Shaikha et al., 2019]. Emergence of nanotechnology has helped further in exploring the unique properties of metals at nano scale [Singh et al., 2017]. Metallic nanoparticles of silver, zinc, copper, titanium, gold and iron have been developed, as an alternative to conventional antibiotics that can possibly overcome the AMR and MDR [Feng et al., 2002; Nomiya et al., 2004; Chaloupka et al., 2010; Haggstrom et al., 2010; Kalishwaralal et al., 2010; Allahverdiyev et al., 2011; Vimbela et al., 2017; Singh et al., 2017: Shaikha et al., 2019]. Unlike conventional antibiotics, metal nanoparticles target multiple structural sites of organisms randomly and simultaneously. Owing to their small particle

size and high surface to volume ratio, metal nanoparticles possess high antibacterial activities, which makes them a potential nano-weapon against pathogenic superbugs [Khurana et al. 2014]. Because of this unique capability of metal nanoparticles, organisms are unlikely to develop resistance against them.

In recent years copper nanoparticles (CuNPs) have gained increasing attention due to their unique physical and chemical antimicrobial properties [Cioffi et al., 2005]. There has been growing interest in synthesis of copper nanoparticles (CuNPs) because of their potential applications in nanomedicine. Copper is a trace element as well as essential micronutrient, which is necessary for growth and maintenance of bone, connective tissue, brain and heart [Azizi et al., 2017]. Deficiency of copper can lead to anemia and improper fetal development during pregnancy. It plays a vital role in oxygen transport and iron homeostasis [Habibovic and Barralet, 2011; Vimbela et al., 2017]. In 2008, Environmental Protection Agency of US approved copper in medicinal products for human usage [Azizi et al., 2017]. CuNPs also helps in collagen cross-linking and in bone matrix formation [Klaine et al., 2008]. CuNPs and their complexes are now used as antibacterial, antiviral, anti-fungal and anti-fouling agents [Ventola, 2015].

CuNPs because of their low oxidation potential (0.34 eV) and high surface to volume ratio are prone to oxidation [Magdassi et al., 2010], which imparts severe limitations on their potential use as antimicrobial agents. Therefore, development of CuNPs, which are resistant to oxidation and aggregation is critical. Another grave challenge, restricting the wide scale utility of CuNPs in clinical applications is their per batch yield, which remained low. Development of scale-up protocols, which can improve per batch yield of CuNPs without affecting their physical, chemical and antibacterial activities, is yet to realize. Environmental accumulation of nanoparticles due to their advertent and inadvertent release is another matter of concern as they possess great threat to microbial communities, which plays an important role in biogeochemical cycling [Bone et al., 2012; Yu et al., 2013].

Considering all gaps in the earlier studies, current research work was undertaken to develop synthesis protocols for the preparation of CuNPs that are stable against aggregation and oxidation by chemical reduction and optimization for the scale-up of nanoparticle's per batch yield. Impact of as-synthesized CuNPs were evaluated for their antibacterial and cytotoxic properties on surrogate bacterial pathogens and some soil bacteria as well as cell lines under *in vitro* conditions.

CHAPTER 2

Review of Literature

Infectious diseases have caused millions of deaths and strained the global health care system with an unprecedented load. Microbial infections cause nearly 9 million deaths annually, which accounts for 41% of the global disease burden, measured in terms of Disability-Adjusted Life Years (DALYS) [GDB, 2015; Hessleng et al., 2017]. Microbial diseases with their estimated mortality from year 1918 to 2020 are presented in Table 2.1.

The word 'antibiotic' hails from the word 'antibiosis' (meaning against life). Antibiotics are chemical compounds that kill or inhibit the growth of microorganisms. Antibiotics are classified as antibacterial, antifungal and antiviral agents depending on their target group. However, all antibacterial compounds are commonly referred to as antibiotics [Etebu et al., 2016]. For decades, antibiotics have been used to treat various diseases. They are also used in various medical procedures like organ transplants and chemotherapy [Etebu et al., 2016]. Broad-spectrum antibiotics target both the Gram-negative and Gram-positive bacteria while narrow spectrum antibiotics only target one of them [Etebu et al., 2016]. Antibiotics are either bactericidal (lethal to bacteria) or bacteriostatic (causing growth inhibition of bacteria) [Kohanski et al., 2010]. They cause cell deaths or the cessation of growth by targeting vital physiology and biochemistry of bacterial cells. Major targets of antibiotics are: bacterial cell walls, cell membranes, DNA and RNA synthesis, protein synthesis and folic acid (vitamin B9) metabolism [Kohanski et al., 2010]. For example, the β-lactam class of antibiotics such as penicillin, cephalosporins and carbapenem block the synthesis of the bacterial cell wall, while antibiotics like tetracycline, aminoglycoside, macrolide targets bacterial ribosomes. Antibacterial action of antibiotics may result in irreversible disruption of the cell integrity by interacting with target molecules through irreversible binding *via* covalent interaction with an enzyme or cellular structure of cells [Kapoor et al., 2017].

Antibiotics have been used extensively for the controlled treatment of infectious diseases and in various surgical procedures like organ transplant and chemotherapy [Wright, 2010]. Excessive and uncontrolled use of antibiotics has resulted into development of Antimicrobial Resistance (AMR) in both intra-hospital and non-hospital strains [Allahverdiyev et al., 2011]. Development of antibiotic resistant strains possesses a serious global threat to the disease management. In European Union alone, an estimated 25,000 deaths per annum was caused by AMR [Pardiyara et al., 2018]. Antibiotic-resistant pathogen-associated hospital acquired infections (HAIs) causes 99,000 deaths per annum in US [Aslam et al., 2018].

Table 2.1 Global mortality due to infectious diseases (1918-2020) [Whitworth, 2018; Hackett, 2018; Bloom and Cadarette, 2019; WHO, 2019; International Association for Medical Assistance, 2019; Coronavirus, 2020]

Year	Pathogen	Geographic region	Cases/Mortality
1918-1920	Influenza (Spanish flu)	Worldwide	500 million cases and 30 to 100 million deaths
1957-1958	Influenza (Asian flu)	Worldwide	1 to 2 million deaths
1968-1969	Influenza (Hong Kong flu)	Worldwide	500,000 to 2 million deaths
1960-present	HIV/AIDS	Worldwide, primarily Africa	70 million cases and 35 million deaths
1961-present	Cholera	Worldwide	1.4 to 4 million annual cases and 21,000 to 143,000 annual deaths
1974	Smallpox	India	130,000 cases and 26000 deaths
1994	Plague	India	693 suspected cases and 56 deaths
2002-2003	SARS	Originated in China, spread to 37 countries	8,098 cases and 774 deaths
2009	Influenza (Swine flu)	Worldwide	284,000 deaths
2014-2016	Ebola	West Africa, primarily Guinea, Liberia, and Sierra Leone	28,600 cases and 11,325 deaths
2015-present	Zika	The Americas, primarily Brazil	Unknown number of cases
2016	Dengue	Worldwide	100 million cases and 38,000 deaths
2017	Plague	Madagascar	2,417 cases and 209 deaths
2017-2018	Cholera	Worldwide	1.2 million cases and 2627 deaths
2018	Listeria	South Africa	1060 cases and 216 deaths
2017-2018	Hepatitis A	USA	10,582 cases
2019-2020	Corona virus	Worldwide	28,687,168 cases and 920, 316 deaths till 12/09/2020

Many intra-hospital pathogens have developed resistance against multiple antibiotics resulting in decrease in the efficiency of treatment. Decline in the effectiveness of existing antibiotics has caused higher morbidity and mortality in patients, which are infected with multidrug-resistant (MDR) strains [Davies et al., 2010; Spellberg and Gilbert, 2014; Gonzalez-Candelas et al., 2017]. Deaths due to MDR alone is nearly 7,00,000 per annum [Betts et al., 2018]. In past two decades, hospitals have witnessed increase in MDR acquired infections due to the production of β-lactamase, which is responsible for development of drug resistance against third generation antibiotics [Blair et al., 2014]. Mechanisms of bacterial resistance against antibiotics are summarized in Fig. 2.1 and listed in Table 2.2 [Kapoor et al., 2017; Aslam et al., 2018].

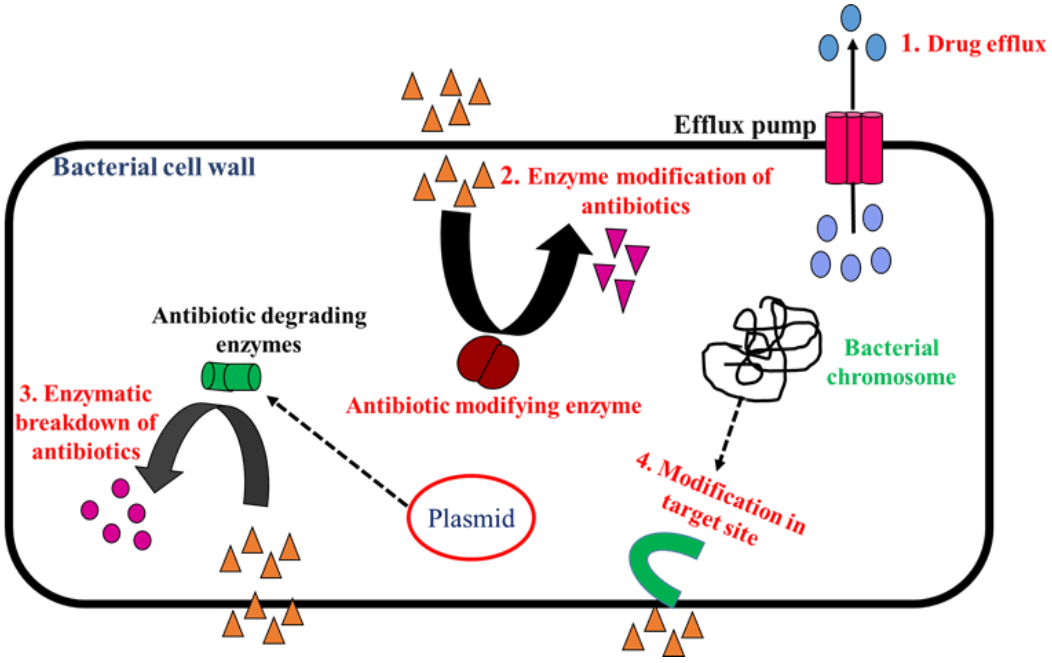

Figure 2.1 Mechanism of antibiotic resistance in microorganisms against conventional antibiotics [Aslam et al., 2018].

Following mechanisms are responsible for antibiotic resistance in microorganisms:

i. Increased efflux of drugs and their reduced uptake.
ii. Development of modifying enzymes / drug degrading inside microorganisms
iii. Enzymatic breakdown of antibiotics.
iv. Alterations in antibiotic targets wherein new biosynthetic machinery is engaged to alter cell-wall structure.
v. Formation of protective biofilm around the bacteria that prevents its exposure to antibiotics.

Table 2.2 Mechanisms of bacterial resistance against different antibiotics [Kapoor et al., 2017]

Antibiotic class	Resistance type	Resistance mechanism	Microorganisms
Aminoglycoside	Decreased uptake Enzyme modification	Changes in the outer membrane Aminoglycoside modifying enzymes (AGEs)	*Pseudomonas aeruginosa* Gram-negative bacteria
Oxazolidinones	Altered target	Mutation leading to reduced binding to active site	*Enterococcus faecium* and *Staphylococcus aureus*
Beta- lactams	Altered PBP Enzyme degradation	Penicillin binding protein (PBP 2a) Penicillinase which are classified as per ambler classification	Mec A in *S. aureus*, *Streptococcus pneumoniae* Gram-negative bacteria
Tetracycline	Efflux	New membrane transporters	*tet* genes encoding efflux proteins in Gram-positive bacteria and Gram-negative bacteria
	Altered target	Production of proteins that bind to the ribosome and alter the conformation of the active site	*tet* (M) and *tet* (O) in Gram-positive and Gram-negative bacteria species
Sulfa drugs	Altered target	Mutations of genes encoding Dihydropteroate synthase	*Escherichia coli*, *S. aureus*, *S. pneumonia*
Macrolides	Altered target	Methylation of ribosomal active site with reduced binding	*erm*-encoded methylases *in S. aureus*, *S. pneumoniae*, and *S. pyogenes*
Chloramphenicol	Antibiotic inactivation	Chloramphenicol acetyl transferase (CAT)	CAT in *S. pneumonia*
Glycopeptides	Altered target	D-alanyl-alanine is changed to D-alanyl-D-lactate.	Vancomycin resistance in *E. faecium* and *Enterococcus faecalis*
Quniolones	Altered target	Mutation leading to reduced binding to active site (s)	Mutations in gyr A in enteric Gram-negative bacteria and *S. aureus*

Injection of antibiotics as a growth promoter in livestock has increased in recent years resulting in greater MDR strains in animals. Antibiotic consumption in livestock is expected to rise to 67% by 2030 [Boeckel et al., 2015]. This could also affect human health, because mobile genetic elements (MGEs) from resistant bacteria make their ways from animals to humans by various means [Molbak, 2004; Humphrey et al., 2005].

Development of new and unconventional antibiotics is the need of the hour to overcome challenges put forward by multiple drug resistance (MDR). Due to their high surface-to-volume ratio, metal nanoparticles exhibit enhanced chemical and biological activities [Khurana et al., 2014]. Nanoparticles impart toxicity on microorganisms (Fig. 2.2; Table 2.3) by disturbing permeability and respiration of cell walls, inhibit enzymes, deactivate proteins, electrolyte imbalance, interfering with metabolic pathways of cells, damage to the cell membrane, reacting with sulfur-containing proteins and phosphorus-containing compounds such as DNA, induce oxidative stress by generating reactive oxygen species (ROS), generation of free radicals, modify gene expression levels, damage biomolecules like proteins, lipids and DNA and prevent biofilm formation [Hemeg, 2017; Shailkha et al., 2019; Martinez et al., 2019].

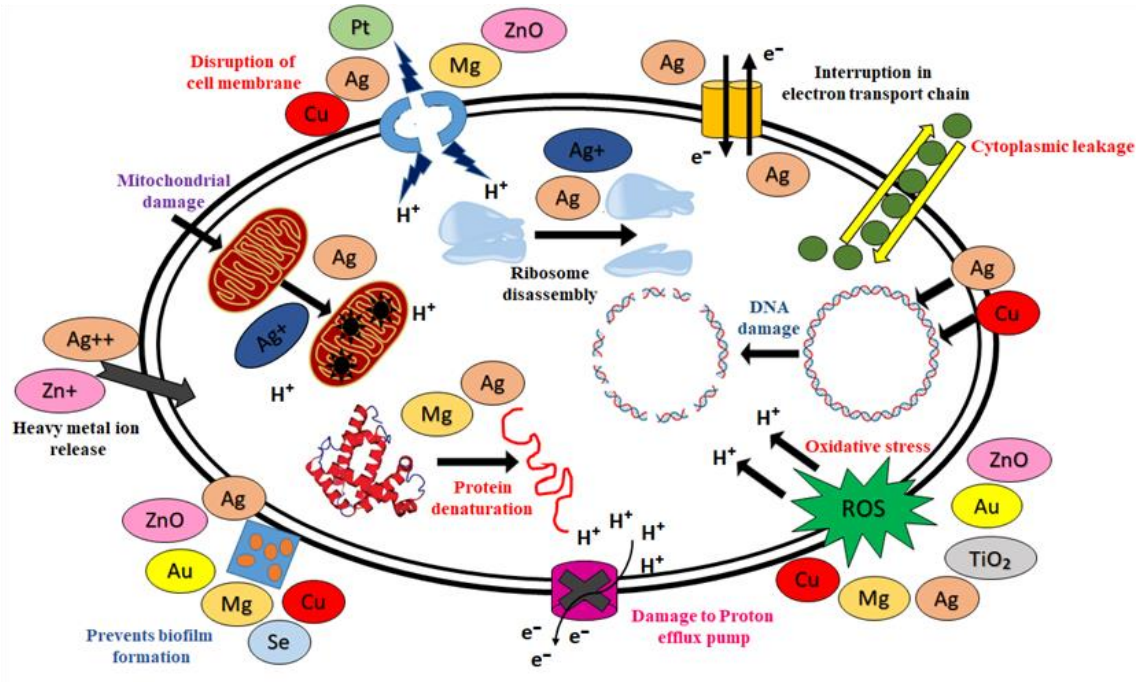

Figure 2.2 Possible mechanisms of antibacterial effect of metal nanoparticles on bacteria [Hemeg, 2017].

Due to the different target sites of metal nanoparticles, the probability of a microorganism developing resistance against metal nanoparticles is very low [Chopra, 2007; Harikumar and Aravind, 2016]. Among metals, gold, silver and copper are known for their antiseptic properties since ancient times [Vimbela et al., 2017]. The gold

nanoparticles have also been developed for PCR based detection of pathogenic bacteria [Singh et al., 2018]. The ligand-based metal (copper complexes) and metal-based formulations of inorganic nanoparticles (barium sulfate) have also shown higher antibacterial activities [Lobana et al., 2020; Sooch et al., 2020].

Table 2.3 Antibacterial effect of metal nanoparticles on different bacteria [Hemeg, 2017]

Nanoparticles	Target Bacteria	Antibacterial mechanism
Silver (Ag)	*Acinetobacter baumannii*, *S. typhi*, *Vibrio cholerae*, *B. subtilis*, *S. aureus* (Multiple drug resistance), *Escherichia coli*, *Streptococcus pyogenes*, *Pseudomonas aeruginosa*, coagulase-negative *Staphylococcus epidermis*, *Enterococcus faecalis*, *Klebsiella pneumoniae*, *Listeria monocytogenes*, *Proteus mirabilis*, *Micrococcus luteus*	ROS generation, lipid peroxidation, inhibition of cytochromes of ETC, bacterial membrane disintegration, inhibition of cell wall synthesis, increase in membrane permeability, dissipation of proton gradient resulting in lysis, adhesion to cell surface causing lipid and protein damage, ribosome destabilization, intercalation between DNA bases, disruption of biofilms.
Copper (Cu)	*Escherichia coli*, *Bacillus subtilis*, *Proteus vulgaris*	ROS generation, disorganization of membrane, inhibition of DNA replication, Dissipation of cell membrane potential, lipid peroxidation, protein oxidation, DNA degradation.
Zinc oxide (ZnO)	*S. aureus*, *E. coli*, *P. aeruginosa*, *B. subtilis*, *Stenotrophomonas acidaminiphila*, Methicillin-resistant *Streptococcus agalactiae*, *E. coli*, *Klebsiella oxytoca*, *S. aureus*, *S. pyogenes*, Methicillin-resistant *Staphylococcus aureus*	ROS production, disruption of membrane, adsorption to cell surface, lipids and protein damage, inhibition of microbial biofilm formation

Nanoparticle–antibiotic conjugates are promising nano-platforms to combat bacterial resistance. They help in lower the dosage by synergistic effect and reduce noxiousness [Sekhon, 2010; Pissuwana et al., 2011]. Further, these conjugates can increase the concentration of antibiotics at the antibiotic–microorganism contact site [Li et al., 2005]. Decrease in the overall drug concentration in the conjugated system makes them less

toxic and improves their dosage limits [Chen at al., 2009]. Possible mechanisms leading to the synergistic effects in antibacterial activities of metal nanoparticles – antibiotic conjugates are summarized in Table 2.4.

Table 2.4 Mechanisms of antibacterial activities of nanoparticles – antibiotic conjugates on different bacteria [Liu et al., 2005; Birla et al., 2009; Banoee et al., 2010; Selvarani, 2010; Mandava et al., 2017]

Nanoparticle	**Antibiotics**	**Bacteria**	**Mechanism**
Silver	Kanamycin, tetracycline, streptomycin, ampicillin, amoxicillin, gentamicin, vancomycin, erythromycin	*S. aureus*, *E. coli*, *Micrococcus luteus*, *Salmonella typhi*, *P. aeruginosa*	Increased antibacterial action of nanoparticles and antibiotics. Ampicillin destroys cell wall and increases penetration of silver nanoparticles. Silver nanoparticles act as antibiotic carrier and facilitate approach of hydrophobic antibiotic drugs into the bacterial cell membrane.
Zinc oxide	15 antibiotics from different groups	*S. aureus*, *E. coli*	Increased activity of ciprofloxacin in the presence of ZnO nanoparticles by influencing activity of membrane.
Copper	Tetracycline, streptomycin, gentamycin, Amoxicillin, Ampicillin, Ciprofloxacin	*E. coli*, *M. luteus*, *Salmonella typhi*, *Streptococcus pyrogenes*, *S. mutans*	Increased activity of nanoparticles in the presence of antibiotics either by penetrating membrane or by ROS formation.

Apart from antibacterial activities, metal/metal oxide nanoparticles (such as silver, zinc oxide, copper, and titanium dioxide) exhibit strong cytotoxic activities (Table 2.5) [Kreuter, 2007; Sharma et al., 2017]. In most of these studies, it has been found that metal nanoparticles exhibits significant toxicity even at low dose levels, where their bulk counterparts were otherwise biocompatible [Morones et al., 2005; Giannousi et al., 2014; Azam and El-Said, 2014; Sukar and Albadran, 2015; Nayak et al., 2016; Chakraborty and Basu, 2017; Azam et al., 2012]. High active surface area and smaller size of nanoparticles, provide them greater biochemical reactivity and membrane permeability [Wang et al., 2017].

Table 2.5 Cytotoxicity studies of metal/metal oxide nanoparticles

Nanoparticles	Cell lines	References
Silver (Ag)	Human hepatoblastoma ($HepG_2$) and Mice liver primary cell lines Human pulmonary cell lines: A549 and THP-1Osteosarcoma MG-63 cell line.	Sondi and Sondi, 2004; Morones et al., 2005; Lanone et al., 2009; Faedmaleki et al., 2014; Nayak et al., 2016
Copper (Cu)	Human pulmonary cell lines: A549 and THP-1 HeLa and MCF-7 breast cancer cell line Human skin cancer cells (A-375)	Sondi and Sondi, 2004; Yoon et al., 2007; Lanone et al., 2009; Giannousi et al., 2014; Azam and El-Said, 2014; Nayak et al., 2016; Ebrahimi et al., 2017; Chakraborty and Basu, 2017
Zinc oxide (ZnO)	Human monocytic cell line THP-1. MCF-7 breast cancer cell line	Nair et al., 2009; Azam et al., 2012; Sahu et al., 2014; Anitha et al., 2018
Titanium dioxide (TiO_2)	Rat embryo Fibroblast cell line (REF-3) HCT116	Deckers et al., 2009; Sukar et al., 2015

Since, CuNPs exhibits interesting antibacterial and cytotoxic activities and synergistic effects with conventional antibiotics. Detailed review of these aspects of CuNPs, is presented in subsequent sections.

2.1 Synthesis and colloidal stability of CuNPs

Copper nanoparticles (CuNPs) can be a potential candidate for replacement of silver and gold nanoparticles in applications that involves surface plasmon resonance [Cioffi et al., 2005; Soomaro et al., 2014]. However, because of low oxidation potential of copper (0.34 eV), it is prone to oxidation [Magdassi et al., 2010; Rahman et al., 2020]. Owing to high surface to volume ratio, the chemical reactivity of metal nanoparticles increases with the decrease in particle size. Therefore, as compared to bulk copper, CuNPs are more susceptible to oxidation [Zhang et al., 2006; Vellora et al., 2013], which limits their utility in many advance applications. Synthesis of oxidation-resistant colloidal CuNPs has always been a challenge.

CuNPs are synthesized by different chemical and physical methods like

mechanical milling [Oleszak et al., 1996], vapor deposition [Liu et al., 2003], thermal reduction [Naisari et al., 2009], sonochemical reduction [Kumar et al., 2011], chemical reduction [Cheng et al., 2006; Pulkkinen et al., 2009; Qiu-Li., 2010, Khanna et al., 2009; Wei et al., 2009; Wu et al., 2006] and green synthesis [Sastary et al., 2013]. Amongst them, chemical reduction method is most widely explored route. It is easy, simple and versatile method for CuNPs synthesis. It provides good control over nanoparticle yield, size, size distribution and morphology. Effect of reaction parameters like reaction temperature, reaction time, concentration of reactants and capping agents on the physical, chemical and plasmonic properties of CuNPs have been studied in literature [Dang et al., 2011; Xie at al., 2004; Li et al., 2013]. Effect of reaction parameters and the colloidal medium on the stability of CuNPs have also been studied [Wu and Chen, 2004; Kinninan et al., 2008; Xiong et al., 2011; Shankar et al., 2014; Maximino et al., 2018].

Wu and Chen, 2004 synthesized CuNPs by reduction of cupric chloride with hydrazine using cetyltrimethylammonium bromide (CTAB) as capping agent in an inert atmosphere. Kanninen et al., 2008 have synthesized CuNPs with different capping agents and studied the effect of ligand-exchange on the stability of CuNPs. They concluded that oleic acid capped nanoparticles possess better stability than the thiol capped nanoparticles. Yu et al., 2009 reported synthesis of monodispersed colloidal CuNPs in polar solvents with a reaction time of 8 hr. They have found that the size of synthesized CuNPs depends on the concentration of PVP.

Dang et al., 2011 studied the effect of colloidal medium on the stability of CuNPs synthesized by chemical reduction method using two different solvents: water and ethylene glycol. Synthesized CuNPs remained stable upto 60 days in ethylene glycol, while it precipitated in water after 22 days, indicating better colloidal stability of CuNPs in ethylene glycol. In another study, Dang et al., 2011 synthesized CuNPs by chemical reduction method using polyethylene glycol (PEG) as capping agent and studied their surface plasmon resonance by varying reaction time, pH and ratio of copper sulfate to surfactant. They obtained well-dispersed nanoparticles with small size at 60 min reaction time at pH 6 and observed that the surface plasmon resonance (SPR) and oxidation resistance of as-synthesized CuNPs have strong dependence on reaction time, pH and relative ratio of surfactant to copper precursor. Xiong et al., 2011 have used L-ascorbic acid as reducing cum capping agent in the synthesis of CuNPs. Synthesized nanoparticles were ultrafine (2 nm) in size and stable up to 60 days in aqueous medium.

Qing-Ming et al., 2012 studied the effect of reaction parameters (reaction temperature, copper sulfate concentration, pH of solution, $NaBH_4$ concentration and $NH_3.H_2O$ concentration) on the properties of CuNPs. They have obtained smallest CuNPs (37 nm) at optimum reaction conditions (40 °C reaction temperature with 0.2 mol/L Cu^{2+}, 0.4 mol/L $NaBH_4$, 1.2 mol/L $NH_3.H_2O$ at 12 pH). Liu et al., 2012 reported synthesis of CuNPs by reducing Cu^{2+} ions in aqueous medium at different pH with L-ascorbic acid.

They obtained CuNPs only at pH 3- 7. No CuNPs were formed when pH was > 7. Li et al., 2013 have developed a chemical reduction method for the synthesis of uncapped CuNPs, which remained stable for several months. They demonstrated that altering the order of addition of chemical reagents in the synthesis process significantly affects the size and size distribution of nanoparticles.

Soomro et al., 2014 synthesized CuNPs by chemical reduction method using $NaBH_4$, ascorbic acid and sodium dodecyl sulfate (SDS). They studied the plasmonic properties of as-synthesized CuNPs in terms of SPR peak position by varying the reaction parameters (reaction time, pH, concentration of copper sulfate and SDS). It was concluded that synthesized CuNPs were air resistant for several days. Shankar et al., 2014 studied the effect of reducing agents (NaOH and ascorbic acid) on the morphology of CuNPs. They obtained rod-like nanoparticles with NaOH and triangular or and spherical nanoparticles with ascorbic acid. Jain et al., 2014 studied the effect of reaction temperature and concentration of copper chloride on the morphology, particles size and colloidal stability of CuNPs. They observed that initial concentration of reactants and reaction temperature has significant effect on the particle size and agglomeration of CuNPs. Synthesized CuNPs were stable up to two months.

Khaid et al., 2015 reported synthesis of CuNPs by chemical reduction method using ascorbic acid as antioxidant and sodium borohydride as reducing agent and polyvinylpyrrolidone (PVP) as capping agent. They obtained CuNPs with copper (Cu^0) as major phase and cuprous oxide (Cu^{1+}) as minor phase. Khan et al., 2016 attempted synthesis of starch-protected zero-valent CuNPs by using copper (II) sulfate pentahydrate, NaOH, ascorbic acid and starch at 80 °C. However, they ended up with a mixed phase of Cu and Cu_2O. Olad et al., 2017 prepared CuNPs by using $Cu(NO_3)_2 \cdot 3H_2O$ as a precursor, hydrazine hydrate as reducing agent and deionized water as solvent. Nanoparticles were stabilized with PVP, PEG and starch. They obtained small size CuNPs with narrow size distribution using PEG as stabilizer with copper precursor to stabilizer ratio of l:1.

Maximino et al., 2018 synthesized CuNPs in the presence of organic ligand (poly(allylamine) and allylamine-glycerol) by reducing copper (II) sulfate pentahydrate with hydrazine. They claimed that synthesized CuNPs were air stable upto 3-5 years, however, no experimental evidence of observed stability was provided in this study. Aguilar et al., 2019 reported synthesis of CuNPs by reducing Cu^{2+} ions with sodium borohydride and PVP. They studied effect of reducing agent/precursor salt (RA/PS) ratio on the size and morphology of the nanoparticles. Small semispherical CuNPs were obtained at RA/PS ratio of 2.6. Cu_2O polyhedral particles were obtained when RA/PS ratio was 2.0–1.84 and Cu_2O particles having star-like morphology were obtained at RA/PS ratio of 1.66. Das et al., 2020 synthesized copper nanoparticles by green route using *Moringa oleifera*, however CuNPs were amorphous in nature.

It was observed from the literature survey, that CuNPs were synthesized with diverse physical, chemical and plasmonic properties by chemical reduction method with a variety of copper precursors, reducing and stabilizing agents, under different reaction pH, time and temperature. Most of these studies are isolated with no direct correlation between the synthesis parameters, their colloidal stability and per batch yield. Therefore, synthesizing stable colloidal CuNPs in aqueous media with moderate yield remains a challenge.

2.2 Antibacterial activity of CuNPs on pathogenic bacteria

Rapid emergence of strains with antibiotic resistance and multiple drug resistance (MDR) has brought focus on nanoparticles with antibacterial properties [Shankar et al., 2014]. Nanoparticle based antibiotics are unlikely to suffer from MDR due to their broad and random targeting characteristics. There are several reports on the antibacterial activity of CuNPs on pathogenic bacteria [Raffi et al., 2010; Chatterjee et al., 2012; Karthik et al., 2013; Muhameed et al., 2013; Shao et al., 2016; Daina et al., 2019].

Cioffi et al., 2005 reported antibacterial activities of CuNPs based polymer metal nanocomposites. Synthesized nanocomposite was capable of releasing metal species in a controlled manner that inhibits the growth of the organism. The biostatic activities of composites were correlated to the nanoparticle loading. Yoon et al., 2007 studied the antimicrobial activity of SNPs (silver nanoparticles) and CuNPs on *Escherichia coli* and *Bacillus subtilis*. They observed that CuNPs exhibited higher antibacterial activities against Gram-positive, *B. subtilis* while SNPs were more active against Gram-negative, *E. coli*. Ruparelia et al., 2008 studied the antibacterial activity of SNPs and CuNPs on *E. coli, Staphylococcus aureus* and *B. subtilis*. SNPs exhibited higher antibacterial activity against *E. coli* and *S. aureus*, while CuNPs were more bactericidal to *B. subtilis*. Mary et al., 2009 synthesized CuNPs-loaded fibers by borohydride induced reduction and tested their antibacterial activities against *E. coli*. These CuNPs loaded fibers can be used in burn/wound dressing.

Raffi et al., 2010 studied the antibacterial activity of CuNPs in liquid and solid medium against Gram-negative *E. coli*. They observed formation of cavities / pits in the bacterial cell wall after their interaction with CuNPs. Rispoli et al., 2010 studied the antimicrobial activity of CuNPs against *E. coli* and evaluated effects of pH, temperature, aeration rate, concentration of nanoparticles and concentration of bacteria. It was concluded that the antibacterial activities of CuNPs not only depend on primary effect of test parameters, but also on the interactive effect of these parameters.

Bagchi et al., 2012 synthesized mullite-based CuNPs and studied their antibacterial activities against pathogenic strains: *E. coli*, *S. aureus*, Methicillin-resistant *Staphylococcus aureus* (MRSA) and *Shigella flexneri*. They reported that 70 µg/mL of CuNPs were able to kill all tested microorganisms. Chatterjee et al., 2012 evaluated the

antibacterial activity of CuNPs against *E. coli*. They observed increase in the number of filamentous bacteria with increase in the concentration of CuNPs indicating that the antibacterial activity of CuNPs was because of the growth of filamentous bacteria.

Karthik et al., 2013 studied antibacterial activities of CuNPs and copper oxide nanoparticles on *E. coli, Streptococcus pyogenes, Pseudomonas aeruginosa* and *S. aureus* and found that CuNPs possess higher antibacterial activities as compared to their oxides. Muhammad et al., 2013 observed that chitosan-coated CuNPs have higher antibacterial activities against Gram-negative bacteria than the Gram-positive bacteria.

Figueroa et al., 2014 investigated antibacterial effects of copper, nickel and bimetallic Cu-Ni nanoparticles on dental pathogens (*S. aureus, E. coli* and *Streptococcus mutans*). They observed that CuNPs exhibits bactericidal effects while Ni and bimetallic Cu-Ni nanoparticles only show bacteriostatic effects on tested microorganisms. Shiv et al., 2014 evaluated antibacterial activity of CuNPs against Gram-positive (*Listeria monocytogenes*) and Gram-negative bacteria (*E. coli*). They observed that Gram-positive bacteria exhibit higher susceptibility towards CuNPs than the Gram-negative bacteria.

Kruk et al., 2015 synthesized CuNPs by the reduction of copper ions with hydrazine in SDS aqueous solution and evaluated their antimicrobial activities against standard and clinical strains of methicillin-resistant *S. aureus (MRSA)* and *Candida* species (*C. albicans* and *C. parapsilosis*). Synthesized CuNPs exhibited strong antibacterial and antifungal activities. The antibacterial activities of CuNPs both against standard and clinical strains were stronger than their antifungal activities. Shao et al., 2016 synthesized CuNPs loaded with regenerated bacterial cellulose (RC) and studied their antibacterial activity against *S. aureus* (ATCC 6538), *B. subtilis* (ATCC 9372), *C. albicans* (CMCC(F)98001), *E. coli* (ATCC 25922) and *P. aeruginosa* (ATCC 27853). They found that CuNPs loaded with regenerated bacterial cellulose exhibits antibacterial activities against all tested microorganisms.

Ebrahimi et al., 2017 studied the antibacterial activities of CuNPs synthesized by green route against Gram-positive (*S. aureus* and *B. cereus*) and Gram-negative (*E. coli* and *K. pneumonia*) bacteria. They observed that Gram-positive strains were more susceptible to CuNPs as compared to the Gram-negative bacteria. Zia et al., 2018 synthesized silver and copper nanoparticles by chemical reduction method and studied their antibacterial activity against common human pathogenic bacteria (*S. aureus* and *E. coli*). They observed dose-dependent antibacterial activity of nanoparticles. Both silver and copper nanoparticles exhibited similar antibacterial activities against *S. aureus*, while *E. coli* was more susceptible to silver nanoparticles.

Diana et al., 2019 synthesized mesoporous silica (MSN) - maleamic and MSN – maleamic - Cu nanoparticles and tested their antimicrobial activities on Gram-positive and Gram-negative bacteria. MIC of *E. coli* and *S. aureus* were 125 µg/mL and 250

µg/mL, respectively. ROS levels in MSN-maleamic-Cu treated *E. coli* were 40% higher, while in *S. aureus*, it was 30% higher as compared to controls, indicating that ROS plays a vital role in their antibacterial activities. Jayarambabu et al., 2019 synthesized CuNPs by using green synthesis route and evaluated their antibacterial activity on Gram-negative (*E. coli*) and Gram-positive (*B. subtilis*) bacteria. They have also observed that Gram-positive strains were more susceptible to CuNPs as compared to the Gram-negative strains.

Das et al., 2020 evaluated antibacterial activity of CuNPs synthesized by green route against *E. coli, Klebsiella pneumoniae*, *S. aureus*, and *E. faecalis*. They observed much higher MIC values of CuNPs against these pathogens as compared to those reported in literature, indicating high susceptibility of biological activities of nanoparticles towards synthesis route and conditions of synthesis.

2.3 Antibacterial activity of CuNPs on environmental friendly bacteria

Nanoparticles have catastrophic fate once they are released into the environment and cause toxic effects on the microbial communities in soil and water bodies, which are critical to environmental recycling and ecosystem [Colman et al., 2013; Bone et al., 2012; Hegde et al., 2015]. Leaching of ions from nanoparticles contaminates soil and groundwater where they migrate into surface and interacts with living systems [Bone et al., 2012; Yu et al., 2013]. Therefore, environmental accumulation of CuNPs is a matter of great concern. Understanding the antibacterial activities of CuNPs against soil bacteria is of great relevance for ecosystem health and sustainable nanotechnology [Kon et al., 2013]. In this section an overview of literature on environmental corners of nanoparticles is provided.

Gajjar et al., 2009 studied the antimicrobial activities of commercial nanoparticles against environmental soil microbe, *Pseudomonas putida* KT2440. They observed that nanoparticles of Ag, Zn and Cu were all toxic and possess dose-dependent toxicity on *Pseudomonas putida*. Rousk et al., 2012 studied the ecotoxicity of ZnO and CuO nanoparticles by measuring their ability to inhibit bacterial growth on two different soils. Dose-dependent toxicity of ZnO and CuO nanoparticles was observed in terms of decrease in bacterial growth in both the soil samples.

Concha-Guerrero et al., 2014 investigated the effect of CuO nanoparticles on native soil bacteria. They have observed formation of cavities, holes, membrane degradation, cellular collapse and lysis in CuO exposed soil bacteria. Generation of reactive oxygen species (ROS) and release of nitric oxides were also observed in nanoparticle treated bacteria suggesting that these mechanisms play vital role in the antibacterial activities. Hsueh et al., 2015 studied the effect of zinc oxide nanoparticles on a plant-beneficial bacterium, *B. subtilis*. They observed that ZnO nanoparticles (> 50 ppm) inhibit the growth of *B. subtilis* and found that ZnO nanoparticles exhibits toxicity

by inhibiting cell growth, cytosolic protein expressions and biofilm formation.

Yerukala et al., 2018 reported antibacterial activities of CuNPs against two plant biocontrol agents *P. fluorescens* and *B. subtilis*. Gram-negative *P. fluorescens* was more sensitive to CuNPs than Gram-positive *B. subtilis*. This difference in toxicity was ascribed to the structural difference in cell membranes of two cultures. Alum et al., 2018 investigated the response of environmental isolates and pathogenic laboratory strains of *E. coli* towards CuNPs. The environmental isolate and laboratory strains of *E. coli* showed different inactivation patterns. Different levels of glutathione reductase (GR) activities, an enzyme critical for protection against radicals (hydroxyl or superoxide) was observed. These results indicated that CuNPs exhibited higher toxicity on environmental isolates than the pathogenic laboratory strains.

Li et al., 2020 evaluated the effect of TiO_2 nanoparticles on the toxicity of copper on two bacterial species (*Bacillus thuringiensis* and *Bacillus megaterium*), which were isolated from sediments. They observed that TiO_2 nanoparticles inhibited the growth of *B. thuringiensis* and enhanced ROS induced cell damage by copper, whereas in *B. megaterium* no ROS formation was observed.

2.4 Cytotoxicity of CuNPs on RAW 264.7 murine macrophage cell line

Copper nanoparticles (CuNPs) can conjugate with proteins and enzymes [Saranya et al., 2017] and by doing so, it can disrupt many critical cellular functions by inducing intra and extra cellular stresses leading to cell death by apoptosis or necrosis pathways [Laha et al., 2014; Tardito et al., 2009]. Therefore, it is imperative to study putative toxicity of CuNPs especially in mammalian cells like macrophages [Bostos et al., 2017; Park et al., 2011].

Chen et al., 2006 studied the *in-vivo* toxicity of CuNPs (23.5 nm), micro-copper particles (17 μm) and cupric ions ($CuCl_2 \cdot 2H_2O$) on mice. They have found that CuNPs induced greater toxicological effects and pathological injuries to the kidney, liver and spleen of mice as compared to the bulk copper. Lanone et al., 2009 studied the comparative toxicity of 24 nanoparticles including CuNPs on human alveolar epithelial and macrophage cell lines. They have observed that toxic concentration (TC50) of copper and zinc-based nanoparticles show similar concentration-dependent effects on human alveolar epithelial and macrophage cells.

Bucchianico et al., 2013 studied the cytotoxic and genotoxic effects of copper oxide nanoparticles having different morphologies on RAW 264.7 and peripheral whole blood cells. They have observed dose-dependent increase in oxidative stress on DNA. Triboulet et al., 2013 studied the molecular responses of macrophages (RAW 264.7 and primary macrophages) towards copper and copper oxide nanoparticles by a combination of proteomic and biochemical approaches with copper ions and zirconium oxide

nanoparticles as controls. LD20 (lethal dose) of Cu and CuO nanoparticles was 10 μg/mL for RAW264.7 cell line and 5 μg/mL for primary macrophages.

Libalova et al., 2017 reported the toxicity of CuONPs (12 nm±4 nm) with different surface modifiers (anionic sodium citrate, sodium ascorbate, neutral PVP, cationic ployethylenimine, uncoated CuONPs on RAW 264.7 murine macrophage cell line. They observed that toxicity was because of synergistic interactions between nanoparticles, their dissolution, formation of ROS and toxicity of different coating agents in RAW 264.7. (Something is missing). Kumar et al., 2020 studied cytotoxicity of thoil stabilized CuNPs against RAW 264.7. They observed that at low concentrations (below 60 μg/mL) CuNPs were less toxic and toxicity increased at higher concentrations. The toxicity was caused by generation of ROS in RAW 264.7.

2.5 Cytotoxicity of CuNPs on MCF-7 human breast cancer cell line

Breast cancer is most invasive type of cancer and difficult to treat by conventional therapeutic methods [Franco-Molina et al., 2010]. In United States alone, 1.7 million new breast cancer cases have been reported in 2018 [Janic et al., 2018]. In Indian population, particularly in the age group of 20-30, multifold increase in the aggressive cases of breast cancer has been reported [Fridhouse and Lalitha, 2015]. Therefore, finding an effective treatment with fewer side-effects is important [Fridhouse and Lalitha, 2015; Janic et al., 2018]. CuNPs have impressive binding and conjugation ability with proteins and enzymes that could cause necrosis in malignant tumors, causing breast cancer [Saranya et al., 2017]. In this section existing literature on the cytotoxicity of CuNPs on MCF-7 human breast cancer cells have been reviewed.

Laha et al., 2015 studied the anticancer properties of folic acid conjugated copper oxide nanoparticles (CuO-FA NPs) against MCF-7. MTT assay, flow cytometric analysis, ROS assay, expression of apoptotic proteins indicated that most cell death occurred through apoptosis in CuO-FA NPs treated MCF-7 cells. In *in-vivo* study, Dalton's lymphoma (DL) cells were used. LD50 of CuONPs was 0.6 mM/L and for CuO-FA NPs it was 0.1 mM/L, indicating the higher affinity and toxicity of folic acid coated nanoparticles. 1.6 fold increased ROS production with reference to control cells and higher expression of apoptotic proteins indicated that most of cell death occurred through apoptosis in CuO-FA treated cells. In another study, the same group has demonstrated that CuO NPs induce autophagy in MCF-7 cell line in a time and dose-dependent manner, which was due to the induction of apoptosis.

Maqusood et al., 2016 studied the toxicity of copper ferrite nanoparticles on MCF-7 cell line where they demonstrated dose and time dependent toxicity by membrane damage. Copper ferrite nanoparticles induce oxidative stress in MCF-7 cells by generating reactive oxygen species (ROS). Depletion of glutathione and induced oxidative stress causes cell death in MCF-7. Saranya et al., 2017 have studied cytotoxicity

of colloidal CuNPs on MCF-7 by MTT assay. The synthesized CuNPs showed cytotoxic effects against MCF-7 with 50 % cell inhibition at 250 μg/mL of CuNPs.

Azizi et al., 2017 evaluated cytotoxic effect of albumin coated silver and CuNPs on human breast cancer cells MDA-MB 231 and normal cells MCF-10A by MTT assay, ROS assay, fluorescent microscopy and DNA fragmentation. As compared to uncoated CuNPs, albumin coated CuNPs significantly suppresses viability of cancer cells, while they were less toxic to normal cells. Compared to the untreated cells, MDA-MB 231 cells treated with CuNPs exhibit higher ROS levels causing cell apoptosis.

Hassanient et al., 2018 studied anticancer properties of CuNPs against human colon cancer Caco-2 cells, human hepatic cancer HepG2 cells and human breast cancer MCF-7 cells. Dose-dependent anticancer property was observed in each tested cell lines with IC_{50} of 11.21 μg, 19.88 μg and 12.21 μg for Caco-2 cells, HepG2 cells and MCF-7 cells, respectively. Aditi et al., 2019 evaluated cytotoxic effects of copper oxide nanoparticles on MCF-7 and Hela cells. Toxicity was caused by cellular uptake of Cu^{+2} ions, which inflicted significant ROS generation inside the cells and DNA fragmentation. In *in-vivo* model, copper oxide nanoparticles reduced the breast tumor volume in Balb/C mice and increased the mean survival time through the alteration of pro-inflammatory cytokines level.

Shobha et al., 2019 studied cytotoxicity and genotoxicity of CuNPs on MCF-7 cancer cells and on normal cell line (3T3L1). Morphological changes have been observed in CuNPs treated MCF-7 cells. For MCF-7, the IC_{50} dose of CuNPs was 1.71 μg/mL, whereas at this concentration, no cytotoxicity was observed on normal cell lines (3T3L1). MCF-7 showed the chromosomal condensation and fragmentation of DNA after their treatment with the CuNPs.

2.6 Synergistic effect of antimicrobial activity of CuNPs with antibiotics

To overcome increasing resistance in microorganism options available is to combine antibiotics with other antimicrobial agents or drugs that can improve antibacterial efficacy and are not prone to develop resistance in microorganisms [Li et al., 2005; Sekhon et al., 2010; Pissuwana et al., 2011]. Researchers have made several attempts to improve the antibacterial activities and MDR of existing antibiotics by conjugating them with metal/metal oxide nanoparticles.

Usman et al., 2012 evaluated synergistic effects of chitosan-copper nanoparticles on Gram-positive bacteria (methicillin-resistant *S. aureus* (MRSA) and *Bacillus subtilis*), Gram-negative bacteria (*Salmonella choleraesuis* and *Pseudomonas aeruginosa*) and yeast (*Candida albicans*) with nystatin (for yeast), ampicillin (for Gram-negative bacteria), and streptomycin (for Gram-positive bacteria). They have concluded that CuNPs, in combination with antibiotics, exhibits higher antibacterial activities against

tested bacteria. Khurana et al., 2016 studied the synergistic effects of metal nanoparticles (silver and copper) on environmentally friendly bacteria (*B. subtilis* and *P. fluorescens*) with antibiotics (tetracycline and kanamycin). The antimicrobial activity of tetracycline was improved by 286-346% and 0-28% with silver and CuNPs, respectively whereas the improvement was 154-289% for silver and 3-20% for CuNPs with kanamycin.

Mandava et al., 2017 reported the synergistic effects of CuNPs with antibiotics ampicillin, amoxicillin, gentamicin and ciprofloxacillin on bacterial strains *E. coli, S. typii, M. luteus* and *S. mutans*. Amongst the tested antibiotics, CuNPs - Ampicillin conjugates have highest synergistic antibacterial activities. Selvarani et al., 2018 investigated the synergistic effects of CuNPs with commercial antibiotics (tetracycline, rifampicin, chloramphenicol, vancomycin, gentamycin, streptomycin, kanamycin, tobramycin, penicillin, and ampicillin) against *B. cereus, E. coli, P. aeruginosa* and *S. aureus*. Strong synergy of CuNPs was observed with all tested antibiotics.

Kaur et al., 2019 reported synergistic activity of CuNPs with erythromycin, azithromycin and norfloxacin against Gram-positive and Gram-negative bacterial strains. In case of antibiotics, the test bacteria (*Klebsiella sp* and *Pseudomonas sp*) showed resistance at all tested concentrations. In conjugation with CuNPs, the antibacterial activity of all antibiotics increased suggesting that combination of antibiotics with nanoparticles has significant synergistic antibacterial effects on *Klebsiella sp* and *Pseudomonas sp*. Yaqub et al., 2020 prepared CuNPs by chemical and biological synthesis and evaluated their synergistic effects with doxycycline against *E.coli* and *P. aeruginosa.* They reported that chemically synthesized CuNPs showed higher antimicrobial activity with doxycycline as compared to green synthesized CuNPs.

2.7 Conclusion

Due to the development of multidrug-resistance (MDR) in microorganisms there is an urgent need for development of new antimicrobial agents that will overcome the threats put up by MDR. Metal nanoparticles owing to their high surface-to-volume ratio exhibits enhanced chemical and biological activities that makes them a potential candidate for development of antimicrobial drugs. There are various metal nanoparticles like gold, silver and copper, which possess enhanced antibacterial and cytotoxic activities. In recent years, there has been growing interest in synthesis of copper nanoparticles (CuNPs) because of their potential applications in nanomedicine. CuNPs and their complexes are now used as antibacterial, antiviral, anti-fungal and anti-fouling agents. Compare to the bulk, copper at nano-scale possess higher antibacterial activities and greater toxicity. Because of high sensitivity towards aggregation and oxidation, the preparation of single phase copper nanoparticles and its scale-up remains a challenge. The antibacterial and cytotoxic activities also changed dramatically by scaling up of nanoparticle yield. Further, the correlation between per batch yield of nanoparticles and their antibacterial activities

and cytotoxicity was completely missing in literature. Therefore, development of synthesis protocols leading to a successful scale-up of nanoparticle per batch yield without altering their antibacterial and toxicological activities remain a subject of great interest to the researchers.

Based on the literature survey and identified gaps, following objectives have been proposed for this thesis:

Objectives

1. Synthesis of single phase, oxidation resistant hydrophilic-engineered copper nanoparticles (CuNPs) by chemical reduction method.
2. Physical and chemical characterization of as-synthesized and aged CuNPs.
3. *In vitro* evaluation of antibacterial activity and cytotoxicity of CuNPs.

CHAPTER 3

Objective 1: Synthesis of single phase, oxidation resistant hydrophilic engineered copper nanoparticles (CuNPs) by chemical reduction method

Effect of synthesis variables (type of copper precursor, reaction temperature and reaction time) on nanoparticle yield, their plasmonic properties, hydrodynamic size and size distribution were studied. Synthesized CuNPs were characterized by UV-visible spectroscopy, photon correlation spectroscopy (PCS) and inductively coupled plasma atomic emission spectroscopy (ICP-AES) to understand the effect of reaction parameters on their surface plasmon resonance (SPR), hydrodynamic particle size and nanoparticle yield. Effect of aging on the colloidal stability of CuNPs and its correlation with nanoparticles' yield was also evaluated by monitoring the hydrodynamic size (D_H) and surface plasmon resonance (SPR) band position (λ_{max}).

3.1 Material

Copper chloride ($CuCl_2$. $2H_2O$), copper acetate ($Cu(OAc_2)$), copper sulfate ($CuSO_4$), copper nitrate ($Cu(NO_3)_2$), sodium borohydride ($NaBH_4$), polyvinylpyrrolidone (PVP 10,000) were purchased from sigma-Aldrich. L-ascorbic acid was procured from Merck. Spectroscopy grade nitric acid used in ICP-AES analysis was purchased from Sigma-Aldrich. All aqueous solutions were prepared in Milli-Q ultrapure water (ρ = 18.2 MΩ). All chemicals are of AR grade and used as received without any further purification.

3.2 Synthesis of copper nanoparticles (CuNPs)

Colloidal copper nanoparticles (CuNPs) were prepared by chemical reduction method in ambient atmosphere [Khurana et al., 2016]. Synthesis protocol is summarized in Fig. 3.1 and conditions of experiments are given in Table 3.1. To optimize the conditions for the synthesis of CuNPs, a series of CuNPs were prepared by using four different copper precursors i.e. $CuCl_2$, $CuSO_4$, $Cu(NO_3)_2$ and $Cu(OAc)_2$. The reaction was carried out at 60-100 ^oC for reaction time of 5-30 min. $NaBH_4$ and ascorbic acid were used as primary (strong) and secondary (weak) reducing agents.

In brief, 5 mM PVP 10,000 was dissolved in 25 mL warm distilled water under constant magnetic stirring. This results into light yellow solution. Aqueous solution of 1 mM copper precursor ($CuCl_2$. $2H_2O$, $CuSO_4$, $Cu(NO_3)_2$, $Cu(OAc)_2$) was added drop-wise into the preheated solution of PVP. On addition of copper precursor, the color of the solution changes from light yellow to green. Then, 10 mM $NaBH_4$ was added. The solution color turned black. Now, 10 mM aqueous solution of ascorbic acid (10 mL) was added and allowed to react for another 5 min at 60 -100 ^oC under constant magnetic

stirring for another 5 min. This turns the solution color to dark red indicating the reduction of copper ions to Cu^0 and formation of CuNPs. The colloids were then cooled to room temperature and centrifuged at 6000 rpm for 10 min to remove clusters of nanoparticles, if any. CuNPs were preserved at room temperature for further analysis.

Effect of following synthesis variables on the properties of CuNPs was investigated.

(i) Copper precursors ($CuCl_2$. $2H_2O$, $CuSO_4$, $Cu(NO_3)_2$, $Cu(OAc)_2$) - [Sample S1-S4].
(ii) Reaction time (5-30 min) - [Sample S5-S8].
(iii) Reaction temperature (60-100 ^oC) - [Sample S9-S13].

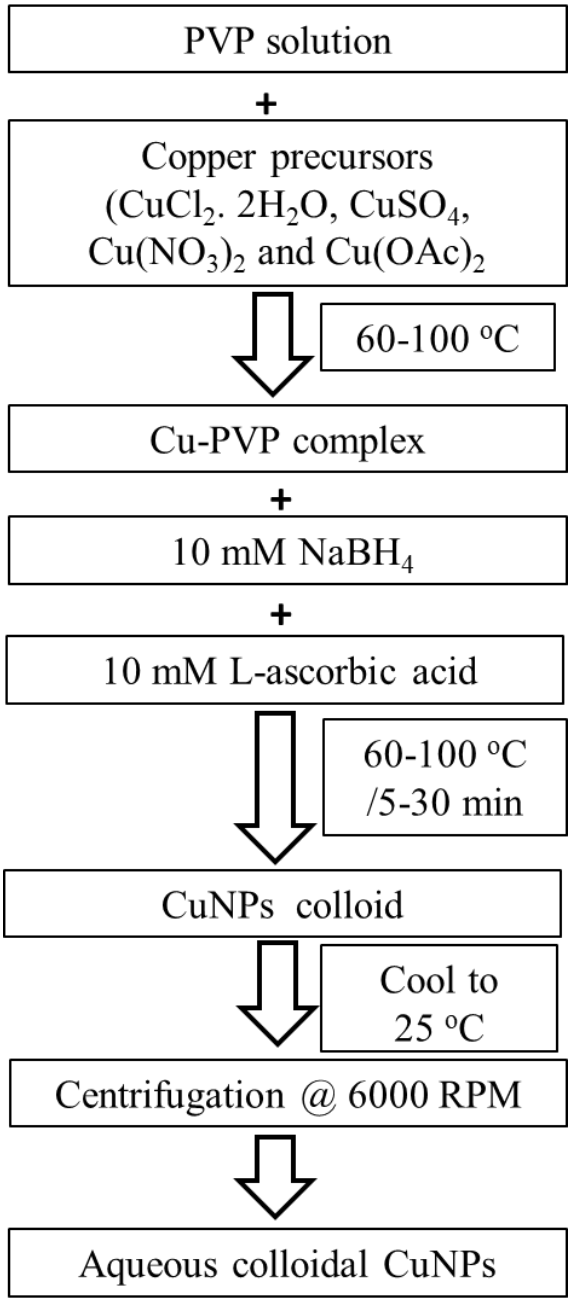

Figure 3.1 Flowchart of synthesis protocols used for the preparation of colloidal CuNPs.

Table 3.1 Summary of synthesis conditions (copper precursors, reaction time and reaction temperature) of CuNPs along with their SPR properties (λ_{max}, A_{max}), hydrodynamic particle size and Cu concentration in colloids

Sample	**Copper precursor**	**Reaction Time (**min**)**	**Reaction Temperature (**^{o}C**)**	**λ_{max} (nm)**	**A_{max}**	**Hydrodynamic size (nm)**	**Cu Concentration (µg/mL)**
S1	$CuSO_4$	5	80	575	0.27	37 ± 0.53	191.2 ± 9.5
S2	$CuCl_2.2H_2O$	5	80	569	0.32	38 ± 0.52	118 ± 6.0
S3	$Cu(OAc)_2$	5	80	569	0.18	55 ± 0.49	82.0 ± 4.0
S4	$Cu(NO_3)_2$	5	80	568	0.10	102 ± 0.53	72.0 ± 3.0
S5	$CuCl_2.2H_2O$	5	80	569	0.32	38 ± 0.52	191.2 ± 9.5
S6	$CuCl_2.2H_2O$	10	80	569	0.19	39 ± 0.51	193.3 ± 9.6
S7	$CuCl_2.2H_2O$	20	80	569	0.18	47 ± 0.51	194.6 ± 9.7
S8	$CuCl_2.2H_2O$	30	80	567	0.30	56 ± 0.51	195.9 ± 9.8
S9	$CuCl_2.2H_2O$	5	60	564	0.27	66 ± 0.51	169.9 ± 8.4
S10	$CuCl_2.2H_2O$	5	70	565	0.25	59 ± 0.51	183.6 ± 9.1
S11	$CuCl_2.2H_2O$	5	80	569	0.32	38 ± 0.52	191.2 ± 9.5
S12	$CuCl_2.2H_2O$	5	90	567	0.29	47 ± 0.51	157.5 ± 7.8
S13	$CuCl_2.2H_2O$	5	100	566	0.21	67 ± 0.51	162.5 ± 8.1

Objective 2: Physical and chemical characterization of as-synthesized and aged CuNPs

As-synthesized CuNPs were characterized by UV-visible absorption spectroscopy, X-ray diffraction (XRD), photon correction spectroscopy, transmission electron microscopy (TEM), and inductively coupled plasma atomic emission spectroscopy (ICP-AES). The plasmon resonance spectra of CuNPs were recorded in the spectral range of 400-700 nm at room temperature on Shimadzu UV-2600 spectrophotometer. Structural characterization of as-synthesized CuNPs was carried out by powder X-ray diffraction (XRD). The XRD patterns of as-synthesized CuNPs were recorded in the 2θ range of 30° to 95° on PANalytical X'Pert Pro diffractometer, which was operated at 45 kV and 40 mA with monochromatic CuKα radiation (λ = 0.15406 nm) with a scan speed of 3° per minute. Hydrodynamic particle size and size distribution of CuNPs were determined by photon correction spectroscopy. Hydrodynamic size was measured on Brookhaven 90 plus particle size analyzer. Colloidal stability of as-synthesized nanoparticles was determined by zeta potential measurement. Zeta potential of colloidal CuNPs were measured by phase angle light scattering (PALS) on Brookhaven 90 plus zeta potential analyzer. Measurements were carried out at 25 °C with gold coated electrodes. For zeta potential measurements, each CuNPs samples were adequately diluted in Milli-Q ultra-pure water and sonicated well prior to the measurement. 1.5 mL of CuNPs sample was filled in disposable polystyrene cuvettes. Electrophoretic mobility of the nanoparticles was determined by measuring the Doppler shift in scattered light under constant potential. From this, zeta potential was calculated by using Smoluchowsky equation. Transmission electron microscopy (TEM) of as-synthesized CuNPs was recorded on Philips CM200 transmission electron microscope operated at an accelerating voltage of 200 KV. Samples for TEM measurements were prepared by placing a drop of adequately diluted colloidal CuNPs on an amorphous carbon-coated copper grid having 200 mesh size. Samples were vacuum dried overnight before the microscopy. Elemental analysis of as-synthesized colloidal CuNPs was performed on inductively coupled plasma atomic emission spectroscopy (ICP-AES). Measurements were performed on Leeman labs Prodigy ICP-AES spectrometer. Before each measurement, the spectrometer was calibrated with VHG multi-element standard. CuNPs samples for ICP analysis were prepared by digesting them with concentrated nitric acid at 90 °C.

3.3 Effect of synthesis variables

3.3.1 Copper precursor

To understand the effect of copper precursors on the physical and plasmonic properties of as-synthesized CuNPs, four copper precursors $CuCl_2.2H_2O$, $CuSO_4$, $Cu(NO_3)_2$ and $Cu(OAc)_2$ were used. All other parameters were kept constant. Reaction temperature was kept at 80 ^oC and reaction time of 5 min. Synthesis protocols were summarized in Table

3.1 (sample S1-S4). Effect of copper precursors on the surface plasmon resonance (SPR) and hydrodynamic size of CuNPs was studied by UV-Visible absorption spectroscopy and photon correlation spectroscopy (PCS). The UV-Visible spectra of colloids synthesized with different copper precursors ($CuCl_2.2H_2O$, $CuSO_4$, $Cu(NO_3)_2$ and $Cu(OAc)_2$) were shown in Fig. 3.2.

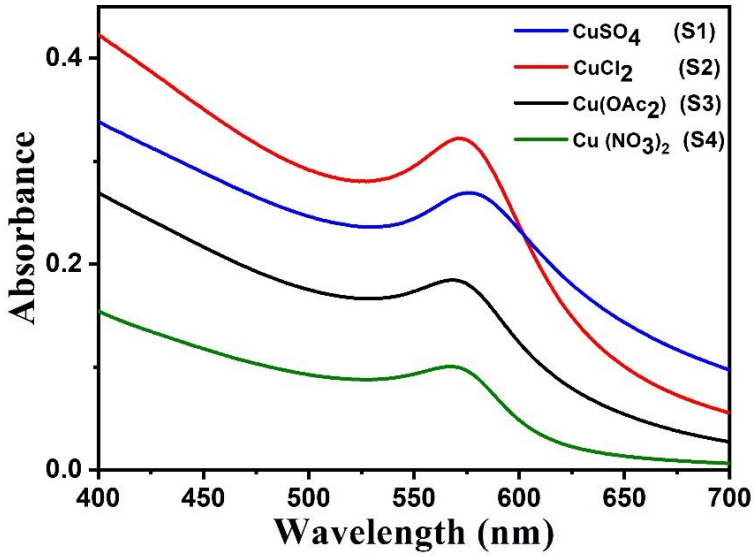

Figure 3.2 UV-visible absorption spectra of CuNPs prepared with (S1) $CuSO_4$, (S2) $CuCl_2$. $2H_2O$, (S3) $Cu(OAc)_2$ and (S4) $Cu(NO_3)_2$.

A single plasmon resonance band centered between 560-580 nm was observed indicating the formation of CuNPs in Cu^0 state. The position of plasmon resonance band (λ_{max}) of CuNPs synthesized with $CuSO_4$ was highest (575.5 ± 10 nm) followed by that of $CuCl_2$ (569 ± 10 nm), $Cu(NO_3)_2$ (569 ± 10 nm) and $Cu(OAc)_2$ (568 ± 10 nm). A significant blue shift to 370 nm was expected in SPR band position, if Cu oxidizes to Cu^{2+} (i.e. CuO). Similarly, if Cu oxidizes to Cu^{1+} (i.e. Cu_2O), an SPR band was expected at 450 nm [Hu et al., 2006]. Absence of SPR bands at 370 nm and 450 nm in the UV-visible spectra (Fig. 3.2) of CuNPs indicates that the synthesized CuNPs were in native Cu^0 state.

Presence of single SPR band also indicates that the synthesized nanoparticles have symmetric (spherical) morphology [Castanon et al., 2008]. For non-symmetric plasmonic nanostructures more than one SPR band was expected in their UV-visible spectra [Khurana et al., 2014]. The SPR band position of CuNPs was dependent on the nanoparticle shape, size and surface adsorbed species [Dang et al., 2011]. The small difference observed in the position of SPR bands of CuNPs prepared with different copper precursors might be because of difference in their hydrodynamic particle sizes, as no change in the shape of nanoparticles was evident from the UV-visible spectra (Fig. 3.2).

Effect of copper precursors on the hydrodynamic particle size and size distributions of CuNPs prepared with four different copper precursors ($CuCl_2.2H_2O$,

$CuSO_4$, $Cu(NO_3)_2$) and $Cu(OAc)_2$) was shown in Fig. 3.3. Each histogram was fitted with lognormal particle size distribution function [Khurana et al., 2014].

$$P(D) = \frac{1}{(D\sigma\sqrt{2\pi})} \exp\left[-\frac{(\ln(\frac{D}{Do}))^2}{2\sigma^2}\right] \quad (3.1)$$

Where σ is the standard deviation, D is the hydrodynamic particle diameter and ln Do the mean of ln D.

From the best fit, mean hydrodynamic size was determined which was reported in Table 3.1. The minimum hydrodynamic size of CuNPs (37 ± 0.53 nm) was observed for particles prepared with $CuSO_4$, followed by $CuCl_2$ (38 ± 0.52 nm) and $Cu(OAc)_2$ (55 ± 0.49 nm). The largest hydrodynamic size (102 ± 0.53 nm) was observed for CuNPs that were prepared with $Cu(NO_3)_2$ (Fig. 3.3). Further, irrespective of the copper precursor used, the hydrodynamic particle size follows a monomodal distribution (Fig. 3.3), confirming the spherical morphology of the nanoparticles [Sharma et al., 2019].

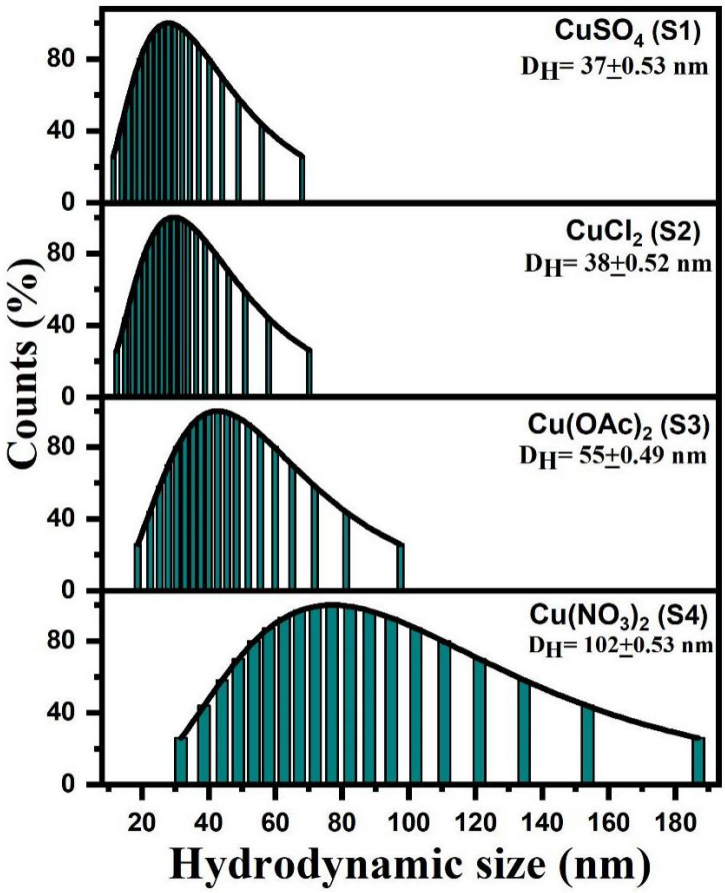

Figure 3.3 Hydrodynamic particle size distribution histograms of as-synthesized CuNPs prepared with (S1) $CuSO_4$, (S2) $CuCl_2$. $2H_2O$, (S3) $Cu(OAc)_2$, and (S4) $Cu(NO_3)_2$. Histograms were fitted with lognormal particle size distribution function.

To estimate the per batch yield of CuNPs prepared with four different copper precursors, Cu concentration of as-synthesized CuNPs colloids were measured with ICP-AES, which were reported in Table 3.1. The yield was highest for $CuCl_2$ (191.2 ± 9.5 µg/mL) followed by $CuSO_4$ (118 ± 6 µg/mL), $Cu(NO_3)_2$ (82 ± 4 µg/mL) and $Cu(OAc)_2$ (72 ± 3 µg/mL). CuNPs with stable SPR band, smallest hydrodynamic particle size and highest CuNPs yield were prepared with $CuCl_2$. Therefore, it was concluded that $CuCl_2$ was the most appropriate copper precursor for the synthesis of colloidal CuNPs.

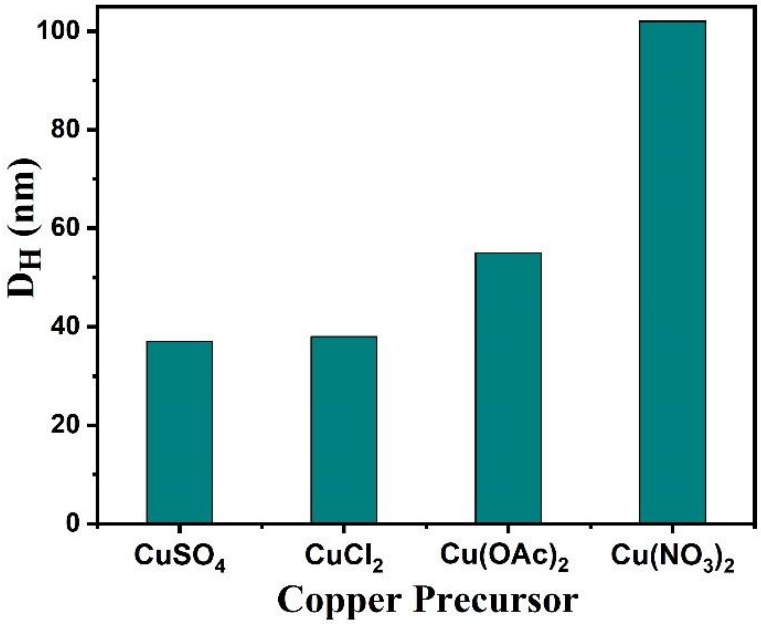

Figure 3.4 Effect of copper precursors (S1) $CuSO_4$, (S2) $CuCl_2$. $2H_2O$, (S3) $Cu(OAc)_2$ and (S4) $Cu(NO_3)_2$ on the hydrodynamic particle size of CuNPs.

3.3.2 Reaction Time

To further understand the effect of reaction time on the plasmonic properties, hydrodynamic size and yield of CuNPs, four sets (S5-S8) of CuNPs were prepared with reaction time varied from 5 to 30 min. Rest of the synthesis protocols were same as explained previously in section 3.3. $CuCl_2$ was used as copper precursor. UV-visible absorption spectra of CuNPs colloids synthesized at a reaction time 5, 10, 20 and 30 min were shown in Fig. 3.5.

SPR band positions of CuNPs colloids synthesized with 5, 10, 20, 30 min reaction time were also reported in Table 3.1. A single plasmon resonance band centered around 570 ± 10 nm was observed. This indicates that irrespective of reaction time, CuNPs with symmetric (spherical) morphology have been formed. No significant shift was observed in the plasmon resonance band positions of CuNPs colloids. This suggests that plasmonic properties of synthesized CuNPs were independent of reaction time. The SPR band centered at 570 ± 10 nm was also a characteristic signature of formation of CuNPs in Cu^0 state [Sharma et al., 2019]. If CuNPs changes their ionic state from Cu^0 to Cu^{1+}, a

significant blue shift was expected in their SPR band position [Khurana et al., 2013]. SPR band from 570 nm was expected to blue shift to 370 nm or 450 nm if Cu^0 oxidizes to Cu^{2+} (CuO) or Cu^{1+} (Cu_2O), respectively [Hu et al., 2006]. In this case also, absence of additional SPR bands at 370 and 450 nm in Fig. 3.5 indicates that the synthesized CuNPs were in their native metallic Cu^0 state.

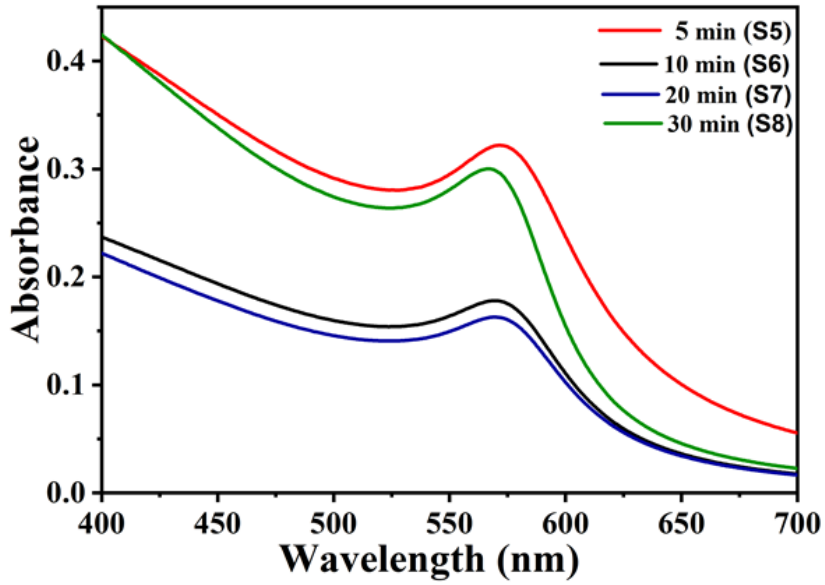

Figure 3.5 UV-visible absorption spectra of CuNPs prepared with (S5) 5 min, (S6) 10 min, (S7) 20 min and (S8) 30 min reaction time.

The size distribution histograms of CuNPs prepared with 5-30 min reaction time were shown in Fig. 3.6. Each histogram was fitted with lognormal particle size distribution function (Equation 3.1). From the fits, mean hydrodynamic sizes were determined, which were plotted as a function of reaction time in Fig. 3.7.

As observed in Fig. 3.7, when the reaction time was 5 min, the hydrodynamic size of synthesized CuNPs was 38 ± 0.52 nm and it increases to 56 ± 0.53 nm when reaction time was increased to 30 min indicating that the hydrodynamic size of CuNPs increases with the increase in reaction time. This increase in the hydrodynamic size of CuNPs might be because of the spontaneous and narrow nucleation stage followed by an extended growth stage, which has resulted in the formation of larger sized nanoparticles [Dang et al., 2011].

Yield of CuNPs colloids prepared at 5-30 min reaction time was measured in terms of Cu concentration by inductively coupled plasma atomic emission spectroscopy (ICP-AES), which was reported in Table 3.1. Irrespective of reaction time, no significant change was observed in the Cu concentration in CuNPs colloids, which indicates that entire reduction reaction was spontaneous and completed within first 5 min of reaction. The SPR band position and CuNPs yield was independent of reaction time, whereas their

hydrodynamic size depends on the reaction time. Since the hydrodynamic size was smallest for 5 min reaction time, therefore, 5 min of was chosen as the optimized reaction time for further studies.

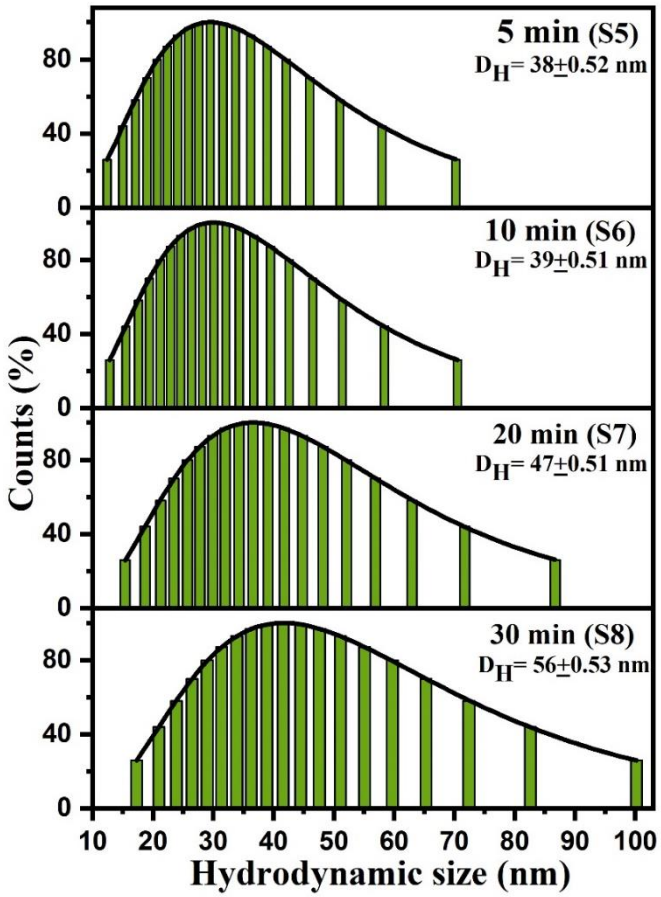

Figure 3.6 Hydrodynamic particle size distribution histograms of as-synthesized CuNPs prepared with (S5) 5 min, (S6) 10 min, (S7) 20 min and (S8) 30 min reaction time. Each histogram was fitted with lognormal particle size distribution function.

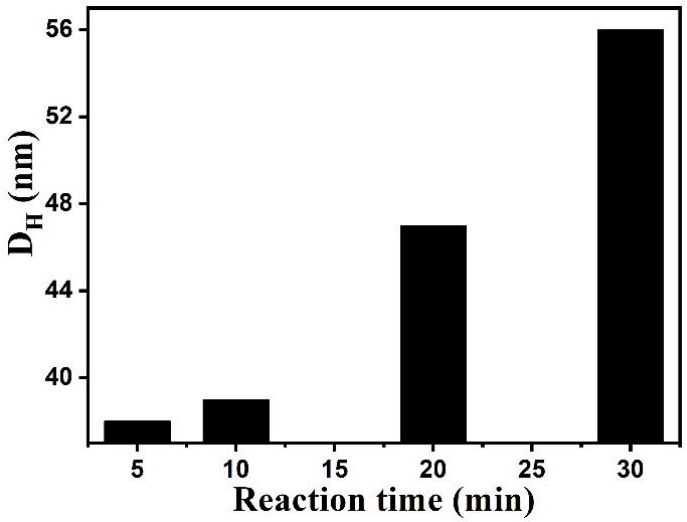

Figure 3.7 Effect of reaction time on the hydrodynamic particle size of CuNPs prepared with (S5) 5 min, (S6) 10 min, (S7) 20 min and (S8) 30 min reaction time.

3.3.3 Reaction Temperature

To investigate the effect of reaction temperature on the colloidal synthesis of CuNPs, a series of samples (S9-S13) were prepared by following identical protocols as described in section 3.3 by altering the reaction temperature from 60-100 ^{o}C. $CuCl_2$ was used as copper precursors and reaction was carried out for previously optimized reaction time of 5 min. Effect of reaction temperature on the properties of CuNPs have been investigated by measuring their plasmon resonance, hydrodynamic particle size and Cu concentration. UV-visible absorption spectra of as-synthesized CuNPs colloids prepared with 60-100 ^{o}C reaction temperature were shown in Fig. 3.8.

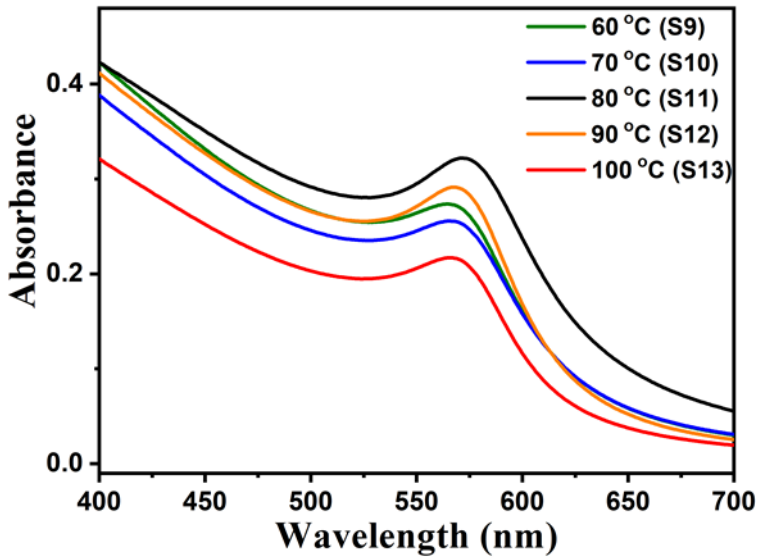

Figure 3.8 UV-visible absorption spectra of CuNPs prepared at (S9) 60 ^{o}C, (S10) 70 ^{o}C, (S11) 80 ^{o}C, (S12) 90 ^{o}C and (S13) 100 ^{o}C reaction temperature.

As observed previously, irrespective of the reaction temperature; all synthesized CuNPs colloids exhibited a single plasmon resonance band centered around 570 ± 10 nm indicating the formation of CuNPs with symmetric (spherical) morphology. No significant shift was observed in the plasmon resonance band positions of CuNPs colloids. This suggests that the plasmonic properties of synthesized CuNPs were independent of the reaction time. The SPR band positioned at 570 nm was also a characteristic signature of formation of CuNPs in Cu^0 state [Sharma et al., 2019]. If CuNPs changes their ionic state from Cu^0 to Cu^{1+} or Cu^{2+}, a significant blue shift was expected in their SPR band position [Khurana et al., 2014]. SPR band from 570 nm was expected to blue shift to 370 nm or 450 nm if Cu^0 oxidizes to Cu^{2+} (CuO) or Cu^{1+} (Cu_2O), respectively [Hu et al., 2006]. Absence of SPR bands at 370 and 450 nm in Fig. 3.8 indicates that synthesized CuNPs were in their native metallic Cu^0 state.

Hydrodynamic size of as-synthesized CuNPs colloids was measured by photon correction spectroscopy. Histograms were fitted with the lognormal particle size

distribution function (equation 3.1), from which mean hydrodynamic size was determined (Fig. 3.9). It was observed that the hydrodynamic size of CuNPs depends on the reaction temperature. Till 80°C, the hydrodynamic size of CuNPs colloids decreases with the increase in the reaction temperature. This might be because of increase in the nucleation density resulting in large number of CuNPs with smaller hydrodynamic size.

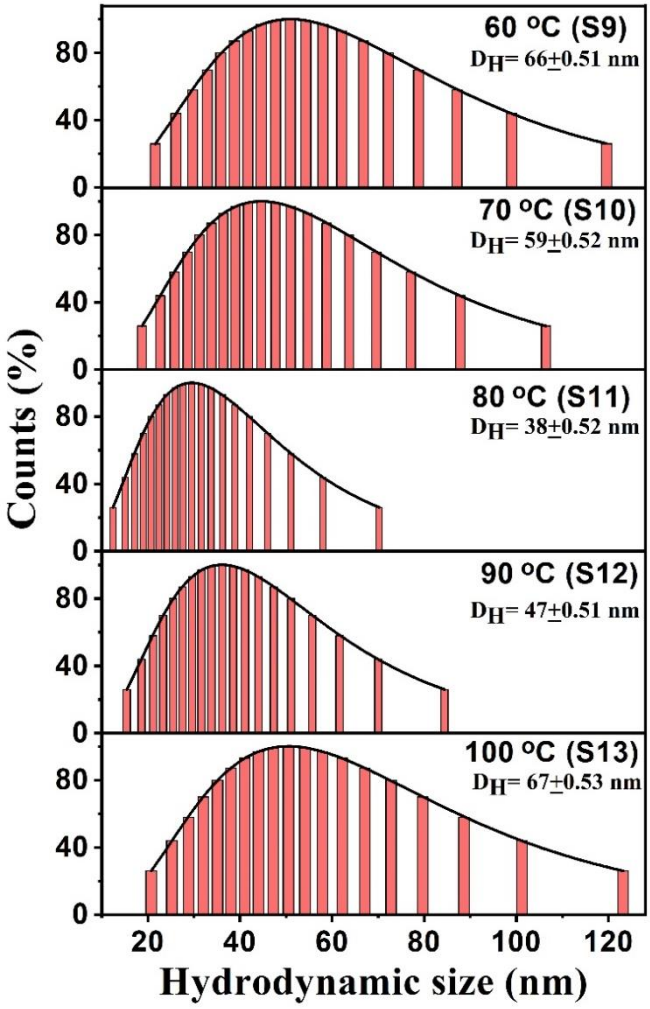

Figure 3.9 Hydrodynamic particle size distribution of as-synthesized CuNPs prepared at (S9) 60 ^{o}C, (S10) 70 ^{o}C, (S11) 80 ^{o}C, (S12) 90 ^{o}C and (S13) 100 ^{o}C reaction temperature. Histograms were fitted with lognormal particle size distribution function.

The minimum in hydrodynamic size (38 ± 0.52 nm) of CuNPs colloids was observed at 80 ^{o}C (Fig. 3.10). With further increase in the reaction temperature, the hydrodynamic size of CuNPs colloids increases. This might be because of Ostwald ripening during the growth stage that resulted in fewer numbers of nanoparticles with larger hydrodynamic sizes [Khurana et al., 2013].

To further understand the effect of reaction temperature on CuNPs yield, Cu concentration in synthesized CuNPs colloids were measured by inductively coupled plasma atomic emission spectroscopy (ICP-AES). Nanoparticle yield in terms of Cu

concentration in CuNPs colloids is reported in Table 3.1. With the increase in reaction temperature, the Cu concentration in CuNPs colloids increases, till 80 ºC. Further increase in reaction temperatures (90 °C and 100 °C) lead to the decrease in the Cu concentration in the CuNPs colloids. This might be because of an increase in the number of thermal fluctuations at higher temperature causing the redissolution of CuNPs. Based on SPR band position, smallest hydrodynamic size and highest nanoparticle yield, 80 ºC was chosen as the optimum reaction temperature and was fixed in subsequent studies. Therefore, $CuCl_2$ as copper precursor, reaction time of 5 min and reaction temperature of 80 ºC were the optimized reduction reaction conditions for the preparation of colloidal CuNPs.

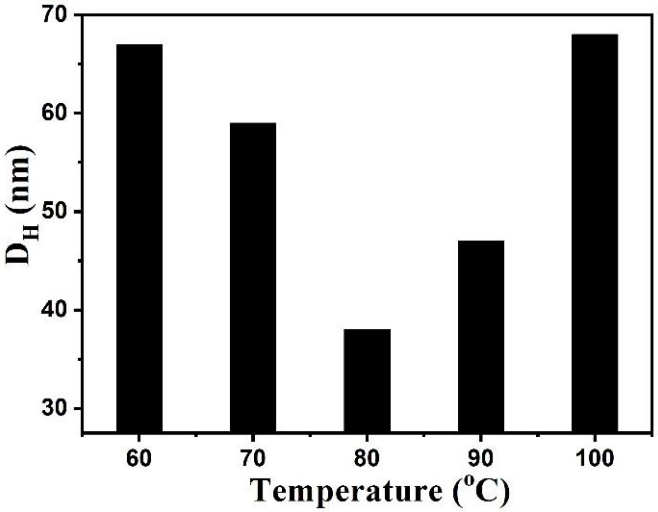

Figure 3.10 Effect of reaction temperature on the hydrodynamic particle size of CuNPs prepared at (S9) 60 ºC, (S10) 70 ºC, (S11) 80 ºC, (S12) 90 ºC and (S13) 100 ºC reaction temperature.

3.4 Development of scale-up (yield) protocol for synthesis of CuNPs

Physical and chemical properties of nanoparticles are dramatically altered when an attempt is made to increase the per batch yield of nanoparticles. It is a major challenge in nanomaterials chemistry to develop scale-up (yield) protocols for nanoparticles synthesis, which do not affect adversely on the physical and chemical properties of CuNPs. In this study, three identical sets of CuNPs with similar physical properties and hydrodynamic size were prepared by chemical reduction method with nanoparticle per batch yield 0.2 g, 0.3 g and 0.4 g. Three sets of colloidal CuNPs with target yield 0.2 g (sample A), 0.3 g (sample B) and 0.4 g (sample C) were prepared by chemical reduction method as per the protocols developed in section 3.3 [Khurana et al., 2016]. In short, 5 mM, PVP 10000 was dissolved in 25 mL warm distilled water under constant magnetic stirring. To this, requisite quantity of aqueous solution of $CuCl_2.2H_2O$ was added and heated to 80 ºC under constant magnetic stirring. 10 mM $NaBH_4$ was then added. Followed by the addition of $NaBH_4$, 10 mM ascorbic acid was also added under constant magnetic stirring at 80 °C. Reaction was allowed to proceed further for another 5 min. Color of the solution changes from black to dark red indicating the reduction of Cu^{2+} to Cu^0, which

spontaneously aggregates to form colloidal CuNPs [Khurana et al., 2016]. This colloidal dispersion of CuNPs was cooled to room temperature and centrifuged at 6000 rpm for 10 min to remove clusters of CuNPs, if any. Colloidal CuNPs were preserved at room temperature in air tight container for further analysis.

To understand the effect of per batch yield on the plasmonic properties, particle size and Cu concentration, as-synthesized CuNPs were characterized by UV-visible spectroscopy, photon correlation spectroscopy, transmission electron microscopy (TEM) and inductively coupled plasma atomic emission spectroscopy (ICP-AES). The UV-visible absorption spectra of as-synthesized CuNPs (A: 0.2 g, B: 0.3 g and C: 0.4 g yield) were shown in Fig. 3.11(a). A single plasmon resonance band centered at 570-580 nm was observed in the UV-visible spectra of CuNPs. As can be seen in Fig. 3.11(a), irrespective of the CuNPs per batch yield, their SPR band positions were similar (Table 3.2), indicating the successful scale-up of CuNPs yield from 0.2 g to 0.4 g without any significant deviation in their plasmonic properties. Presence of SPR band around 570-580 nm (Fig. 3.11(a)) was also a characteristic signature of formation of CuNPs in Cu^0 state [Sharma et al., 2019]. If CuNPs changes their ionic state from Cu^0 to Cu^{1+}, a significant blue shift was expected in their SPR band position [Hauman et al., 2011]. An SPR band from 570-580 was expected to blue shift to 370 nm if Cu^0 oxidizes to Cu^{2+} (CuO). The SPR band was expected to shift to 450 nm if Cu^0 oxidizes to Cu^{1+} (Cu_2O) [Hu et al., 2006]. Absence of any additional SPR bands around 370 and 450 nm indicated that as-synthesized CuNPs were in their native metallic Cu^0 state (Fig. 3.11(a)). Two or more SPR bands were expected in the UV-visible absorption spectra of asymmetric nanoparticles [Kaur and Chudasama, 2014]. Irrespective of nanoparticle per batch yield, single SPR band was observed in Fig. 3.11(a), which was also an indication of the formation of nanoparticles with symmetric (spherical) morphology [Kaur and Chudasama, 2014].

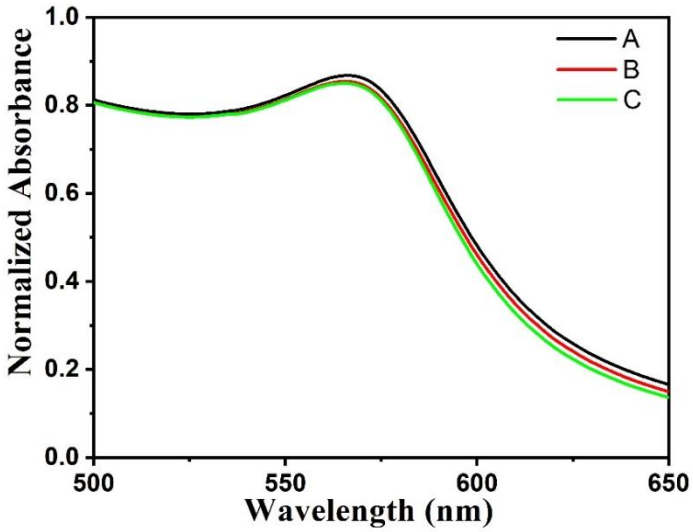

Figure 3.11(a) UV visible absorption spectra of as-synthesized CuNPs [Sample A (yield 0.2 g), B (yield 0.3 g) and C (yield 0.4 g)].

X-ray powder diffraction was used to confirm the crystallographic phase of synthesized nanoparticles. XRD patterns of as-synthesized CuNPs (sample A, B and C) were shown in Fig. 3.11(b). Diffraction peak positions observed in Fig. 3.11(b) were in good agreement with the standard diffraction pattern of FCC copper [JCPDS card No.01-085-1326]. No evidence of any of the impurity or oxide phases (CuO and Cu_2O) has been observed in the diffractograms of CuNPs confirming that as-synthesized CuNPs were in Cu^0 state. Highest intense diffraction peak (111) was fitted with pseudo-voigt peak function. From the best fit, full width half maximum (FWHM) of (111) diffraction peak was determined, which was further used to estimate the crystallite size of CuNPs by Scherrer formula [Khurana et al., 2014]. The average crystallite size of CuNPs ranges between 25.5-27.4 nm (Table 3.2). Lattice parameter (a) was also determined from Bragg's equation for each CuNPs, which was also reported in Table 3.2. The calculated value of lattice parameter (a=0.3615 nm) was in good agreement with that reported in JCPDS card No.01-085-1326.

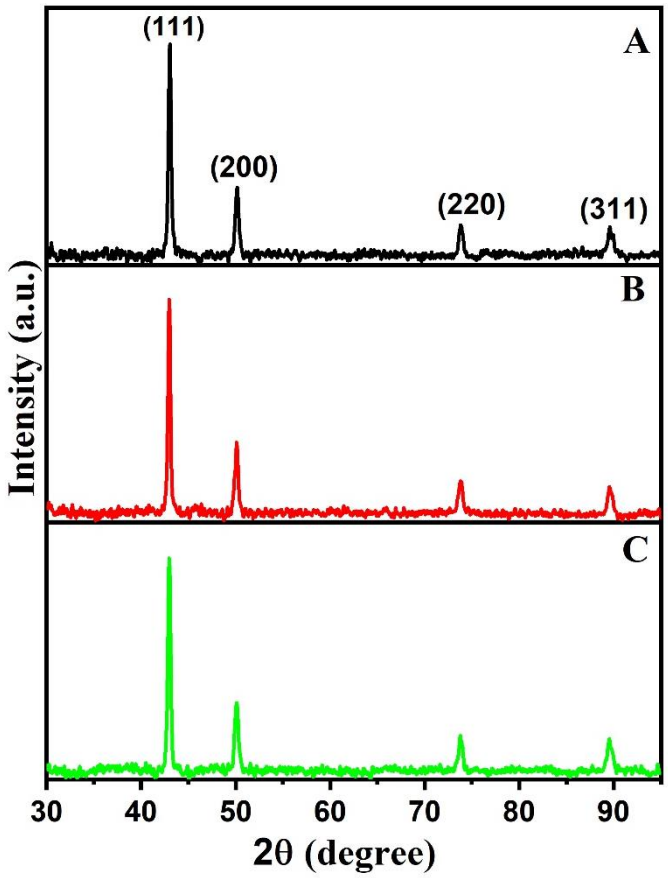

Figure 3.11 (b) X- ray diffraction patterns of CuNPs [(Sample A (yield 0.2 g), B (yield 0.3 g) and C (yield 0.4 g)]. Each pattern is in good agreement with the FCC structure of CuNPs.

Effect of per batch yield on the hydrodynamic size of CuNPs was shown in Fig. 3.12. Each histogram in Fig. 3.12 was fitted with lognormal particles size distribution function

(Equation 3.1). The mean hydrodynamic size of sample A, B and C obtained from the best fits were 11.34 nm, 12.19 nm and 13.70 nm, respectively. Irrespective of per batch yield, monomodal size distribution was observed in each histogram, which was in good agreement with the observation of single SPR band in the UV-visible spectra of CuNPs (Fig. 3.11(a)) with a possible symmetric (spherical) morphology.

Table 3.2 Important parameters of as-synthesized CuNPs [Sample A (yield 0.2 g), B (yield 0.3 g) and C (yield 0.4 g)]

Parameters	**A**	**B**	**C**
Nanoparticle Yield (g)	0.2	0.3	0.4
λ_{SPR} (nm)	568	568	568
Crystallite size (nm)	25.5	27	27.4
Lactic parameter (nm)	0.36	0.36	0.36
Hydrodynamic particle size (nm)	11.34	12.19	13.70
Physical size (nm)	9.88 ± 0.39	10.94 ± 0.95	11.49 ± 0.75
Zeta potential (mV)	-44.88 ± 0.03	-45.93 ± 0.02	-46.00 ±0.02
Cu concentration (μg/mL)	1147	1601	2873

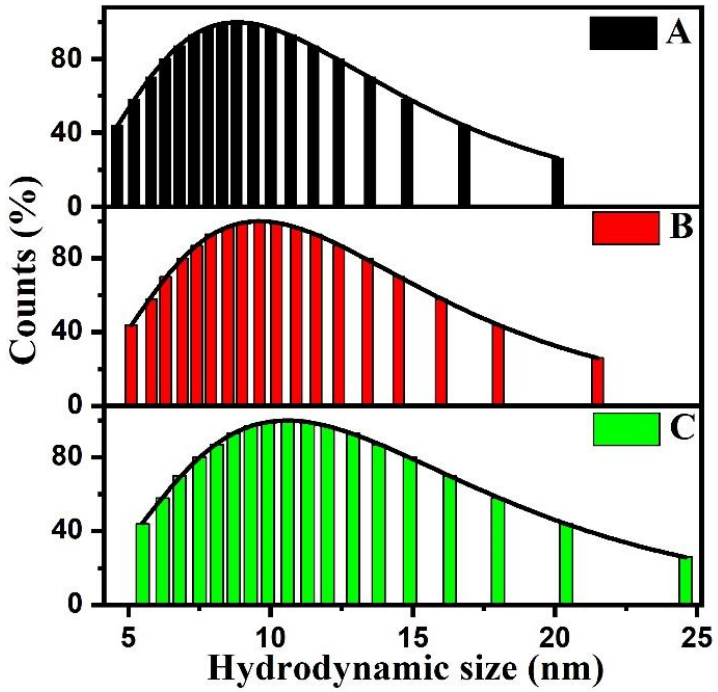

Figure 3.12 Hydrodynamic particle size distribution histograms of CuNPs [(Sample A (yield 0.2 g), B (yield 0.3 g) and C (yield 0.4 g)]. Each histogram was fitted with lognormal particle size distribution function.

To confirm the morphology of nanoparticles, transmission electron microscopy (TEM) was performed. TEM images of CuNPs (A: 0.2 g, B: 0.3 g and C: 0.4 g) are shown in Fig. 3.13.

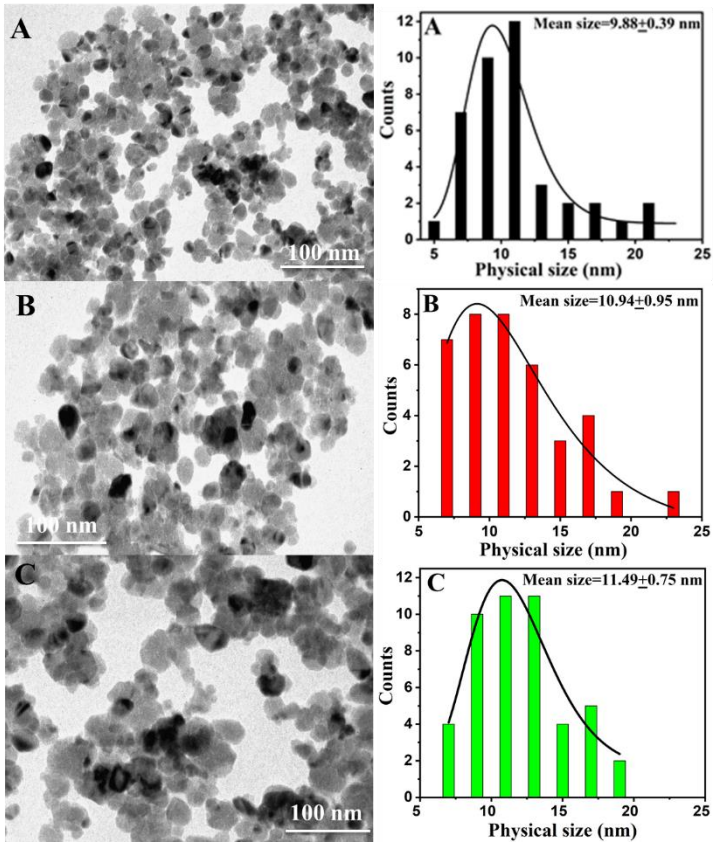

Figure 3.13 TEM micrographs and corresponding size distribution histograms of as-synthesized CuNPs [Sample A (yield 0.2 g), B (yield 0.3 g) and C (yield 0.4 g)]. Histograms were fitted with lognormal particle size distribution function.

Aggregated nanoparticles with near spherical morphology can be seen in the micrographs. Size distribution histograms prepared from TEM micrographs were fitted with lognormal particle size distribution function (Equation 3.1). From the best fits, mean physical sizes of CuNPs were determined, which were reported in Table 3.2. The physical sizes of CuNPs range between 9.88 to 11.49 nm, which were smaller than corresponding hydrodynamic particle sizes. This marked difference in two sizes was because the hydrodynamic size determined from PCS includes the size of CuNPs core and the polymeric PVP shell around it, while the physical size determined from the TEM microscopy only refers to the core size of CuNPs [Khurana et al., 2016].

Zeta potential is considered to be an important physical measure for the colloidal stability of nanoparticles, since the magnitude of the zeta potential determines the extent of the electrostatic repulsion between the same species constituting the colloid [Mohameed, 2020]. Zeta potential of as-synthesized CuNPs was determined from electrophoretic mobility measured by the phase angle light scattering (PALS). In this technique, Doppler shift of scattered laser beam from the sample was measured at constant potential applied across the metal electrodes. From the best fit of the phase shift using Smoluchowksy algorithm, the electrophoretic mobility of the nanoparticles was determined and from this the zeta potential was calculated. Raw data of phase shift in

CuNPs from which the zeta potential of CuNPs was calculated was in Fig. 3.14.

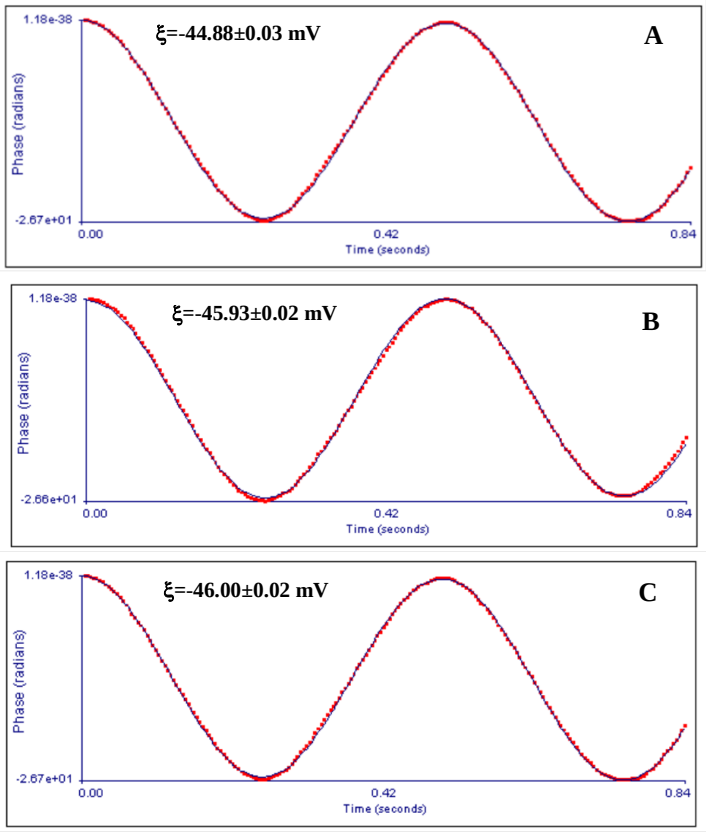

Figure 3.14 Time dependence of phase angle of CuNPs [Sample A (yield 0.2 g), B (yield 0.3 g) and C (yield 0.4 g)]. From the fits, electrophoretic mobility was determined from which the zeta potential (ξ) of CuNPs was calculated.

Zeta potential of as-synthesized CuNPs was -44.88±0.03 mV (sample A), -45.93±0.02 mV (sample B) and 46.00±0.02 mV (sample C). For all the three CuNPs samples, the zeta potential lies between -44.88 mV to -46.00 mV. Any colloid having its zeta potential ≥ ± 30 mV is being considered to be stable [Mohameed, 2020]. Therefore, it was concluded that the as-synthesized CuNPs (Sample A, B and C) colloids exhibited good colloidal stability.

Concentration of Cu in CuNPs colloids was also determined by ICP-AES measurements. As the nanoparticle yield was increased from 0.2 to 0.4 g, Cu concentration in CuNPs colloids increases from 1147 µg/mL to 2873 µg/mL (Table 3.2). This was in good agreement with expected per batch yield.

3.5 Colloidal stability of CuNPs

Stability of CuNPs towards oxidation and aggregation is very important. CuNPs have tendency to aggregate and oxidize to CuO or Cu_2O. To monitor the effect of the aging on the colloidal stability of CuNPs against oxidation and aggregation, UV-visible and photon correlation spectroscopy was used. Colloidal stability of nanoparticles (sample A, B and

C) was evaluated in terms of changes in the hydrodynamic size (D_H) of CuNPs and its influence on the plasmon resonance band (λ_{SPR} and A_{max}). With aging a gradual red shift in the SPR band position was observed indicating a possible aggregation of nanoparticles (Fig. 3.15) [Xiong et al., 2011]. Irrespective of CuNPs yield, the overall change in the λ_{SPR} for an ageing period of 180 days was less than 2 % indicating the impressive colloidal stability of nanoparticles. A gradual decrease in the A_{max} of CuNPs with ageing was also observed (Fig. 3.16). This might be because of increase in the hydrodynamic size of CuNPs caused by aggregation of nanoparticles.

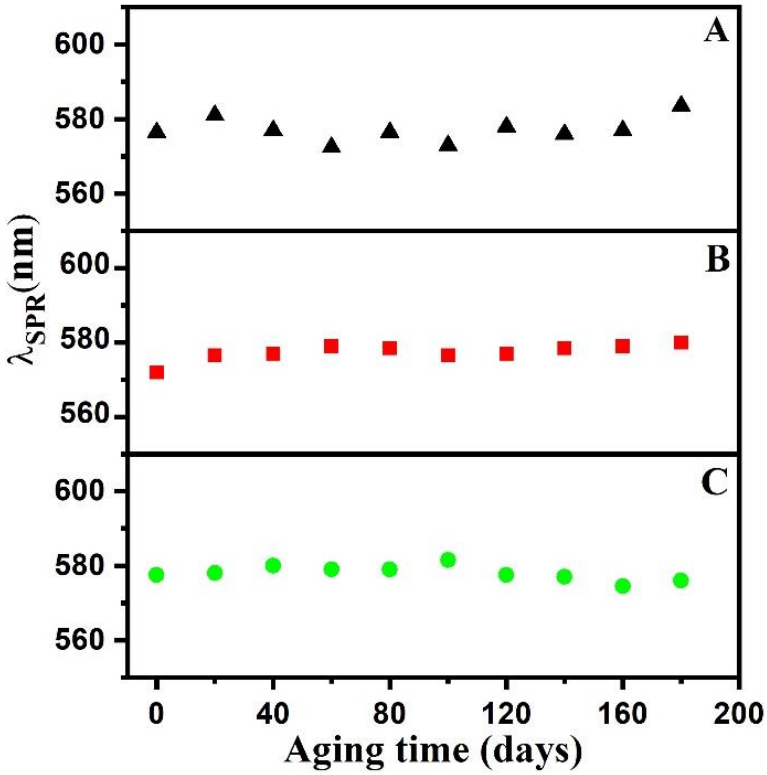

Figure 3.15 Effect of aging on the position of SPR (λ_{SPR}) band of CuNPs [Sample A (yield 0.2 g), B (yield 0.3 g) and C (yield 0.4 g)].

Hydrodynamic particle size was also measured at periodic intervals of 20 days. The plot of mean hydrodynamic size of CuNPs as a function of aging time was shown in Fig. 3.17. Each curve in Fig. 3.17 was fitted with the following equation:

$$D_H(t) = D_{H0} \exp (t/\tau) \qquad (3.2)$$

where $D_H(t)$ was the hydrodynamic particle size of the colloids measured after the ageing for time t, D_{H0} was the hydrodynamic particle size at t = 0 day and τ was the shelf life of the colloid.

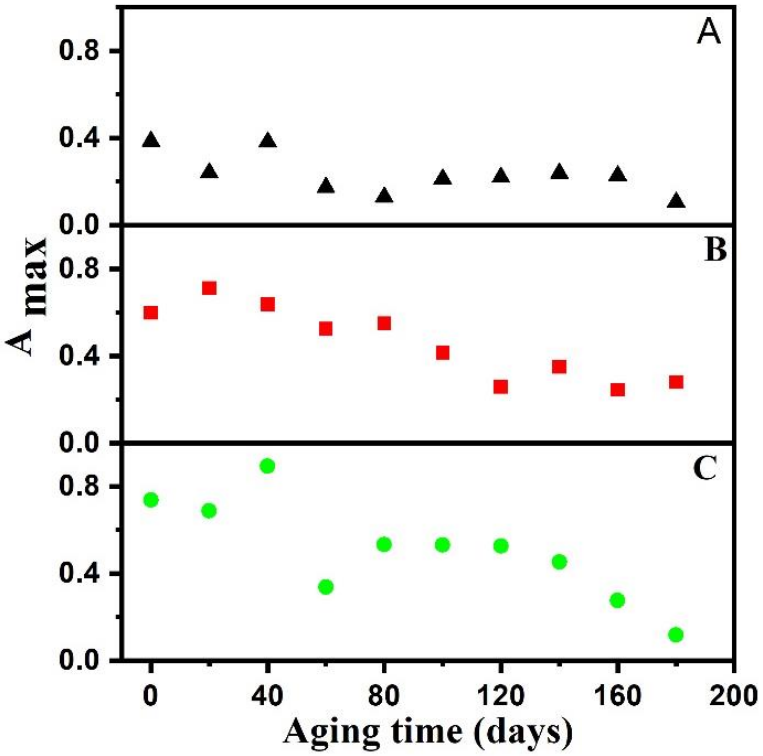

Figure 3.16 Effect of aging on the absorption maximum (A_{max}) of SPR of CuNPs [Sample A (yield 0.2 g), B (yield 0.3 g) and C (yield 0.4 g)].

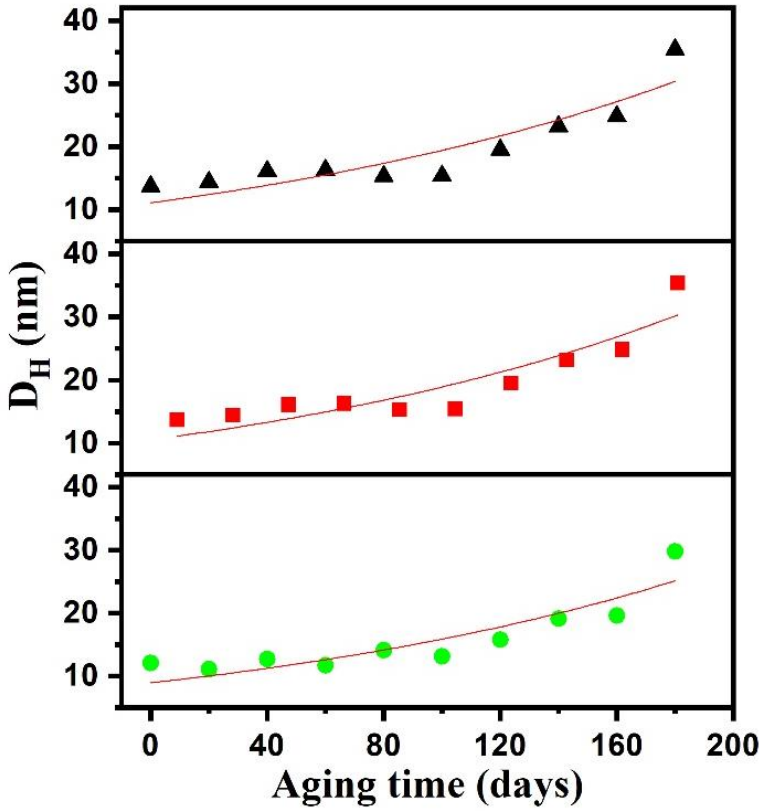

Figure 3.17 Effect of aging on the hydrodynamic particle size of CuNPs [Sample A (yield 0.2 g), B (yield 0.3 g) and C (yield 0.4 g)].

From these fits, the shelf life of CuNPs samples A, B and C were determined, which were 179, 179 and 174 days, respectively. As evident from Fig. 3.17, irrespective of per batch yield of CuNPs, their hydrodynamic particle size increases with ageing. This might be because of the cluster formation in the dispersion caused by desorption of the protective layer of surfactant from the surface of nanoparticles [Khurana et al., 2016]. Colloids lose their dispersion stability and plasmonic properties beyond 180 days.

Copper nanoparticles (CuNPs) used in the present study were synthesized by chemical reduction of copper chloride under the mild reaction condition by using a unique combination of reducing agents (sodium borohydride, L-ascorbic acid) and polyvinylpyrrolidone (PVP) as stabilizer. In addition to strong reducing agent ($NaBH_4$), an excess secondary weak reducing agent (L-ascorbic acid) used in the reduction reaction simulates a dynamic equilibrium around CuNPs, which minimizes their oxidation by reducing any oxidised Cu^{1+} ions back to Cu^0 [Khurana et al., 2016]. Thus, as-synthesized CuNPs remain protected in their native metallic (Cu^0) phase by the capping of L-ascorbic acid over 180 days.

3.6 Conclusion

Colloidal CuNPs when prepared by chemical reduction method exhibited strong dependence on the source of copper precursor, the reaction time and the reaction temperature. $CuCl_2$ as copper precursor, reaction time of 5 min and reaction temperature of 80 °C were the optimized synthesis parameters. Without affecting adversely on the physical and plasmonic properties of CuNPs, scale-up protocols have been developed to increase CuNPs yield from 0.2 g to 0.4 g. The shelf-life of synthesized CuNPs colloids was ≈ 180 days, beyond which CuNPs lose their colloidal stability and plasmonic properties.

CHAPTER 4

Objective 3 (a) *In vitro* evaluation of Antibacterial activity of Copper nanoparticles

Despite several reports on antibacterial activities of CuNPs, no attempts have been made so far to understand the effect of per batch yield of CuNPs on their antibacterial and cytotoxicity. In this chapter, *in vitro* study on antibacterial activity of as-synthesized CuNPs (sample A, B and C) was performed on two pathogenic bacteria [*Escherichia coli* (MTCC No. 739), *Proteus vulgaris* (MTCC No. 426)] and ecotoxicity on two soil bacteria [*Bacillus subtilis* (MTCC No. 441) and *Pseudomonas fluorescens* (MTCC No. 1749)]. Antibacterial activities were measured in terms of minimum inhibitory concentration (MIC) and the minimum bactericidal concentration (MBC). An insight into interaction of nanoparticle with bacterial cultures and the possible underlying mechanism responsible for the observed antibacterial activities were evaluated by estimating cytoplasmic (sugars and proteins) leakage and reactive oxygen species (ROS) generation. Synergistic effect of CuNPs on antibacterial activities of conventional antibiotics (tetracycline, kanamycin, ampicillin and streptomycin) was also studied.

4.1 Material and bacterial cultures

Antibacterial activities of as-synthesized CuNPs, Sample A (yield = 0.2 g), Sample B (yield = 0.3 g) and Sample C (Yield = 0.4 g) were tested. *Escherichia coli* (MTCC No. 739), *Proteus vulgaris* (MTCC No. 426), *Bacillus subtilis* (MTCC No. 441) and *Pseudomonas fluorescens* (MTCC No. 1749) bacterial cultures were procured from Institute of Microbial Technology (IMTECH), Chandigarh, India. Nutrient agar and nutrient broth were purchased from Himedia. 2, 7-dichloroflurorescin diacetate (DCFH-DA), DNS (dinitrosalicylic acid), antibiotics tetracycline, kanamycin, ampicillin and streptomycin were purchased from Himedia. All aqueous solutions were prepared in sterilized Milli-Q ultrapure water (R = 18.2 MΩ). Optical density (OD) was measured on Shimadzu UV-2600 spectrophotometer at room temperature. Amount of reactive oxygen species (ROS) produced in bacterial cultures was measured by fluorescence spectroscopy. Carry Eclipse fluorescence spectrophotometer was used for the fluorescence measurement. Fluorescence was measured at an emission wavelength of 520 nm and excitation wavelength was (λ_{ex}) 485 nm.

4.2 MIC and MBC of CuNPs

Minimum inhibitory concentration (MIC) and minimum bactericidal concentration (MBC) of as-synthesized CuNPs were determined from standard micro-dilution method by following the protocols recommended by national committee of clinical laboratory standards, 2005 (NCCLS) with few modifications [Mirajani et al., 2011]. Strains under

tests were grown to 0.5 McFarland standard turbidity (10^8 cfu/mL) [Ansani et al., 2011]. For the determination of MIC, it was diluted to 10^4 cfu/mL in nutrient broth. Twelve sets of test tubes with 10 mL nutrient broth media containing CuNPs in requisite concentration (sample A - 50 to 90 µg/mL, sample B - 50 to 100 µg/mL and sample C - 20 to 100 µg/mL for *E.coli* and *P. vulgaris* and sample A - 20 to 50 µg/mL, sample B - 20 to 100 µg/mL and sample C - 40 to 70 µg/mL for *B. subtilis* and *P. fluorescens*) were inoculated with 10^4 cfu/mL of respective strain for 24 h at 37 °C for *E.coli*, *P. vulgaris*, *Bacillus subtilis* and at 30 °C for *P. fluorescens*. MIC of CuNPs was determined for each strain by measuring their optical density (OD) at 600 nm. The bacterial cultures without the treatment of CuNPs were used as a control. All experiments were done in triplicates.

To determine MBC, 50 µL aliquots from each test tube used for the determination of MIC was spread on the nutrient agar plates and incubated for 24 h at 37 °C for *E. coli*, *P. vulgaris*, *B. subtilis* and at 30 °C for *P. fluorescens* to check the growth or no growth of organisms [Ansani et al., 2011]. MIC is the lowest concentration of any antimicrobial agent that visually inhibits 99% bacterial growth; whereas MBC is the concentration of antibacterial agent corresponding to which 100 % bacterial growth inhibition is observed. Test results were reported in Table 4.1. Visual representation of MIC and MBC tests of tested bacterial strains are presented in Fig. 4.1 (*E.coli*), Fig. 4.2 (*P. vulgaris*), Fig. 4.3 (*B. subtilis*) and Fig. 4.4 (*P. fluorescens*).

Table 4.1 MIC and MBC (µg/mL) of as-synthesized CuNPs [Sample A (yield 0.2 g), B (yield 0.3 g) and C (yield 0.4 g)] against *E. coli*, *P. vulgaris*, *B. subtilis* and *P. fluorescens* as deduced from visual data presented in Figures (4.1, 4.2, 4.3 and 4.4)

CuNPs	**Strains**							
	E. coli		*P. vulgaris*		*B. subtilis*		*P. fluorescens*	
	MIC (µg/mL)	MBC (µg/mL)	MIC (µg/mL)	MBC (µg/mL)	MIC (µg/mL)	MBC (µg/mL)	MIC (µg/mL)	MBC (µg/mL)
A	65	70	70	75	35	40	35	40
B	80	100	60	70	40	60	40	45
C	90	100	75	80	60	70	55	60

Irrespective of CuNPs yield, all tested samples showed antibacterial activities against both pathogenic and soil microbes. Regardless of the strains both the MIC and the MBC values increase with an increase in the CuNPs yield (sample A $\rightarrow$ C), indicating that strains were more sensitive to sample A and least sensitive to sample C. This might be because of the smaller hydrodynamic size of sample A. Amongst the three CuNPs, the hydrodynamic size of sample A was smallest (11.34 nm) followed by sample B (12.19 nm) and sample C (13.70 nm) (Table 3.2). For CuNPs sample A (yield 0.2 g), the MIC

values for *E. coli* and *P. vulgaris* were nearly identical, which were 65 µg/mL, 70 µg/mL, respectively. Their MBC values were 70 µg/mL and 75 µg/mL, respectively. This indicates that Sample A of CuNPs imparts similar antibacterial activity on both the Gram-negative pathogenic strains. In contrast to this, CuNPs of sample B (yield 0.3 g) and sample C (yield 0.4 g) show higher sensitivity towards *P. vulgaris.* Both MIC and MBC values (Table 4.1) for *E. coli* were higher as compared to *P. vulgaris* indicating the higher sensitivity of CuNPs towards *P. vulgaris.* Similar results were obtained by Manayasree et al., 2017 and Dhanalakshmi et al., 2018 against *E. coli* and *P. vulgaris* (Gram-negative bacteria), where the MIC values of *E. coli* was higher than *P. vulgaris*. The difference in the MIC values of two Gram-negative strains *might* be because of differences in their species and difference in modes of actions of CuNPs in two strains [Chouhan et al., 2017; Slavin et al., 2017].

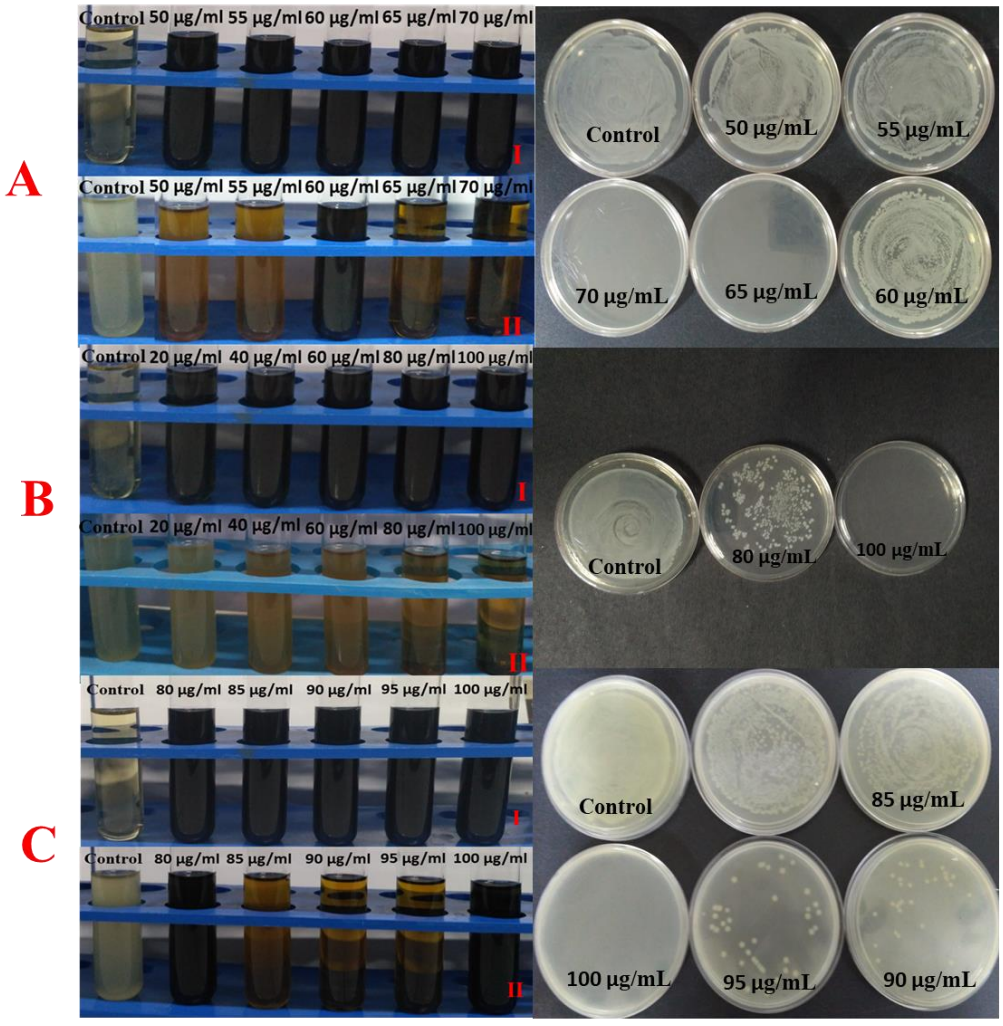

Figure 4.1 Visual observation of MIC and MBC (I - before incubation and II - after incubation) of *E. coli* in presence of different concentrations of CuNPs [Sample A (yield 0.2 g), B (yield 0.3 g) and C (yield 0.4 g)].

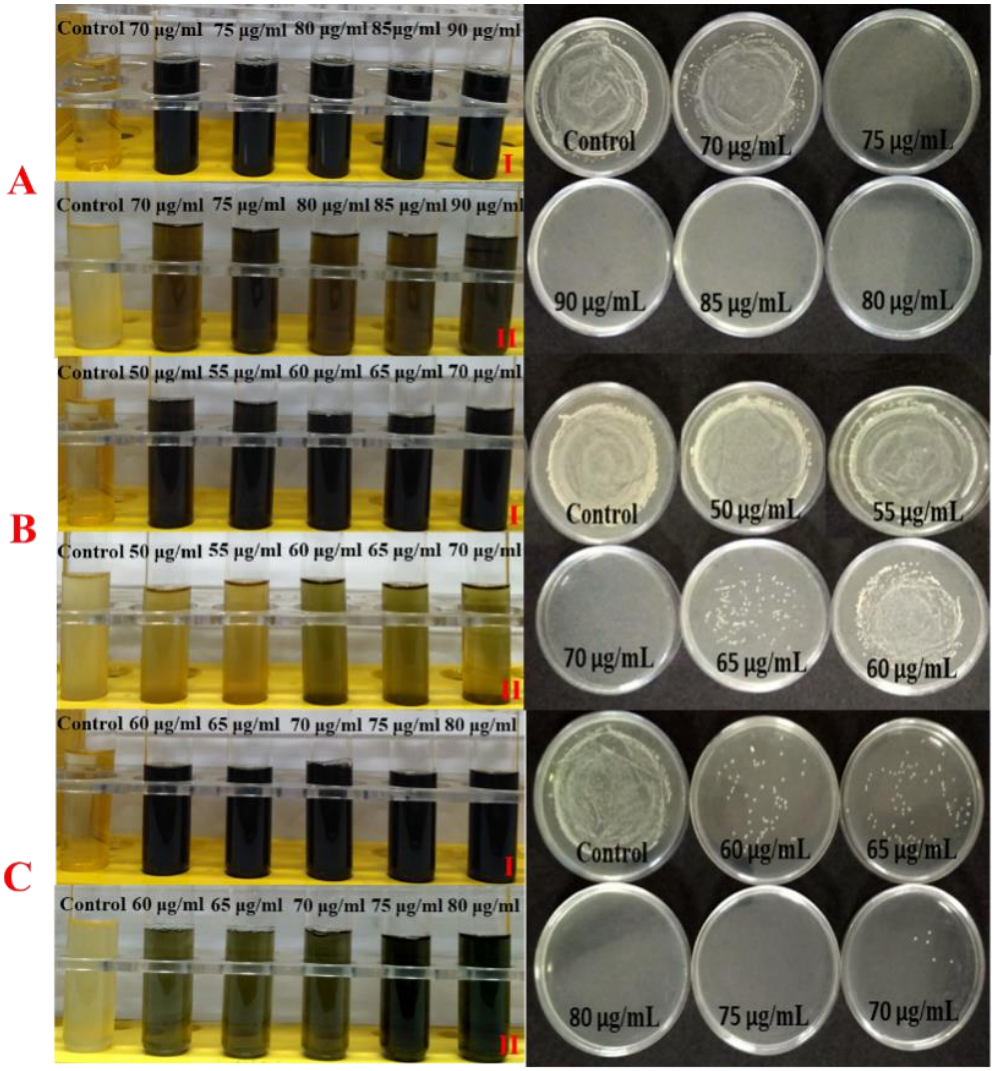

Figure 4.2 Visual observation of MIC and MBC (I - before incubation and II - after incubation) of *P. vulgaris* in presence of different concentrations of CuNPs [Sample A (yield 0.2 g), B (yield 0.3 g) and C (yield 0.4 g)].

In case of soil bacteria, the MIC and MBC values of Sample A (yield 0.2 g) of CuNPs for both the soil bacteria (*B. subtilis* and *P. fluorescens*) were also identical. This indicates that Sample A of CuNPs imparts identical ecotoxicity on both the tested microorganisms irrespective of whether the tested strain is Gram-positive or Gram-negative. In contrast to this, CuNPs of sample B and sample C exhibits little higher toxicity on Gram-negative *P. fluorescens* as compared to Gram-positive *B. subtilis*. This might be because of difference in the bacterial cell membrane wall structure and its composition. Gram-positive bacteria have thick peptidoglycan layer (20-30 nm) and linear polysaccharides chains cross linked by short peptides that make their cell walls rigid and difficult to penetrate by the nanoparticles; where as in Gram-negative bacteria cell walls are made up of thin layer of peptidoglycan (8-12 nm) and a layer of lipopolysaccharides. They lack the strength and rigidity which make them more susceptible to nanoparticles [Fayaz et al., 2010].

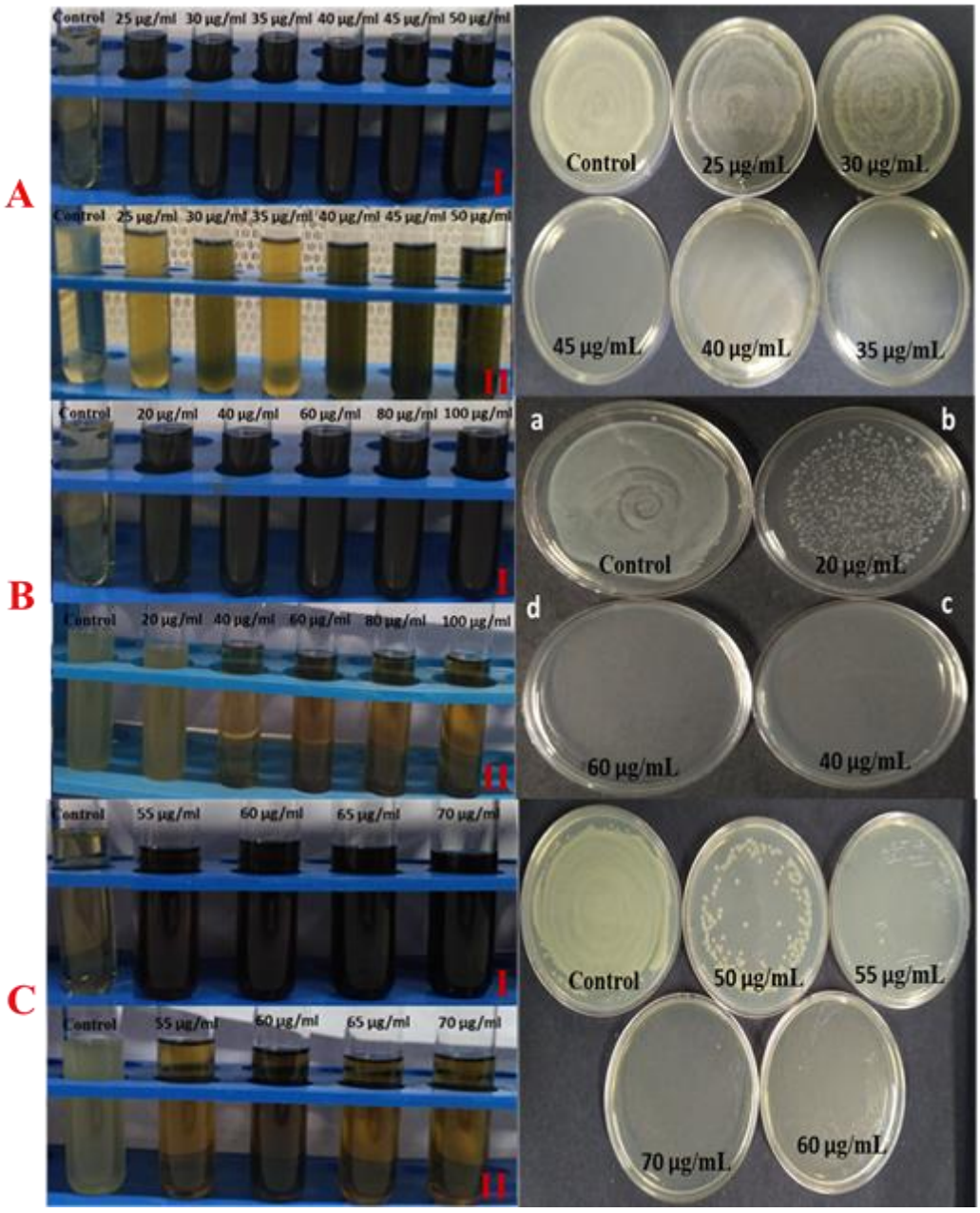

Figure 4.3 Visual observation of MIC and MBC (I - before incubation and II - after incubation) of *B. subtilis* in presence of different concentrations of CuNPs [Sample A (yield 0.2 g), B (yield 0.3 g) and C (yield 0.4 g)].

Because of this difference in the cell wall thickness in two strains penetration of nanoparticles and subsequent interaction was more pronounced in Gram-negative strain (*P. fluorescens*) [Fayaz et al., 2010]. Similar results were reported by Yerukala and Bokka, 2018. Other possible antibacterial mechanism involves leaching of Cu^{2+} ions from nanoparticles, which easily gets absorbed on bacterial cell membrane and damages it by altering their enzyme functions or by solidifying proteins [Raffi et al., 2010; Slavin et al., 2017]. The cell wall of Gram-negative bacteria is made-up of polysaccharides and the negative charge groups such as phosphate, carboxylate, hydroxyl, amine and sulfhydryl

that plays role as membrane active sites [Vinopal et al., 2007]. The copper ions released from CuNPs have grater affinity towards these groups leading to alteration of membrane proteins, electron transport chain and inhibition of cytochromes of Gram-negative cell membrane [Orell et al., 2010]. The MIC and MBC values of CuNPs for soil microbes were low as compared to the pathogenic bacteria. This observation showed that irrespective of yield and hydrodynamic size of CuNPs, soil microbes were more susceptible to CuNPs as compared to pathogenic bacteria.

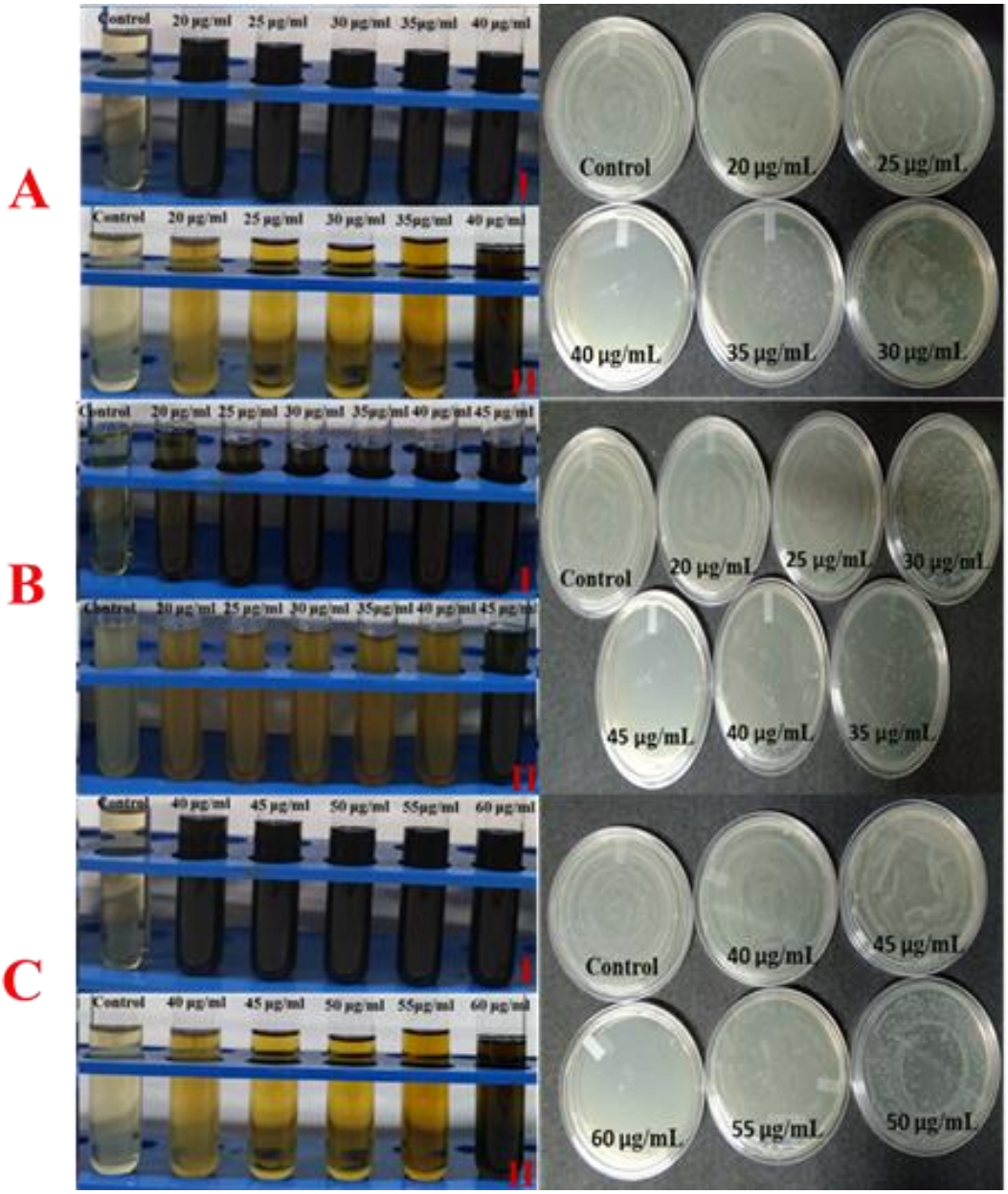

Figure 4.4 Visual observation of MIC and MBC (I - before incubation and II - after incubation) of *P. fluorescens* in presence of different concentrations of CuNPs [Sample A (yield 0.2 g), B (yield 0.3 g) and C (yield 0.4 g)].

4.3 Effect of CuNPs on Growth of bacteria and Cytoplasmic leakage of sugars and proteins

Effect of CuNPs on bacterial growth was studied by following the protocols developed by Ruparelia et al., 2008. Overnight grown culture (OD = 0.01; 10^8cfu/mL) was used to examine the growth pattern of bacteria in broth [Ruparelia et al., 2008; Alshareef et al., 2017]. In each flask containing 50 mL nutrient broth 1 % inoculum was added with requisite concentrations of CuNPs (sample A, B and C). Growth kinetics was studied for four concentrations (two below MIC, one at MIC and one above MIC) for each CuNPs samples. For each bacteria (*E. coli*, *P. vulgaris*, *B. subtilis* and *P. fluorescens*), these concentrations are listed in Table 4.2. Following this, each flask was incubated at 37 °C for *E. coli*, *P. vulgaris* and *B. subtilis* and at 30 °C for *P. fluorescens*. The growth was determined by recording the OD at 600 nm at an interval of 1 h for 0 - 10 h. For reference, the growth kinetics of positive (bacterial culture + media) and negative (media + CuNPs) controls were also studied. The measured OD values were corrected with corresponding negative controls. ODs of CuNPs treated strains were corrected by subtracting the corresponding ODs of negative controls (having equal CuNPs concentration). Each experiment was performed in triplicates. The dynamics of growth was monitored in the presence of CuNPs (sample A, B and C), which was shown in Fig. 4.5 (*E. coli* and *P. vulgaris*) and Fig. 4.6 (*B. subtilis* and *P. fluorescens*). The controls showed normal growth while alterations were observed in the growth patterns of CuNPs treated strains.

Table 4.2 Concentration of CuNPs [Sample A (yield 0.2 g), B (yield 0.3 g) and C (yield 0.4 g)] used in the study of effect of CuNPs on the growth of *E. coli, P. vulgaris, B. subtilis and P. fluorescens*

Bacteria	CuNPs (µg/mL)		
	Sample A	**Sample B**	**Sample C**
E. coli	20, 40, 60, 80	30, 60, 90, 120	40, 60, 80, 100
P. vulgaris	20, 40, 60, 80	20, 40, 60, 80	40, 50, 60, 70, 80
B. subtilis	10, 20, 30, 40	10, 30, 50, 70	20, 40, 60, 80
P. fluorescens	15, 25, 35, 45	20, 30, 40, 50	25, 40, 55, 65

With increase in CuNPs concentration, the bacterial growth declined. In CuNPs treated strains below their MICs, the growth rates were not hindered much. In strains treated with CuNPs with MIC as their concentrations, the growth rate was inhibited significantly. With reference to controls, ≈ 80 % decline in the test bacteria were observed after 7 - 8 h. In strains treated with CuNPs with MBC as their concentrations, the bacterial growth was completely inhibited (Fig. 4.5 and Fig. 4.6). CuNPs exhibited concentration dependent antibacterial activities.

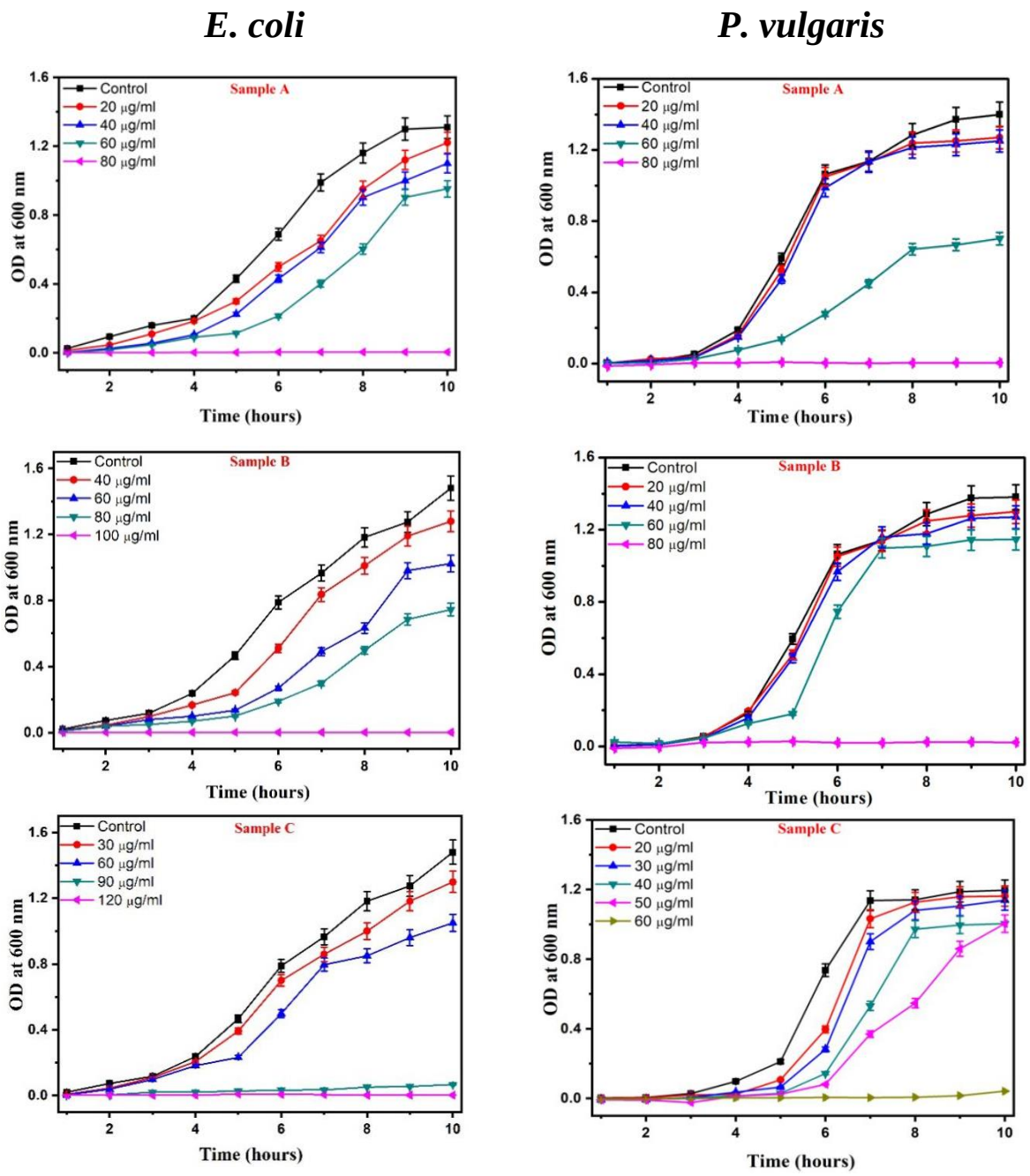

Figure 4.5 Effect of CuNPs [Sample A (yield 0.2 g), B (yield 0.3 g) and C (yield 0.4 g)] on growth of *E. coli* and *P. vulgaris.* Each point on curve was average of three replicates and *error bars* represents standard deviation.

At low concentrations, CuNPs act as micro nutrient essential for cell metabolism, a cofactor in multiple proteins; takes part in redox reactions such as electron transport and oxidative respiration [Samanovic et al., 2012; Tokeer et al., 2013]. While at higher concentrations, excess of Cu induces severe toxicity by multiple pathways [Arguello et al., 2013].

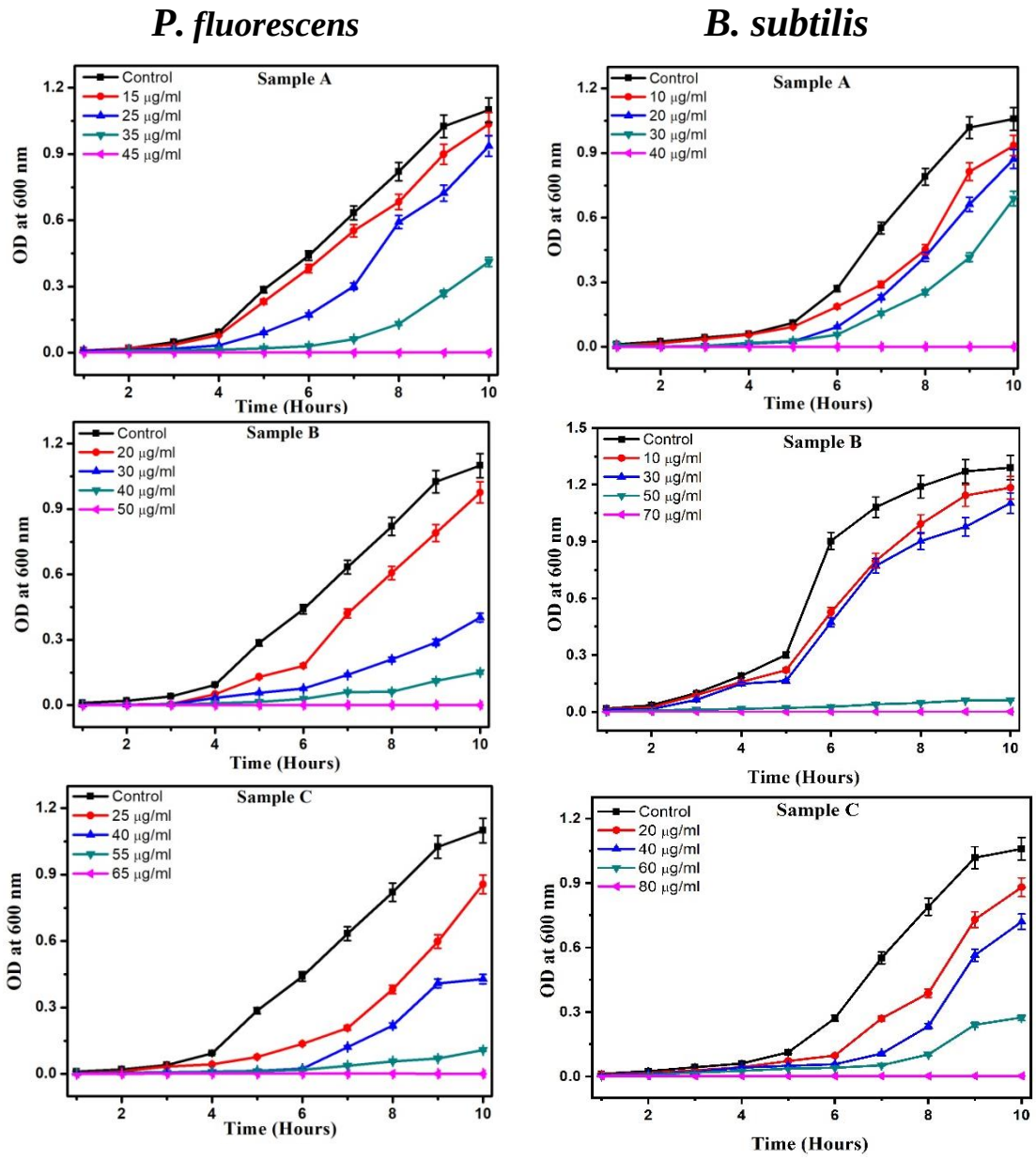

Figure 4.6 Effect of CuNPs [Sample A (yield 0.2 g), B (yield 0.3 g) and C (yield 0.4 g)] on growth of *B. subtilis* and *P. fluorescens.* Each point on curve was average of three replicates and *error bars* represents standard deviation.

4.3.1 Effect of CuNPs on sugar and protein leakage by bacterial cells

Determination of cytoplasmic leakage is one of the methods used to study the effect of nanoparticles on metabolic activities of bacteria [Yuan et al., 2017]. To check the effect of CuNPs on metabolic activities of *E. coli, P. vulgaris, B. subtilis and P. fluorescens*, cytoplasmic leakage of intracellular macromolecules such as sugars and proteins was studied by DNS (dinitrosalicylic acid) and Folin-Lowry method respectively.

Sugar Leakage

Bursting of bacterial cells releases their intracellular materials like sugars and proteins. DNS (dinitrosalicylic acid) method was used to estimate the leakage of reducing sugars from bacterial cultures [Miller, 1959; Fellahi et al., 2013]. Five sets of test tubes with 10 mL nutrient broth media containing CuNPs in requisite concentrations (40-100 µg/mL for *E. coli,* 30-80 µg/mL for *P. vulgaris,* 10-70 µg/mL for *B. subtilis* and 20-60 µg/mL for *P. fluorescens*) were inoculated with 10^7 cfu/mL of respective strain for 24 h at 37 °C for *E.coli*, *P. vulgaris*, *B. subtilis* and at 30 °C for *P. fluorescens*. Tubes incubated without CuNPs were treated as controls. After incubation, they were centrifuged at 12,000 rpm at 4 °C for 30 min and immediately frozen at -20 °C for further analysis. 1 mL supernatant from each tube was taken and 3 mL DNS (3,5-dintrosalicycline acid) reagent was added into it. Tubes were then heated at 90 °C for 15 min. After cooling, OD was measured at 540 nm. A standard curve of glucose was used for estimation of leakage of reducing sugar from test samples [Miller, 1959; Fellahi et al., 2013]. Bacterial cultures without CuNPs treatment were used as controls. Each experiment was performed in triplicates.

Protein Leakage

Folin-Lowry method was used to estimate the protein leakage from the bacterial strains treated with CuNPs [Lowry et al., 1951; Rajesh et al., 2014]. Five sets of test tubes with 10 mL nutrient broth media containing CuNPs in requisite concentrations (40-100 µg/mL for *E. coli,* 30-80 µg/mL for *P. vulgaris,* 10-70 µg/mL for *B. subtilis* and 20-60 µg/mL for *P. fluorescens*) were inoculated with 10^7 cfu/mL of respective strain for 24 h at 37 °C for *E.coli*, *P. vulgaris*, *Bacillus subtilis* and at 30 °C for *P. fluorescens*. Tubes incubated without CuNPs were treated as controls. After incubation, they were centrifuged at 12,000 rpm at 4 °C for 30 min and immediately frozen at -20 °C for further analysis. 1 mL supernatant from each test tube was taken and 5 mL Folin-Lowry reagent [Lowry et al., 1951] was added into it. OD was measured at 660 nm. Experiments were performed in triplicates. A standard curve of bovine serum albumin (BSA) was used to estimate the protein. Bacterial cultures without treatment with CuNPs were used as controls.

Concentration dependence of cytoplasmic leakage in CuNPs (Sample A, B and C) treated cultures were shown in Fig. 4.7 (*E. coli* and *P. vulgaris*) and Fig. 4.8 (*B. subtilis* and *P. fluorescens*). Cytoplasmic leakage was minimum in cultures not treated with CuNPs (controls). Irrespective of strains or nanoparticles, an increase in the leakage of sugars and proteins was observed with the increase in CuNPs concentrations. Both in controls and CuNPs treated cultures, the cytoplasmic leakages were higher in *E. coli* as compared to *P. vulgaris.* The outer membrane of *E. coli* is predominantly constructed from tightly packed lipopolysaccharide (LPS) molecules, which act as an effective permeability barrier for nanoparticles [Sondi and Sondi, 2004]. Tamayo et al., 2015 proposed the bacteriolytic mode (cell wall lysis) of action by copper ions by alternating

the semipermeable property of membrane leaving the bacterial cells incapable of regulating transport through the plasma membrane causing cell lysis and release of cytoplasmic materials outside the membrane [Tamayo et al., 2015]. Therefore, *E. coli* allows greater transport of copper ions towards plasma membrane increases its permeability and induces higher cytoplasmic leakages [Manayasree et al., 2017].

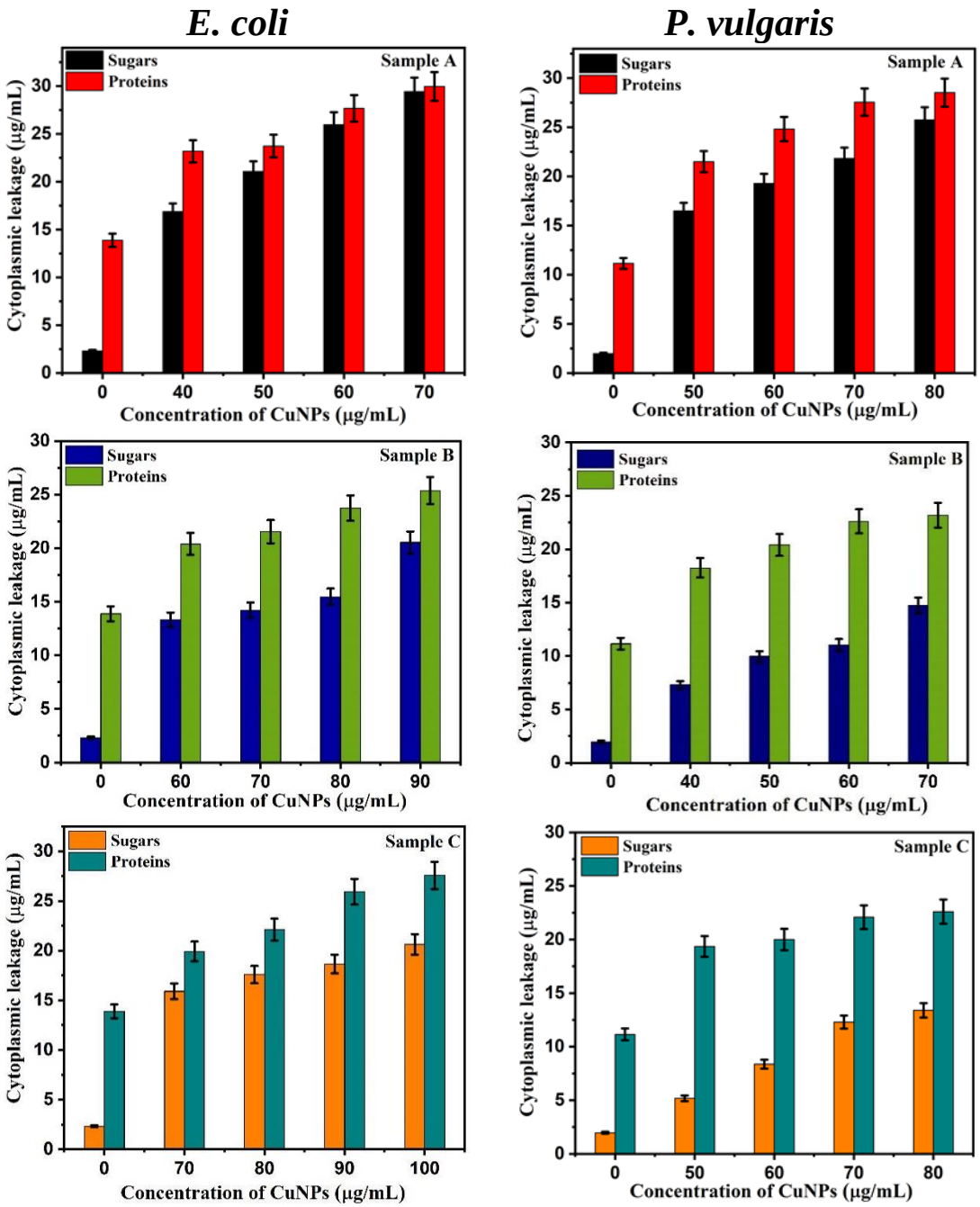

Figure 4.7 Effect of CuNPs [Sample A (yield 0.2 g), B (yield 0.3 g) and C (yield 0.4 g)] on cytoplasmic leakage of sugars and proteins by *E. coli*, *P. vulgaris*. 0 µg/mL CuNPs concentration represents negative control (i.e. media + bacteria). Values are average of three replicates and error bars represents standard deviation.

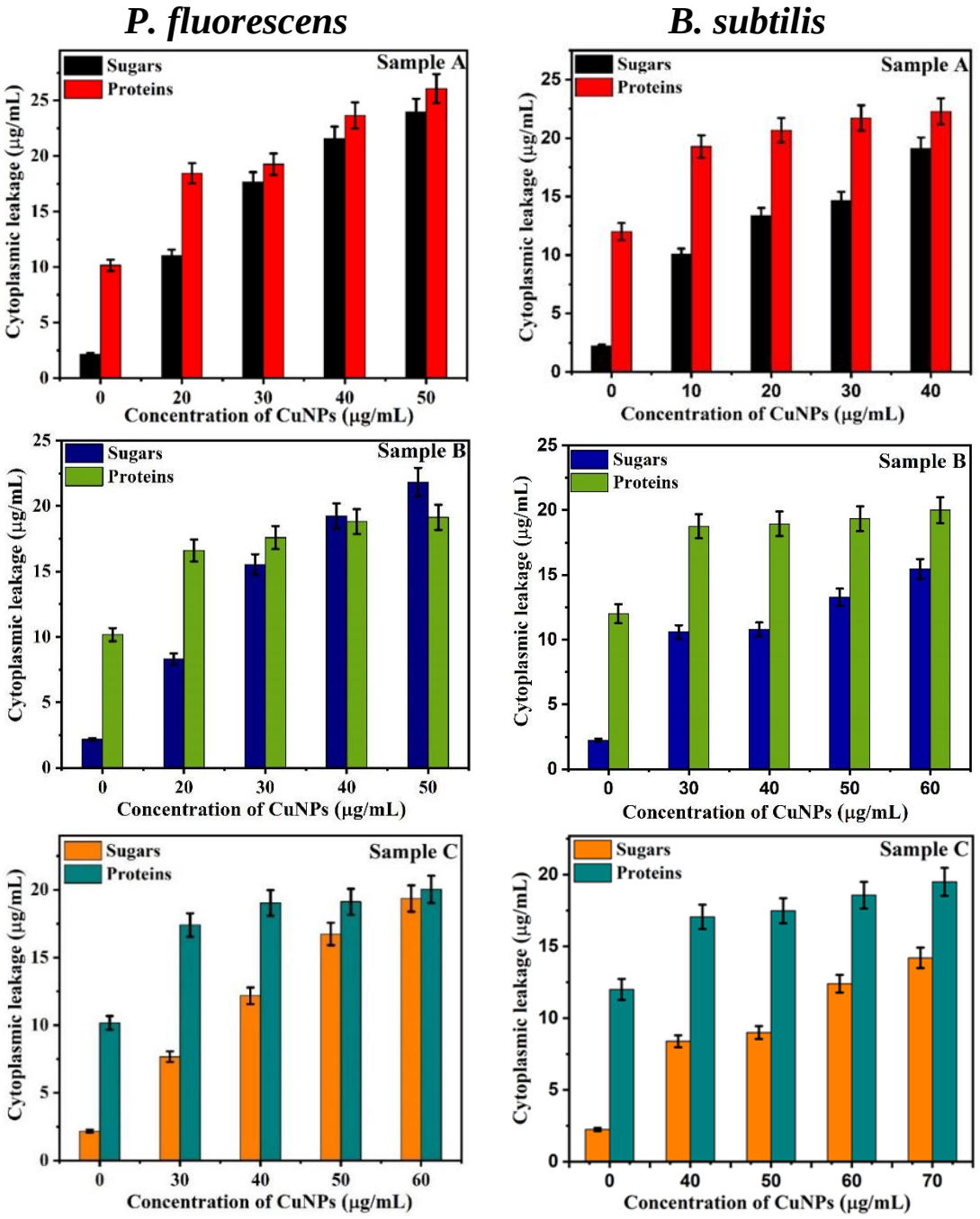

Figure 4.8 Effect of CuNPs [Sample A (yield 0.2 g), B (yield 0.3 g) and C (yield 0.4 g)] on cytoplasmic leakage of sugars and proteins by *P. fluorescens*, *B. subtilis*. 0 µg/mL CuNPs concentration represents negative control (i.e. media + bacteria). Values are average of three replicates and error bars represents standard deviation.

In soil bacteria, the cytoplasmic leakage was lowest in cultures not treated with CuNPs (controls). Irrespective of strains or nanoparticles, an increase in the leakage of sugars and proteins were observed with the increase in CuNPs concentrations. Both in controls and CuNPs treated cultures, the cytoplasmic leakages were more pronounced in *P. fluorescens* as compared to *B. subtilis*. Thick cell wall in Gram-positive *B. subtilis*

functions as barrier against antimicrobial agents and protects contents of cytoplasm from leaking. Yuan et al., 2017 and Saratale et al., 2020 have also reported higher sugar and protein leakages in Gram-negative strains. These observations were in good correlation with those reported by Yuan et al., 2017 and Saratale et al., 2020 and with those observed in MIC and MBC tests.

Amongst the three tested CuNPs (sample A, B and C), the leakage was highest for Sample A followed by sample B and sample C in both pathogenic and soil bacteria (Fig. 4.7 and Fig. 4.8). This was in correlation with their hydrodynamic sizes, which was lowest for sample A (11.34 nm) followed by sample B (12.19 nm) and sample C (13.70 nm). Particles with smaller hydrodynamic sizes were able to penetrate more through the bacterial cell walls and disrupt their biochemical activities. Earlier studies suggests that metallic nanoparticles disrupts the permeability of cell membranes, affects membrane transport system and induces release of cellular macromolecules [Kim et al., 2011; Tiwari et al., 2018; Saratale et al., 2020]. Irrespective of CuNPs yield, all tested samples induces leakage of cytoplasmic content both in pathogenic and soil bacteria, indicating that scale-up of CuNPs yield has no significant effect on their bioactivities.

4.4 Effect of CuNPs on Reactive Oxygen Species (ROS)

Interactions of nanoparticles with microorganisms can produce oxidative stress that can cause external or internal cell damage [Nel et al., 2006]. Intracellular reactive oxygen species (ROS) generation in bacterial cultures after treating them with CuNPs was measured with the help of DCFH-DA (dichloro-dihydro-fluorescein diacetate). DCFH-DA has no fluorescence until it enters into the cell through the plasma membrane. Inside the cell, intracellular esterase converts DCFH-DA to DCFH, which cannot pass through the cell membrane and gets oxidized by cellular ROS into highly fluorescent derivative DCF (2', 7'-dichlorofluorescein) whose fluorescence intensity is directly proportional to the intracellular ROS [Yuan et al., 2017].

To measure the intracellular ROS levels five sets of test tubes with 10 mL nutrient broth media containing CuNPs in requisite concentrations (40-100 µg/mL for *E. coli*, 30-80 µg/mL for *P. vulgaris*, 10-70 µg/mL for *B. subtilis* and 20-60 µg/mL for *P. fluorescens*) were inoculated with 10^7 cfu/mL of respective strain for 24 h at 37 °C for *E.coli*, *P. vulgaris*, *Bacillus subtilis* and at 30 °C for *P. fluorescens*. Tubes incubated without CuNPs were treated as controls. After incubation, they were centrifuged at 12,000 rpm at 4 °C for 30 min. After centrifugation supernatant was treated with 100 µM DCFHDA and incubated for 1 h in dark [Yuan et al., 2017]. After the incubation, fluorescence (λ_{ex} = 485 nm) was measured at 520 nm on Carry Eclipse fluorescence spectrophotometer. This fluorescence intensity was directly proportional to the intracellular ROS.

Concentration dependence of intracellular ROS generated in CuNPs treated

bacterial cultures were measured in terms of fluorescence intensity of DCF, which is shown in Fig. 4.9 (*E. coli* and *P. vulgaris*) and Fig. 4.10 (*B. subtilis* and *P. fluorescens*). The fluorescence intensity was lowest in cultures not treated with CuNPs (controls). In CuNPs treated cultures, irrespective of CuNPs (sample A, B and C), the fluorescence intensity increases with the increase in CuNPs concentration. In each strain, the fluorescence intensity peaks at CuNPs concentrations, which were their MIC values. Beyond MIC, the fluorescence intensity (and hence the ROS levels) quenched in all strains. This decrease in ROS levels at CuNPs concentrations > MIC was because of large drop in number of surviving (live) cells at higher CuNPs concentrations.

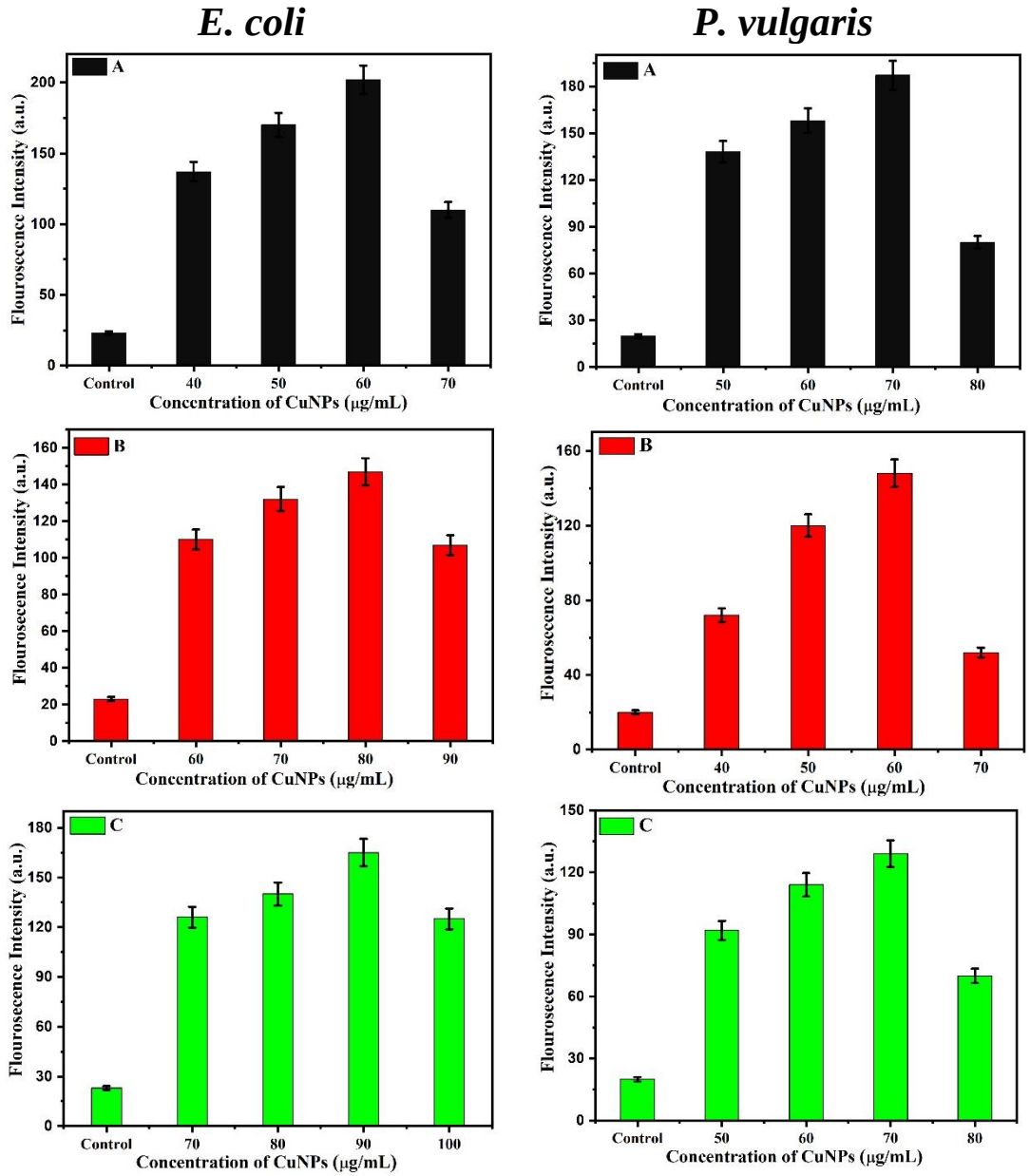

Figure 4.9 Effect of CuNPs [Sample A (yield 0.2 g), B (yield 0.3 g) and C (yield 0.4 g)] on ROS generation (measured in terms of fluorescence intensity of DCF) in *E. coli* and *P. vulgaris*. Control represents negative control without CuNPs. Values are average of three replicates and error bars represents standard deviation.

The ROS levels (measured in terms of fluorescence intensity of DCF) generated in *E. coli* after their treatment with CuNPs (at MIC) was slightly higher than that measured in *P. vulgaris*. This difference in ROS levels can be ascribed to Cu^{+2} ions, which can energetically move across a lipid bilayer [Bogdanovic et al., 2014]. It was previously reported that *E. coli* possesses higher membrane permeability and because of which it allows greater transport of Cu^{+2} ions across the cell membrane [Chatterjee et al., 2014].

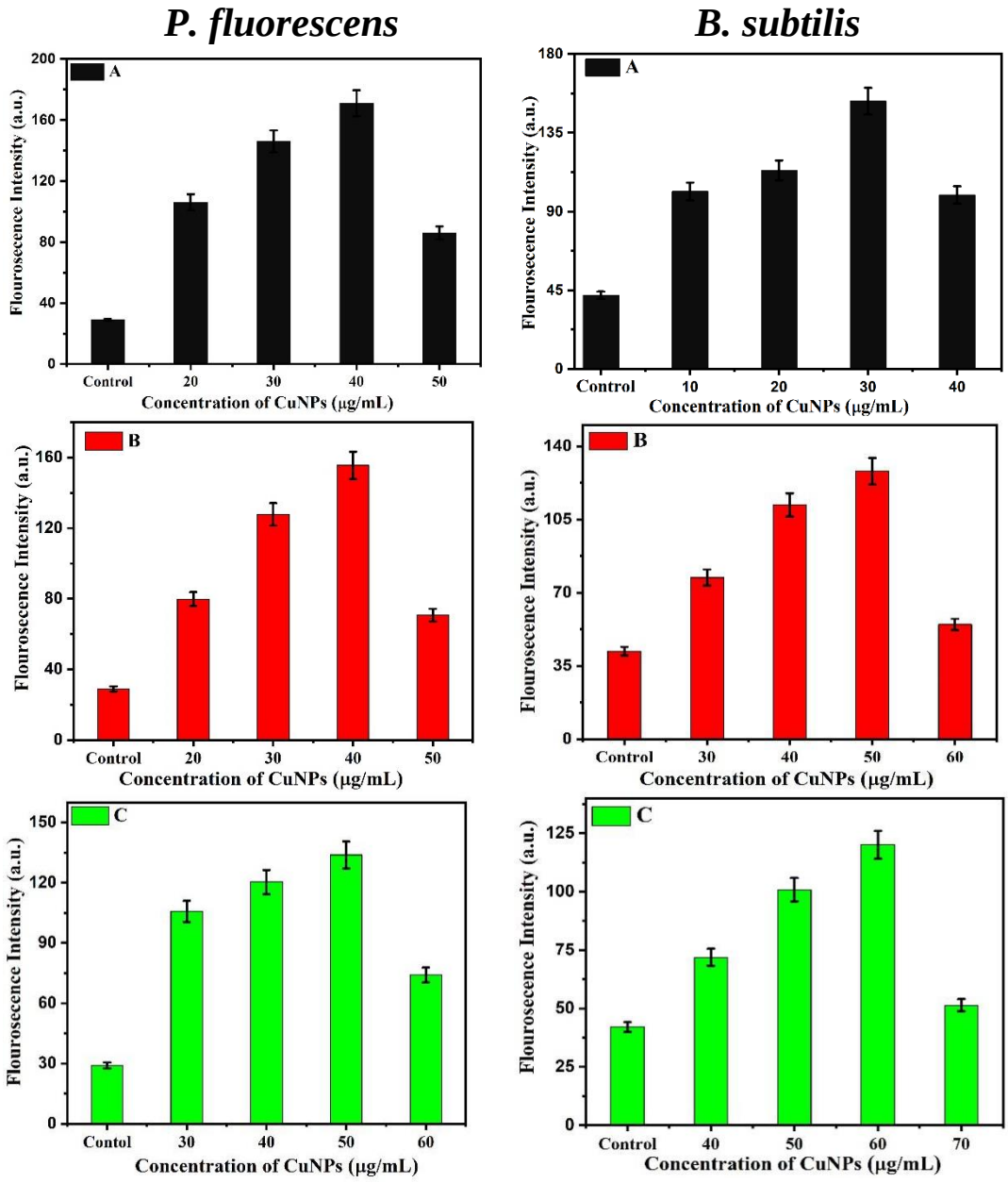

Figure 4.10 Effect of CuNPs [Sample A (yield 0.2 g), B (yield 0.3 g) and C (yield 0.4 g)] on ROS generation (measured in terms of fluorescence intensity of DCF) in *P. fluorescens* and *B. subtilis*. Control represents negative control without CuNPs. Values are average of three replicates and error bars represents standard deviation.

Both in controls and CuNPs treated cultures, the ROS levels (measured in terms of fluorescence intensity of DCF) were more pronounced in Gram-negative *P. fluorescens* as compared to Gram-positive *B. subtilis*. This difference in ROS levels can be ascribed to the distinction in internalization of CuNPs in both the strains caused by the differences in their cell membrane structures [Yuan et al., 2017].

Further, decrease in ROS levels in all tested bacteria was observed with increase in the hydrodynamic size of CuNPs (sample A $\rightarrow$ C). This might be because of the greater penetration power of smaller sized CuNPs. This observation is in line with those observed in MIC, MBC and cytoplasmic leakage tests. Metal nanoparticle – bacterial strain interaction can produce four different types of reactive oxygen species such as hydrogen peroxide (H_2O_2), hydroxyl radicals (OH), hydroperoxyl radicals (HO_2) and super oxide ions (O_2^-). It has been reported that CuNPs can produce all four types of reactive oxygen species and hence can cause greater intracellular damage [Wang et al., 2017]. CuNPs induced oxidative stress causes cell death by nucleic acid and protein oxidation, or through loss of cell membrane integrity and intracellular respiratory failure [Carlson et al., 2008].

4.5 Synergistic effect of CuNPs with Antibiotics on antibacterial activity

Synergistic effect of CuNPs (sample A, B and C) on antibacterial activities of conventional antibiotics (tetracycline, kanamycin, ampicillin and streptomycin) was evaluated against pathogenic (*E. coli* and *P. vulgaris*) and soil (*B. subtilis* and *P. fluorescens*) bacteria through zone of inhibition (ZIH) measurements. Nutrient agar plates (90 mm) were used for ZIH measurements. Once the agar got solidified, bacterial suspension of 100 µL (10^3-10^4 cfu/mL grown according McFarland standard) was uniformly spread over each plate. 9 mm well was bored at the center of each plate with the help of sterile cork-borer. The requisite quantities of CuNPs (10 - 100 µg/mL for *E. coli*, 10 - 80 µg/mL for *P. vulgaris*, 10 - 80 µg/mL for *B. subtilis* and 10 - 60 µg/mL for *P. fluorescens*) or antibiotics (10 mg/mL, 10 µL) or their combinations were added in wells. Wells without CuNPs or antibiotics (i.e. filled with deionized water) were treated as controls. Agar plates were then incubated at 37 °C for *E. coli, P. vulgaris, B. subtilis* and at 30 °C for *P. fluorescens* for 24 h. After 24 h, the zone of inhibition (ZIH) was measured with the help of a scale [Naqui et al., 2013]. Synergistic effects of CuNPs on the antibacterial activities of antibiotics were determined in terms of % synergy, which was defined by following equation:

$$\text{Synergy (\%)} = \frac{[A]}{[B+C]} \times 100 \qquad (4.1)$$

Where, A represents ZIH of combination (i.e. CuNPs + antibiotics), B represents volume normalized ZIH of CuNPs and C represents volume normalized ZIH of antibiotics. Here,

$$B = \frac{Volume\ of\ CuNPs}{Total\ volume} \times ZIH\ of\ CuNPs \quad (4.2)$$

and $$C = \frac{Volume\ of\ Antibiotics}{Total\ volume} \times ZIH\ of\ Antibiotics \quad (4.3)$$

ZIH of CuNPs (sample A, B, C), antibiotics (tetracycline, kanamycin, ampicillin and streptomycin) and CuNPs + antibiotics for *E.coli* and *P. vulgaris* are shown in Fig. 4.11 and Fig. 4.12, respectively. ZIH values of CuNPs, antibiotics and CuNPs – antibiotics combinations against *E. coli* were listed in Table 4.3 (Sample A), Table 4.4 (Sample B) and Table 4.5 (Sample C). For *E. coli* the ZIH of antibiotics; tetracycline, streptomycin, kanamycin and ampicillin were 32, 28, 30 and 34 mm, respectively. ZIH of CuNPs was in range of 13-20 mm (for sample A), 15-22 mm (for sample B) and 15-27 mm (for sample C). The % synergy calculated from equation 4.1 was also reported in Table 4.3 (Sample A), Table 4.4 (Sample B) and Table 4.5 (Sample C). Irrespective of CuNPs, with increase in their concentration, the % synergy decreases (Fig. 4.13). Synergy of CuNPs with tetracycline and ampicillin was much higher as compared to their synergy with streptomycin. CuNPs with antibiotics exhibits synergistic antibacterial activities against *E.coli* [Selvarani, 2010].

Table 4.3 Synergistic effect of CuNPs [Sample A (yield 0.2 g)] and antibiotics (tetracycline, streptomycin, kanamycin and ampicillin) on Zone of Inhibition (ZIH) against *E.coli*

CuNPs (µg/mL)	**Zone of Inhibition (ZIH) (mm)**			**Synergy (%)**
	CuNPs	**Antibiotics**	**CuNPs + Antibiotic**	
10	13	Tetracycline (32)	30	177
30	16		34	198
50	17		30	169
70	20		31	152
10	13	Streptomycin (28)	25	155
30	16		24	141
50	17		21	119
70	20		21	103
10	13	Kanamycin (30)	29	176
30	16		26	162
50	17		26	161
70	20		27	145
10	13	Ampicillin (34)	31	173
30	16		32	192
50	17		34	187
70	20		35	167

Table 4.4 Synergistic effect of CuNPs [Sample B (yield 0.3 g)] and antibiotics (tetracycline, streptomycin, kanamycin and ampicillin) on Zone of Inhibition (ZIH) against *E.coli*

CuNPs (µg/mL)	Zone of Inhibition (ZIH) (mm)			Synergy (%)
	CuNPs	Antibiotics	CuNPs + Antibiotic	
30	15	Tetracycline (32)	29	175
50	16		30	176
70	20		30	145
90	22		31	138
30	15	Streptomycin (28)	20	123
50	16		21	121
70	20		21	102
90	22		23	100
30	15	Kanamycin (30)	25	152
50	16		25	148
70	20		26	126
90	22		27	120
30	15	Ampicillin (34)	30	178
50	16		30	175
70	20		32	145
90	22		33	138

Table 4.5 Synergistic effect of CuNPs [Sample C (yield 0.4 g)] and antibiotics (tetracycline, streptomycin, kanamycin and ampicillin) on Zone of Inhibition (ZIH) against *E.coli*

CuNPs (µg/mL)	Zone of Inhibition (ZIH) (mm)			Synergy (%)
	CuNPs	Antibiotics	CuNPs + Antibiotic	
40	15	Tetracycline (32)	33	190
60	17		30	164
80	22		31	150
100	27		31	113
40	15	Streptomycin (28)	25	149
60	17		26	145
80	22		23	102
100	27		23	73
40	15	Kanamycin (30)	28	164
60	17		26	144
80	22		25	111
100	27		28	103
40	15	Ampicillin (34)	30	170
60	17		32	174
80	22		31	136
100	27		32	117

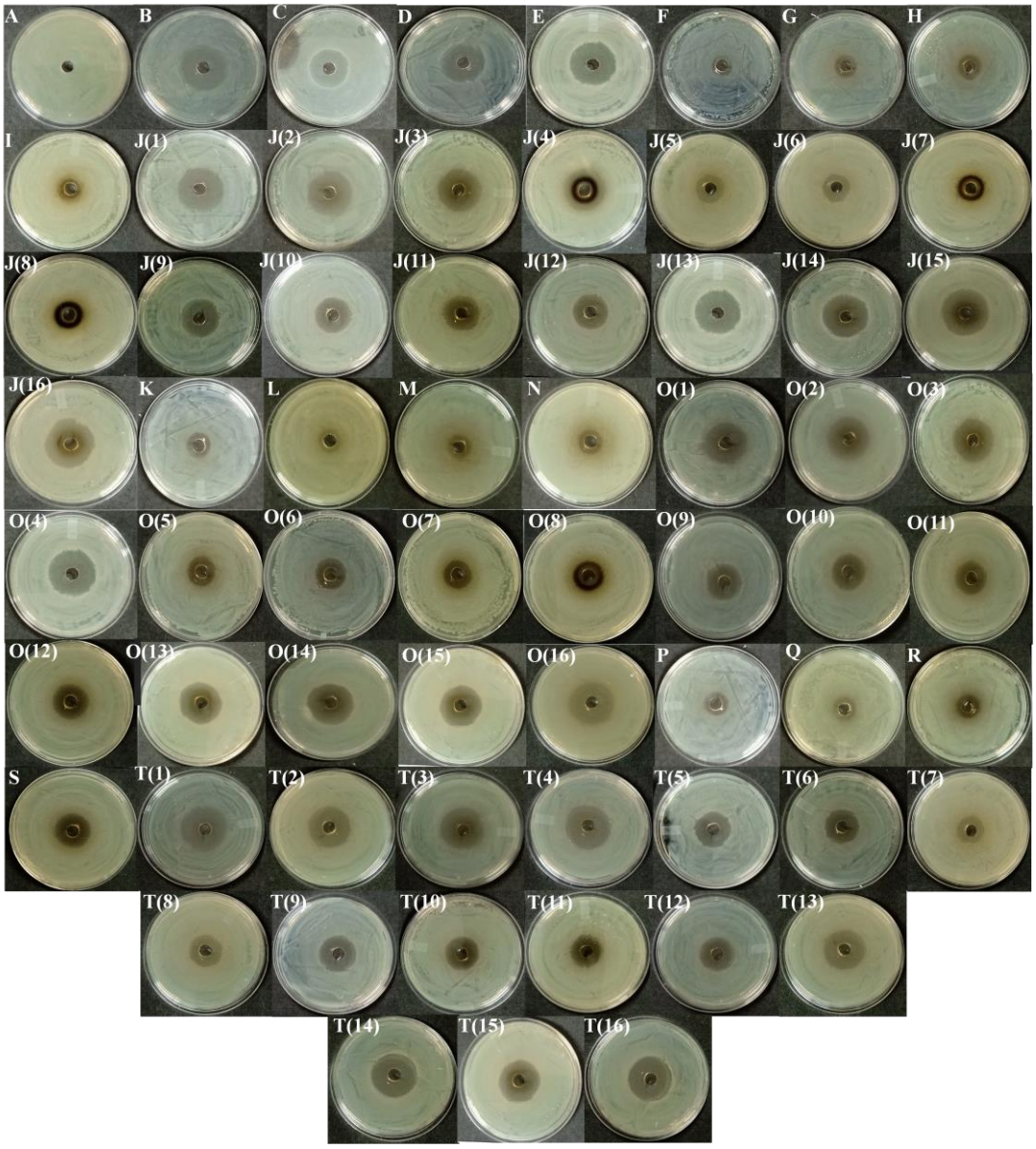

Figure 4.11 Zone of inhibition (ZIH) of CuNPs / Antibiotics / CuNPs + Antibiotics treated *E. coli*. Order of frames: A is control (without CuNPs or antibiotics), B = tetracycline, C = streptomycin, D = kanamycin, E = ampicillin, F, G, H, I = 10, 30, 50, 70 µg/mL CuNPs (sample A), J(1) to J(4) = tetracycline + 10, 30, 50, 70 µg/mL CuNPs (sample A), J(5) to J(8) = streptomycin + 10, 30, 50, 70 µg/mL CuNPs (sample A), J(9) to J(12) = kanamycin + 10, 30, 50, 70 µg/mL CuNPs (sample A), J(13)to J(16) = ampicillin + 10, 30, 50, 70 µg/mL CuNPs (sample A), K, L, M, N = 30, 50, 70, 90 µg/mL CuNPs (sample B), O(1) to O(4)= tetracycline + 30, 50, 70, 90 µg/mL CuNPs (sample B), O(5) to O(8) = streptomycin + 30, 50, 70, 90 µg/mL CuNPs (sample B), O(9) to O(12) = kanamycin + 30, 50, 70, 90 µg/mL CuNPs (sample B), O(13) to O(16) = ampicillin + 30, 50, 70, 90 µg/mL CuNPs (sample B), P, Q, R, S = 40, 60, 80, 100 µg/mL CuNPs (sample C), T(1)-T(4)= tetracycline + 40, 60, 80, 100 µg/mL CuNPs (sample C), T(5) to T(8) = streptomycin + 40, 60, 80, 100 µg/mL CuNPs (sample C), T(9)to T(12) = kanamycin + 40, 60, 80, 100 µg/mL CuNPs (sample C), T(13) to T(16) = ampicillin + 40, 60, 80, 100 µg/mL CuNPs (sample C). Each antibiotic concentration was 10 mg/mL.

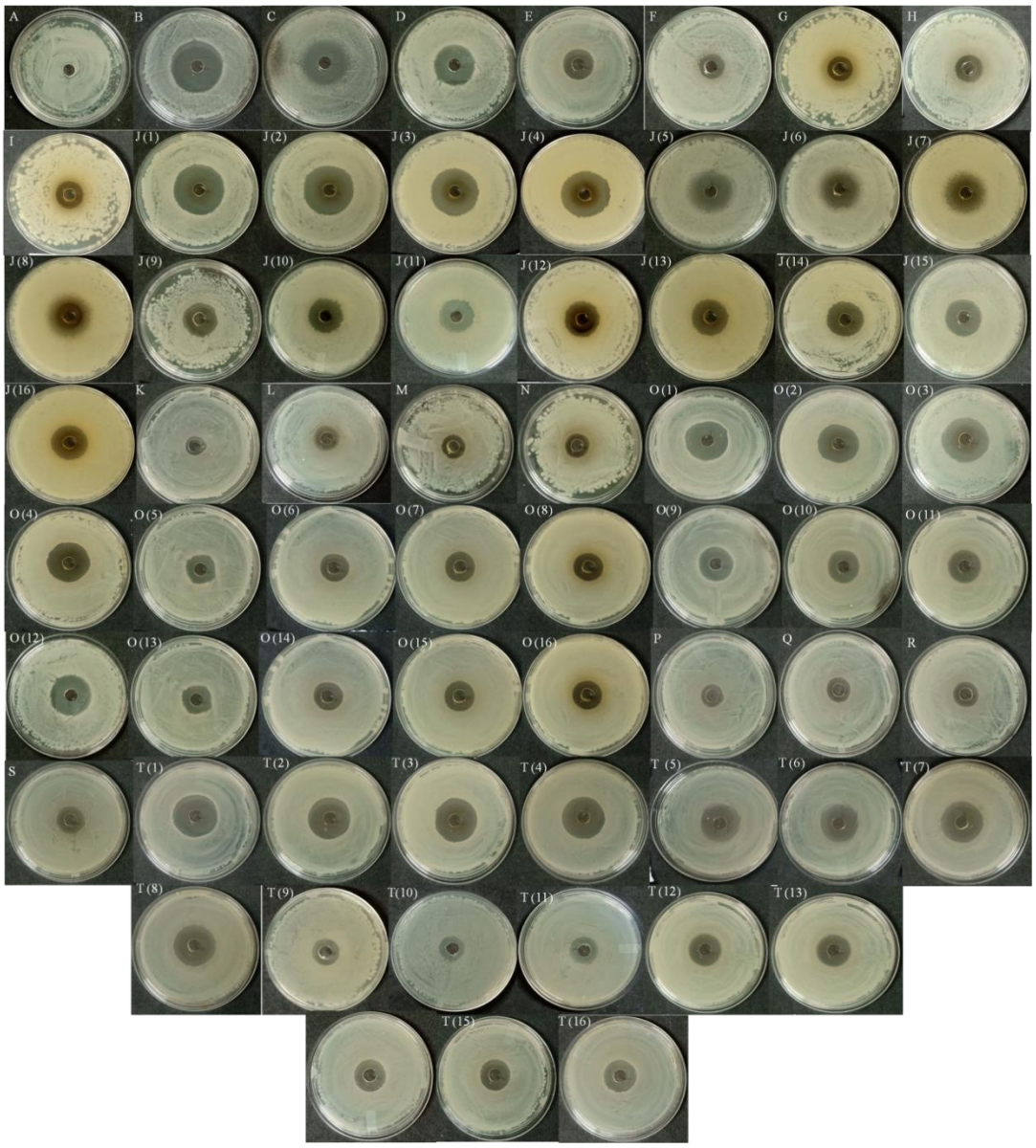

Figure 4.12. Zone of inhibition (ZIH) of CuNPs / Antibiotics / CuNPs + Antibiotics treated *P. vulgaris*. Order of frames: A is control (without CuNPs or antibiotics), B = tetracycline, C = streptomycin, D = kanamycin, E = ampicillin, F, G, H, I = 10, 30, 50, 70 µg/mL CuNPs (sample A), J(1) to J(4) = tetracycline + 10, 30, 50, 70 µg/mL CuNPs (sample A), J(5) to J(8) = streptomycin + 10, 30, 50, 70 µg/mL CuNPs (sample A), J(9) to J(12) = kanamycin + 10, 30, 50, 70 µg/mL CuNPs (sample A), J(13)to J(16) = ampicillin + 10, 30, 50, 70 µg/mL CuNPs (sample A), K, L, M, N = 30, 50, 70, 90 µg/mL CuNPs (sample B), O(1) to O(4)= tetracycline + 30, 50, 70, 90 µg/mL CuNPs (sample B), O(5) to O(8) = streptomycin + 30, 50, 70, 90 µg/mL CuNPs (sample B), O(9) to O(12) = kanamycin + 30, 50, 70, 90 µg/mL CuNPs (sample B), O(13) to O(16) = ampicillin + 30, 50, 70, 90 µg/mL CuNPs (sample B), P, Q, R, S = 40, 60, 80, 100 µg/mL CuNPs (sample C), T(1)-T(4)= tetracycline + 40, 60, 80, 100 µg/mL CuNPs (sample C), T(5) to T(8) = streptomycin + 40, 60, 80, 100 µg/mL CuNPs (sample C), T(9)to T(12) = kanamycin + 40, 60, 80, 100 µg/mL CuNPs (sample C), T(13) to T(16) = ampicillin + 40, 60, 80, 100 µg/mL CuNPs (sample C). Each antibiotic concentration was 10 mg/mL.

In case of *P. vulgaris* the ZIH for tetracycline, streptomycin, kanamycin and ampicillin was 38, 36, 30 and 24 mm, respectively. ZIH of CuNPs sample A, B, C were in the range of 17-22 mm, 14-19 mm and 17-20 mm (Table 4.6, Table 4.7 and Table 4.8). Regardless of nanoparticle yield, CuNPs (sample A, B and C) exhibited synergistic effects with antibiotics (tetracycline, streptomycin, kanamycin and ampicillin). Irrespective of CuNPs, with increase in their concentration, the % synergy decreases (Fig. 4.13). Highest synergy of CuNPs was observed with tetracycline, while the synergy was lowest with ampicillin.

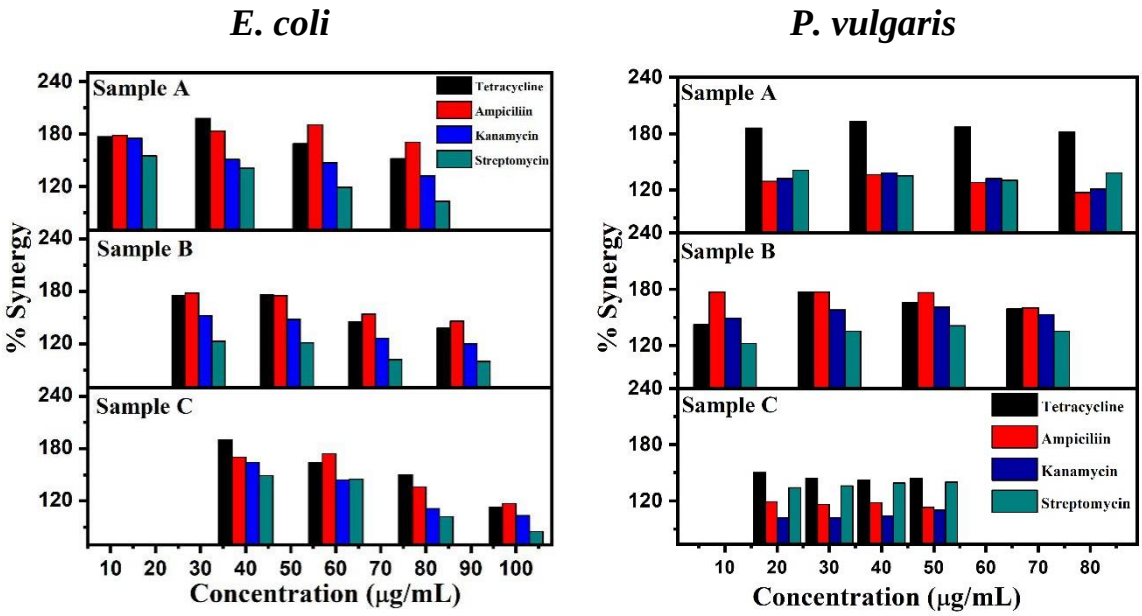

Figure 4.13 Concentration dependence of % Synergy of CuNPs [Sample A (yield 0.2 g), B (yield 0.3 g) and C (yield 0.4 g)] with antibiotics (tetracycline, streptomycin, kanamycin and ampicillin) against pathogenic strains of *E. coli* and *P. vulgaris*.

Photographic view of ZIH of CuNPs (sample A, B, C), antibiotics (tetracycline, kanamycin, ampicillin and streptomycin) and CuNPs + antibiotics for *B. subtilis* and *P. fluorescens* were shown in Fig. 4.14 and Fig. 4.15, respectively. ZIH values of CuNPs, antibiotics and CuNPs – antibiotics combinations against *B. subtilis* were listed in Table 4.9 (Sample A), Table 4.10 (Sample B) and Table 4.11 (Sample C). For *B. subtilis* the ZIH of antibiotics; tetracycline, streptomycin, kanamycin and ampicillin were 40, 38, 38 and 34 mm, respectively. ZIH of CuNPs was in range of 11-23 mm (for sample A), 21-24 mm (for sample B) and 19-28 mm (for sample C). The % synergy calculated from equation 4.1 was also reported in Table 4.9 (Sample A), Table 4.10 (Sample B) and Table 4.11 (Sample C). Against *B. subtilis*, the synergy of CuNPs with ampicillin was highest while it was lowest for streptomycin (Fig. 4.16). All CuNPs irrespective of their yield exhibits synergistic antibacterial activities with antibiotics against *B. subtilis*.

Table 4.6 Synergistic effect of CuNPs [Sample A (yield 0.2 g)] and antibiotics (tetracycline, streptomycin, kanamycin and ampicillin) on Zone of Inhibition (ZIH) against *P. vulgaris*

CuNPs (µg/mL)	Zone of Inhibition (ZIH) (mm)			Synergy (%)
	CuNPs	Antibiotics	CuNPs + Antibiotic	
20	17	Tetracycline (38)	36	186
40	18		37	193
60	20		39	187
80	22		41	182
20	17	Streptomycin (36)	27	141
40	18		26	135
60	20		27	130
80	22		31	138
20	17	Kanamycin (30)	25	132
40	18		26	138
60	20		27	132
80	22		37	131
20	17	Ampicillin (24)	25	129
40	18		26	136
60	20		27	128
80	22		37	117

Table 4.7 Synergistic effect of CuNPs [Sample B (yield 0.3 g)] and antibiotics (tetracycline, streptomycin, kanamycin and ampicillin) on Zone of Inhibition (ZIH) against *P. vulgaris*

CuNPs (µg/mL)	Zone of Inhibition (ZIH) (mm)			Synergy (%)
	CuNPs	Antibiotics	CuNPs + Antibiotic	
10	14	Tetracycline (38)	30	142
30	16		33	177
50	17		31	166
70	19		32	159
10	14	Streptomycin (36)	25	122
30	16		25	135
50	17		26	141
70	19		27	135
10	14	Kanamycin (30)	28	149
30	16		28	158
50	17		29	161
70	19		30	153
10	14	Ampicillin (24)	30	177
30	16		30	177
50	17		31	177
70	19		31	160

Table 4.8 Synergistic effect of CuNPs [Sample C (yield 0.4 g)] and antibiotics (tetracycline, streptomycin, kanamycin and ampicillin) on Zone of Inhibition (ZIH) against *P. vulgaris*

CuNPs (µg/mL)	Zone of Inhibition (ZIH) (mm)			Synergy (%)
	CuNPs	Antibiotics	CuNPs + Antibiotic	
20	17	Tetracycline (38)	32	150
30	18		30	144
40	19		30	142
50	20		31	144
20	17	Streptomycin (36)	20	134
30	18		20	136
40	19		21	139
50	20		23	140
20	17	Kanamycin (30)	28	102
30	18		28	102
40	19		29	104
50	20		30	110
20	17	Ampicillin (24)	22	119
30	18		22	116
40	19		23	118
50	20		23	113

Table 4.9 Synergistic effect of CuNPs [Sample A (yield 0.2 g)] and antibiotics (tetracycline, streptomycin, kanamycin and ampicillin) on Zone of Inhibition (ZIH) against *B. subtilis*

CuNPs (µg/mL)	Zone of Inhibition (ZIH) (mm)			Synergy (%)
	CuNPs	Antibiotics	CuNPs + Antibiotic	
10	11	Tetracycline (40)	37	217
20	20		37	166
30	22		36	154
40	23		37	154
10	11	Streptomycin (38)	33	198
20	20		31	140
30	22		31	133
40	23		32	134
10	11	Kanamycin (38)	32	202
20	20		31	143
30	22		31	135
40	23		32	135
10	11	Ampicillin (34)	38	237
20	20		36	166
30	22		37	161
40	23		38	161

Table 4.10 Synergistic effect of CuNPs [Sample B (yield 0.3 g)] and antibiotics (tetracycline, streptomycin, kanamycin and ampicillin) on Zone of Inhibition (ZIH) against *B. subtilis*

CuNPs (µg/mL)	Zone of Inhibition (ZIH) (mm)			Synergy (%)
	CuNPs	Antibiotics	CuNPs + Antibiotic	
10	21	Tetracycline (40)	33	136
30	23		34	142
50	23		35	141
70	24		37	149
10	21	Streptomycin (38)	31	129
30	23		32	131
50	23		33	137
70	24		35	141
10	21	Kanamycin (38)	30	129
30	23		31	129
50	23		32	135
70	24		33	134
10	21	Ampicillin (34)	30	128
30	23		35	145
50	23		33	139
70	24		34	138

Table 4.11 Synergistic effect of CuNPs [Sample C (yield 0.4 g)] and antibiotics (tetracycline, streptomycin, kanamycin and ampicillin) on Zone of Inhibition (ZIH) against *B. subtilis*

CuNPs (µg/mL)	Zone of Inhibition (ZIH) (mm)			Synergy (%)
	CuNPs	Antibiotics	CuNPs + Antibiotic	
20	19	Tetracycline (40)	31	120
40	20		30	131
60	22		30	138
80	28		38	132
20	19	Streptomycin (38)	33	131
40	20		32	142
60	22		32	149
80	28		36	125
20	19	Kanamycin (38)	32	134
40	20		29	132
60	22		30	142
80	28		31	107
20	19	Ampicillin (34)	35	144
40	20		36	163
60	22		36	169
80	28		37	130

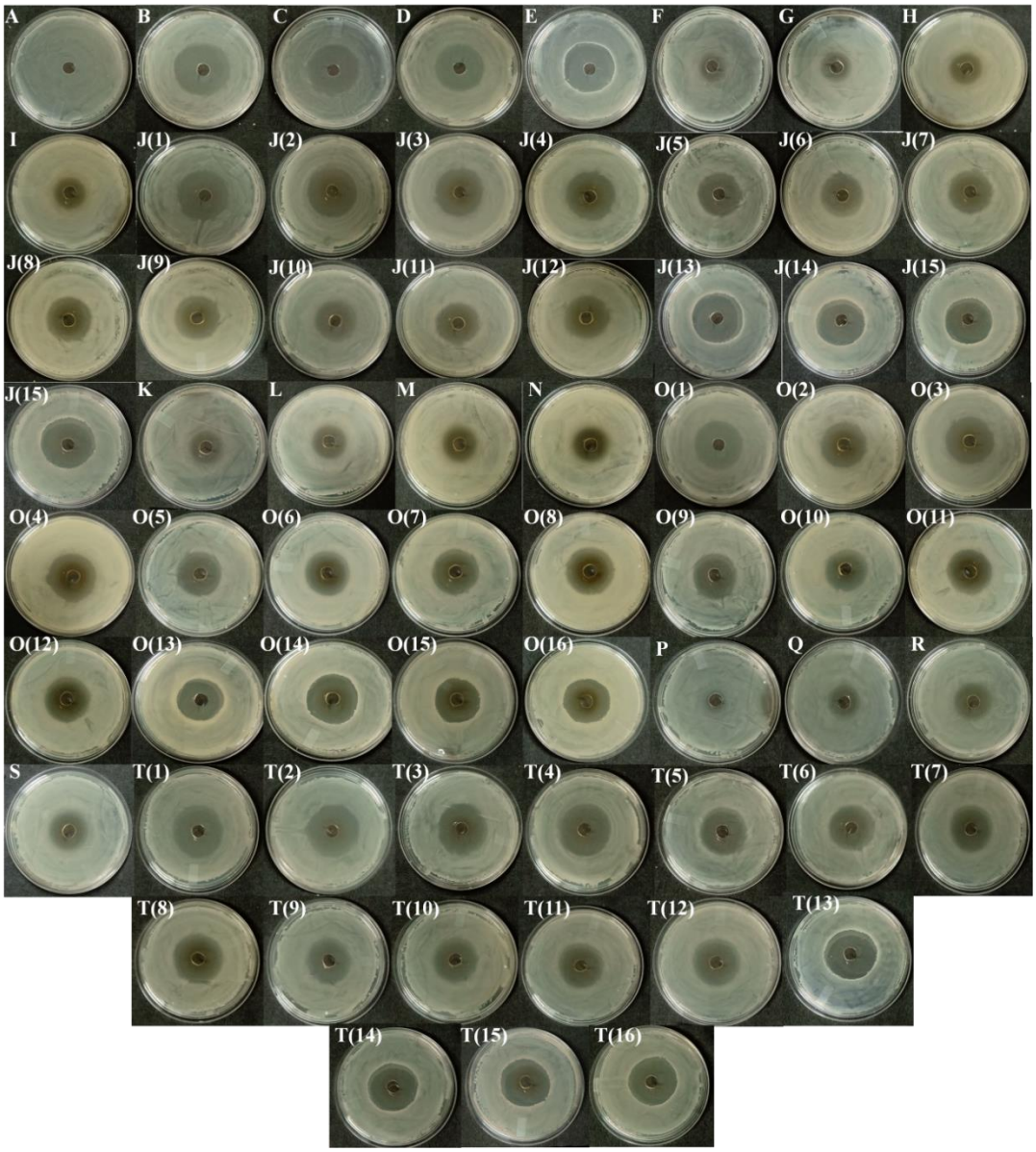

Figure 4.14 Zone of inhibition (ZIH) of CuNPs / Antibiotics / CuNPs + Antibiotics treated *B. subtilis*. Order of frames: A is control (without CuNPs or antibiotics), B = tetracycline, C = streptomycin, D = kanamycin, E = ampicillin, F, G, H, I = 10, 20, 30, 40 µg/mL CuNPs (sample A), J(1) to J(4) = tetracycline + 10, 20, 30, 40 µg/mL CuNPs (sample A), J(5) to J(8) = streptomycin + 10, 20, 30, 40 µg/mL CuNPs (sample A), J(9) to J(12) = kanamycin + 10, 20, 30, 40 µg/mL CuNPs (sample A), J(13)to J(16) = ampicillin + 10, 20, 30, 40 µg/mL CuNPs (sample A), K, L, M, N = 10, 30, 50, 70 µg/mL CuNPs (sample B), O(1) to O(4)= tetracycline + 10, 30, 50, 70 µg/mL CuNPs (sample B), O(5) to O(8) = streptomycin + 10, 30, 50, 70 µg/mL CuNPs (sample B), O(9) to O(12) = kanamycin + 10, 30, 50, 70 µg/mL CuNPs (sample B), O(13) to O(16) = ampicillin + 10, 30, 50, 70 µg/mL CuNPs (sample B), P, Q, R, S = 20, 40, 60, 80 µg/mL CuNPs (sample C), T(1)-T(4)= tetracycline + 20, 40, 60, 80 µg/mL CuNPs (sample C), T(5) to T(8) = streptomycin + 20, 40, 60, 80 µg/mL CuNPs (sample C), T(9)to T(12) = kanamycin + 20, 40, 60, 80 µg/mL CuNPs (sample C), T(13) to T(16) = ampicillin + 20, 40, 60, 80 µg/mL CuNPs (sample C). Each antibiotic concentration was 10 mg/mL.

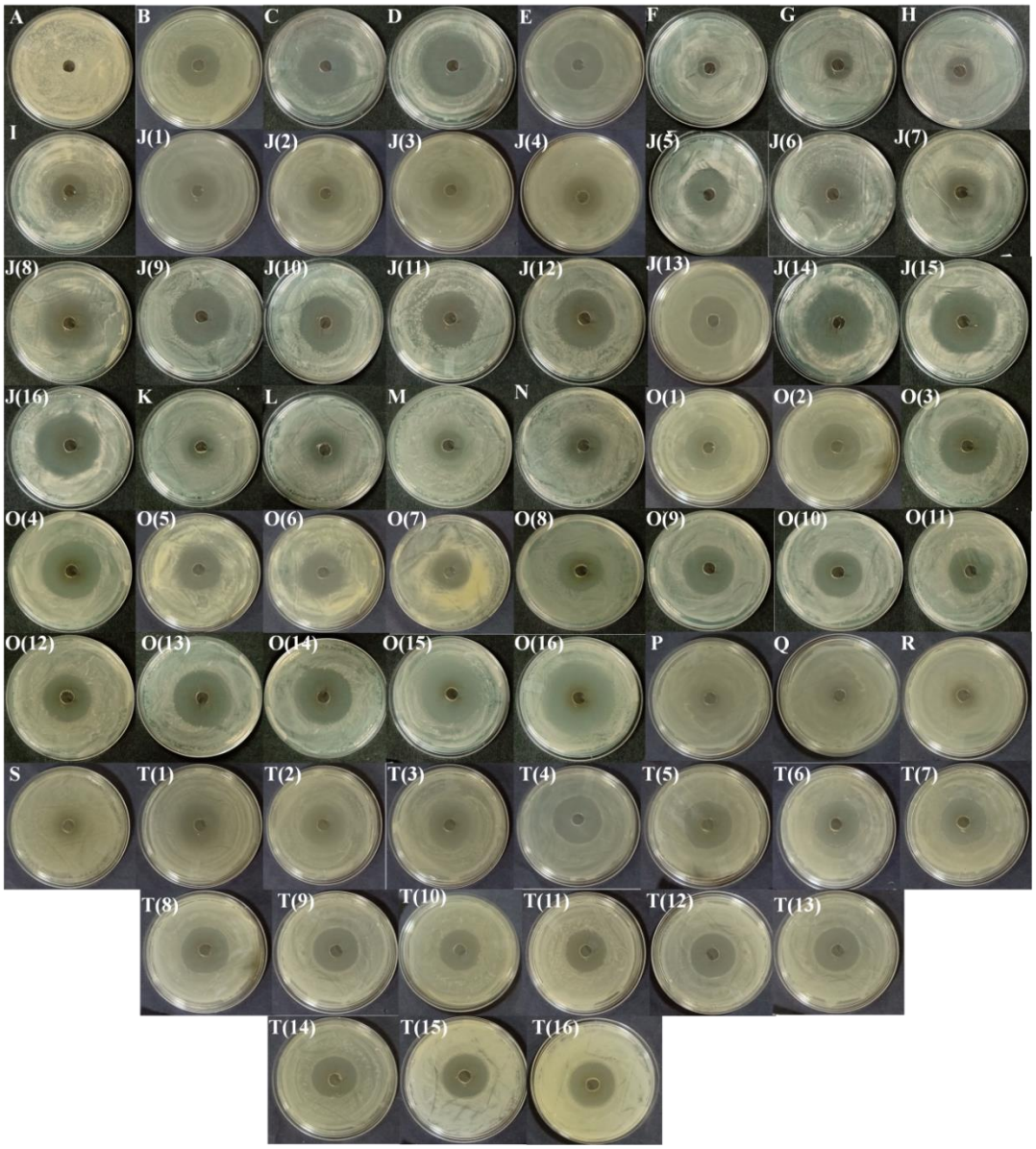

Figure 4.15 Zone of inhibition (ZIH) of CuNPs / Antibiotics / CuNPs + Antibiotics treated *P. fluorescens*. Order of frames: A is control (without CuNPs or antibiotics), B = tetracycline, C = streptomycin, D = kanamycin, E = ampicillin, F, G, H, I = 10, 20, 30, 40 µg/mL CuNPs (sample A), J(1) to J(4) = tetracycline + 10, 20, 30, 40 µg/mL CuNPs (sample A), J(5) to J(8) = streptomycin + 10, 20, 30, 40 µg/mL CuNPs (sample A), J(9) to J(12) = kanamycin + 10, 20, 30, 40 µg/mL CuNPs (sample A), J(13)to J(16) = ampicillin + 10, 20, 30, 40 µg/mL CuNPs (sample A), K, L, M, N = 20, 30, 40, 50 µg/mL CuNPs (sample B), O(1) to O(4)= tetracycline + 20, 30, 40, 50 µg/mL CuNPs (sample B), O(5) to O(8) = streptomycin + 20, 30, 40, 50 µg/mL CuNPs (sample B), O(9) to O(12) = kanamycin + 20, 30, 40, 50 µg/mL CuNPs (sample B), O(13) to O(16) = ampicillin + 20, 30, 40, 50 µg/mL CuNPs (sample B), P, Q, R, S = 30, 40, 50, 60 µg/mL CuNPs (sample C), T(1)-T(4)= tetracycline + 30, 40, 50, 60 µg/mL CuNPs (sample C), T(5) to T(8) = streptomycin + 30, 40, 50, 60 µg/mL CuNPs (sample C), T(9)to T(12) = kanamycin + 30, 40, 50, 60 µg/mL CuNPs (sample C), T(13) to T(16) = ampicillin + 30, 40, 50, 60 µg/mL CuNPs (sample C). Each antibiotic concentration was 10 mg/mL.

In case of *P. fluorescens* the ZIH for tetracycline, streptomycin, kanamycin and ampicillin was 30, 39, 45 and 35 respectively. ZIH of CuNPs against *P. fluorescens* was in the range of 17-27 mm (sample A) (Table 4.12), 18-24 mm (sample B) (Table 4.13) and 12-15 mm (sample C) (Table 4.14). The % synergy calculated from equation 4.1 was also reported in Table 4.12 (Sample A), Table 4.13 (Sample B) and Table 4.14 (Sample C). Against *P. fluorescens*, the synergy of CuNPs with ampicillin was highest while it was lowest for tetracycline (Fig. 4.16). All CuNPs irrespective of their yield exhibits synergistic antibacterial activities with antibiotics against *P. fluorescens*.

Table 4.12 Synergistic effect of CuNPs [Sample A (yield 0.2 g)] and antibiotics (tetracycline, streptomycin, kanamycin and ampicillin) on Zone of Inhibition (ZIH) against *P. fluorescens*

CuNPs (µg/mL)	**Zone of Inhibition (ZIH) (mm)**			**Synergy (%)**
	CuNPs	**Antibiotics**	**CuNPs + Antibiotic**	
10	17	Tetracycline (30)	23	116
20	22		24	104
30	23		28	118
40	27		29	106
10	17	Streptomycin (39)	32	148
20	22		32	135
30	23		36	148
40	27		37	133
10	17	Kanamycin (45)	40	176
20	22		40	162
30	23		40	161
40	27		41	145
10	17	Ampicillin (35)	36	173
20	22		45	192
30	23		45	187
40	27		46	167

Table 4.13 Synergistic effect of CuNPs [Sample B (yield 0.3 g)] and antibiotics (tetracycline, streptomycin, kanamycin and ampicillin) on Zone of Inhibition (ZIH) against *P. fluorescens*

CuNPs (µg/mL)	Zone of Inhibition (ZIH) (mm)			Synergy (%)
	CuNPs	Antibiotics	CuNPs + Antibiotic	
20	18	Tetracycline (30)	34	149
30	20		35	166
40	21		36	164
50	24		40	163
20	18	Streptomycin (39)	31	143
30	20		30	135
40	21		30	132
50	24		31	123
20	18	Kanamycin (45)	36	159
30	20		34	148
40	21		34	146
50	24		35	136
20	18	Ampicillin (35)	36	172
30	20		36	166
40	21		45	202
50	24		50	201

Table 4.14 Synergistic effect of CuNPs [Sample C (yield 0.4 g)] and antibiotics (tetracycline, streptomycin, kanamycin and ampicillin) on Zone of Inhibition (ZIH) against *P. fluorescens*

CuNPs (µg/mL)	Zone of Inhibition (ZIH) (mm)			Synergy (%)
	CuNPs	Antibiotics	CuNPs + Antibiotic	
30	12	Tetracycline (30)	26	179
40	13		29	195
50	14		29	188
60	15		31	192
30	12	Streptomycin (39)	34	216
40	13		32	203
50	14		32	197
60	15		35	209
30	12	Kanamycin (45)	31	187
40	13		30	183
50	14		30	179
60	15		31	180
30	12	Ampicillin (35)	32	211
40	13		31	202
50	14		31	195
60	15		32	194

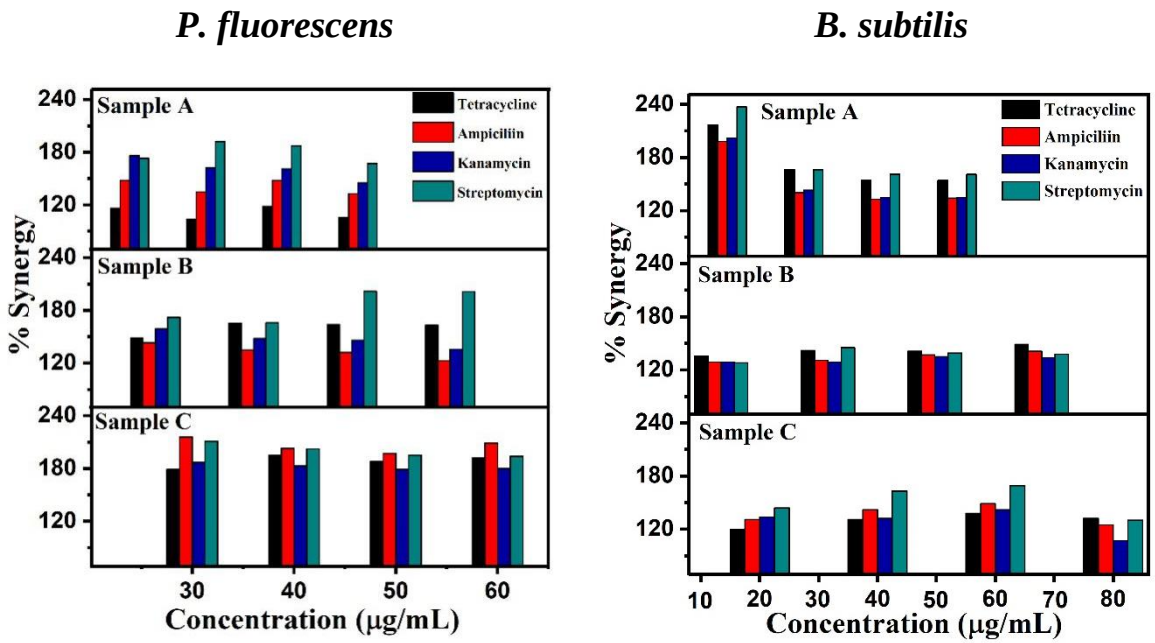

Figure 4.16 Concentration dependence of % Synergy of CuNPs [Sample A (yield 0.2 g), B (yield 0.3 g) and C (yield 0.4 g)] with antibiotics (tetracycline, streptomycin, kanamycin and ampicillin) against pathogenic strains of *B. subtilis* and *P. fluorescens*.

CuNPs irrespective of their yield, exhibits synergistic antibacterial activity with tetracycline, streptomycin, kanamycin and ampicillin against both the tested pathogenic and soil bacteria. The order of observed synergy was: *B. subtilis* > *E. coli* > *P. vulgaris* > *P. fluorescens*. CuNPs – antibiotic synergy was highest against Gram-positive, *B. subtilis,* while it was lowest for Gram-negative *P. fluorescens*. This was in sharp contrast with observed antibacterial activities of CuNPs against these strains. Earlier, it was observed from MIC, MBC, cytoplasmic leakage and ROS assays that Gram-negative strains were more susceptible to antibacterial actions of nanoparticles as compared to the Gram-positive strains. This difference in antibiotic susceptibility was due to the structural and compositional differences in their cell walls. However, as observed in this study, the combination of CuNPs with antibiotics was more lethal to Gram-positive strains.

Synergistic effect of antibacterial activities of CuNPs with conventional antibiotics observed in the present study might be because of the simultaneous action of CuNPs and antibiotics. CuNPs and conventional antibiotics attack bacterial strains differently. Conventional antibiotics target bacterial cells through specific narrow targeting mode(s), while metal nanoparticles attacks bacterial strains through multi-mode random actions. Antibiotics such as tetracycline, streptomycin and kanamycin inhibits the protein synthesis by binding to the ribosomes of the bacterial cells while ampicillin inhibits the cell wall synthesis by acting as irreversible inhibitor of the enzyme transpeptidase [Kapoor et al., 2017]. CuNPs exhibits antibacterial activities through multiple modes such as ROS generation, inhibition of DNA replication, cytoplasmic leakage, DNA degradation, lipid peroxidation, protein oxidation and dissipation of cell

membrane potential, etc. [Hemeg, 2017]. The observed synergy could have been due to the formation of certain complexes between antibiotics and CuNPs, which inhibits the bacterial growth either by inhibiting the cell wall synthesis or by causing their lysis leading to the cell death [Selvarani, 2010]. The close contact between CuNPs and bacteria enhances the transfer of CuNPs to the bacterial cell by bacterial degradation [Mandava et al., 2017]. Antibiotics also contain active groups like hydroxyl ions, which reacts with CuNPs by chelation and thus enhances their cytotoxic effects [Mandava et al., 2017].

4.6 Conclusion

Irrespective of nanoparticle yield or their hydrodynamic size, CuNPs (sample A, B, C) exhibited strong antibacterial activities against pathogenic (*E. coli, P. vulgaris*) and soil (*B. subtilis, P. fluorescence*) bacteria indicating that scale-up of nanoparticle yield has not adversely affected the biochemical activities of CuNPs. As evident from MIC, MBC, cytoplasmic leakage and ROS assays, antibacterial activities of CuNPs decreases with increase in their hydrodynamic size (sample A $\rightarrow$ C). CuNPs can easily penetrate the cell walls in Gram-negative strains and because of this, antibacterial activities of CuNPs were more pronounced in Gram-negative soil bacteria (*P. fluorescens*). CuNPs induced oxidative stress causes cell death due to nucleic acid and protein oxidation, or through loss of cell membrane integrity and intracellular respiratory failure. CuNPs also exhibits strong synergistic effects on antibacterial activities of conventional antibiotics (tetracycline, streptomycin, kanamycin and ampicillin). CuNPs – antibiotic synergy was highest against Gram-positive, *B. subtilis*, which was otherwise protected by thick and rigid peptidoglycan layer. Combination of CuNPs with conventional antibiotics could prove to be more lethal as compared to nanoparticles or antibiotics alone.

CHAPTER 5

Objective 3 (b) *In vitro* evaluation of cytotoxicity of Copper Nanoparticles

Dose-dependent cytotoxicity of CuNPs (sample A, B and C), whose synthesis protocols are previously described in chapter 3, were evaluated against two clinically important cell lines (MCF-7 Human Breast cancer cell line and RAW 264.7 Macrophage cell line). Effect of nanoparticle per batch yield ([Sample A (yield 0.2 g; particle size 11.34 nm), sample B (yield 0.3 g; particle size 12.19 nm) and sample C (yield 0.4 g; particle size 13.7 nm)]) on the dose-dependent cytotoxicity of CuNPs was determined by MTT (3-(4,5-dimethylthiazol-2-yl)-2,5-diphenyltetrazolium bromide) assay, colorimetric cell viability assay and reactive oxygen species (ROS) assay.

5.1 Material and Methods

Dulbecco's modified eagle's medium (DMEM), 2.5 μg/mL amphotericin B (antifungal), antibiotic solution 100X (100 IU/mL penicillin and 100 μg/mL streptomycin), fetal bovine serum (FBS), phosphate buffer saline (PBS 1X), trypsin-EDTA and 2, 5-diphenyltetrazoliumbromide (MTT) salt, 2, 7-dichlorofluorescin diacetate (DCFH-DA) dye, neutral red and trypan blue were purchased from Himedia. Doxorubicin hydrochloride was obtained from Khandelwal Ltd, India. Dimethyl sulfoxide (DMSO) was procured from Sigma-Aldrich. All aqueous solutions were prepared in sterilized Milli-Q ultrapure water (R = 18.2 MΩ). Tecan Infinite microplate reader was used to measure the spectral response of cell cultures / nanoparticles in 96-well plates in MTT assays. Amount of reactive oxygen species (ROS) produced in cell cultures was measured by fluorescence spectroscopy. Carry Eclipse fluorescence spectrophotometer was used for the fluorescence measurement. Fluorescence was measured at 520 nm (λ_{ex} = 485 nm). Optical and fluorescence microscopy was performed on Nikon eclipse TS100 optical microscope and Dewinter trinocular fluorescence microscope, respectively.

5.2 Cell cultures and CuNPs exposure

MCF-7 (Human breast cancer) and RAW 264.7 (murine macrophage) cell lines were procured from National Centre for Cell Culture (NCCS), Pune, India. They were cultured in DMEM growth media supplemented with 10% FBS, 2.5 μg/mL amphotericin and 1 % antibiotic solution (100 IU/mL penicillin and 100 μg/mL streptomycin). Cultures were maintained at 37 ºC under 5% CO_2 humidified atmosphere. At a confluence of 80-90%, cells were washed with 1X phosphate buffer saline (PBS) and then trypsinzed. Suspensions of suitable cell density were prepared after cell counting. Cells were allowed to adhere to wells of microplates for 24 h before the addition of CuNPs (sample A, B and C). Colloidal CuNPs were diluted in DMEM to have their final concentrations as 0.001,

0.005, 0.01, 0.05, 0.1, 0.5, 1, 10, 15, 20, 25, 30, 40, 50 and 100 μg/mL. After dilution they were sonicated for 10 mins to eradicate agglomerates. Wells containing cells without nanoparticles were treated as negative controls while wells containing cells with 12 μg/mL doxorubicin hydrochloride (DOX) were treated as positive control [Aliabadi et al., 2010; Kumari et al., 2020].

Statistical analysis

Data were expressed as mean ± standard deviation of three independent experiments. Statistical analysis was carried out by using analysis of variance and the mean values were compared by t-tests having $p < 0.05$ as limit of significance [Modem et al., 2017].

5.3 MTT assay

To evaluate dose-dependent cytotoxicity of CuNPs, MTT assay was performed on MCF-7 and RAW 264.7 cell lines. It is a sensitive method for the determination of cell integrity and inhibition of cell proliferation that depends on mitochondrial respiration, which occurs outside the mitochondrial inner membrane and involves NADH and NADPH dependent mechanism that eventually triggers cell inhibition [Berridge and Tan, 1993; Avalos et al., 2014; Alhadlaq et al., 2015]. MTT (3-(4,5-dimethylthiazol-2-yl)-2,5 diphenyltetrazolium bromide) is colorimetric assay which is based on reduction of tetrazolium salt to formazone; a blue coloured compound by mitochondrial dehydrogenases of viable cells [Ahmad et al., 2015]. The insoluble formazone formed in this assay was solubilized in DMSO. Cell cultures (MCF-7 and RAW 264.7) at a cell density of 1×10^4 were seeded in 96-well plate. They were allowed to grow for 24 h at 37 ºC in 5% CO_2 humidified atmosphere. After incubation, the growth media was replaced with the aliquots of fresh growth media containing the sonicated and dispersed CuNPs (sample A, B and C) in adequate concentrations (0-100 μg/mL). Details of test concentrations, concentration of stocks and volumes of CuNPs colloids used in the test were provided in Table 5.1. Plates were then incubated for another 24 h at same culture conditions. After incubation, 20 μL MTT (5 mg/mL in PBS) was added in each well and incubated again for 4 h at culture conditions. Supernatant (150 μL) was removed from each well and 100 μL DMSO was added to dissolve the formazone crystals. The optical density (OD) of each well was measured at 570 nm on microplate reader. For each CuNPs concentration; the absorbance of treated wells (media + cells + CuNPs) was corrected by subtracting the corresponding absorbance of wells containing media and CuNPs. This eliminates the CuNPs contribution to the absorbance. Each experiments were performed in triplicates. The % cell inhibition was calculated by using the following equation [Modem et al., 2017]:

$$\text{Cell Inhibition (\%)} = \frac{[A-B]}{[A]} \times 100 \qquad (5.1)$$

Here, A represents mean differential OD obtained by subtracting the OD of negative controls [wells with untreated cells (i.e. media and cells without any CuNPs)] and blanks [wells with media without cells]. B represents mean differential OD obtained by subtracting the OD of wells with and without CuNPs at each CuNPs concentrations. Both A and B were measured after treating wells with MTT.

In-vitro dose-dependent (0.001-100 μg/mL) toxicity of CuNPs (sample A, B and C) was evaluated in terms of % cell inhibition of MCF-7 (Fig. 5.1(a)) and RAW 264.7 (Fig. 5.1(b)) cell lines. Experiments were repeated three times, with three replicates each, and the % cell inhibition was expressed as the mean of nine values. At $p < 0.05$; the % cell inhibitions are significantly different at all tested concentrations (0.001 - 100 μg/mL). Irrespective of nanoparticle per batch yield, CuNPs exhibits strong concentration - dependent cell cytotoxicity on MCF-7 and RAW 264.7 cell lines. In each tested samples, the % cell inhibition increases with increase in CuNPs concentration. In case of MCF-7 (Fig. 5.1(a)), at lower concentration (< 0.005 μg/mL), the inhibition was < 50 %, and at higher concentrations (> 0.005 μg/mL), the % cell inhibition increased exponentially. Cell viability drops to 0% (inhibition = 100 %), when CuNPs concentration was ≥ 20 μg/mL. In RAW 264.7, at lower concentrations (< 1 μg/mL), the % cell inhibition was < 50 % and it increases exponentially in all test samples for CuNPs concentrations > 1 μg/mL. Cell viability drops to 0 % (inhibition = 100 %), when CuNPs concentration was ≥ 40 μg/mL.

Cytotoxicity of CuNPs against both the cell lines is primarily dose-dependent. However, CuNPs of different hydrodynamic sizes (Table 5.2) behaves differently in different concentration region. In case of MCF-7, the % cell viability of smaller sized nanoparticles (sample A, D_H = 11.3 nm) at low concentrations (< 0.1 μg/mL) was lower as compared to the larger sized nanoparticles (Sample C, D_H = 13.7 nm). At low concentrations, CuNPs were unable to release required copper ions and because of this their toxicity was low. With increase in CuNPs concentration (from 0.1 to 15 μg/mL), the number density of nanoparticles in smaller sized CuNPs (sample A, DH = 11.3 nm) were quite high as compared to larger sized CuNPs (Sample C, DH = 13.7 nm). Therefore, at these concentrations (> 0.1 μg/mL) smaller sized nanoparticles (Sample A) with higher surface area exhibits greater cytotoxicity [Prabhu et al., 2010; Tang et al., 2018]. In contrast to this, cytotoxicity of CuNPs against RAW 264.7 macrophage cell lines depends only on nanoparticle dose and it was nearly independent of the hydrodynamic size of CuNPs. Copper is an essential trace element that is involved in several metabolic pathways at lower concentrations [Azizi et al., 2017] and therefore, at low concentrations CuNPs exhibits low toxicity. At higher concentrations, it inhibits cell proliferation resulting into higher toxicity by interfering with catalytic activities, structural integrity and regulatory functions of the cells [Azizi et al., 2017].

Table 5.1 Test concentrations, concentration of stocks (from which dilutions have been made) and volume of colloids (Sample A, B and C)

Tested concentrations (μg/mL)	Stock concentrations (μg/mL)	Volume used for ROS assay* (μL)	Volume used for MTT assay** (μL)
0.001	0.1	20	2
0.005	0.1	--	10
0.010	1.0	20	2
0.05	1.0	--	10
0.100	1.0	200	20
0.500	20.0	--	5
1.000	20.0	100	10
10.000	20.0	1000	100
15.000	50.0	600	60
20.000	50.0	--	80
25.000	50.0	--	100
30.000	50.0	--	120
100.000	1147 (sample A), 1601 (sample B), 2873 (sample C)	--	15

*Calculations were based on the total volume of the well, which was 200 μL for 94-well plates used in the MTT assays.

**These calculations were based on the total volume of the well, which was 2000 μL for 6-well plates used in the ROS assays.

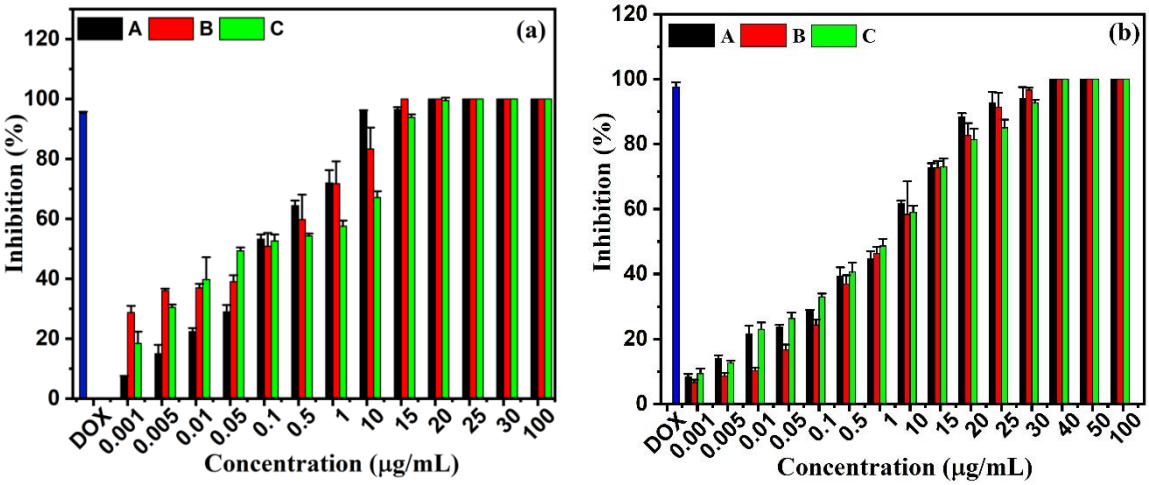

Figure 5.1 Dose-dependent cytotoxicity of CuNPs [Sample A (yield 0.2 g; particle size 11.34 nm), sample B (yield 0.3 g; particle size 12.19 nm) and sample C (yield 0.4 g; particle size 13.7 nm)] determined by MTT assay on (a) MCF-7 human breast cancer cell and (b) RAW 264.7 macrophage cell line. Doxorubicin (DOX) (12 μg/mL) was used as positive control. % Inhibition was expressed as mean ± standard deviation of three set of three independent experiments. As indicated by t-tests, statistical data were significant different at $p < 0.05$.

IC_{50} is a concentration at which the % cell inhibition is reduces to 50%. It is an important pharmacological measure used to determine the effectiveness of the toxicity of nanoparticles. From MTT assay, IC_{50} values of CuNPs (samples A, B and C) against MCF-7 and RAW 264.7 cell lines were determined, which are reported in Table 5.1.

Table 5.2 Nanoparticle yield, hydrodynamic size, Cu concentration in colloids and IC_{50} values of as-synthesized CuNPs

Sample	Yield (g)	Hydrodynamic size (nm)	Cu concentration (μg/mL)	IC_{50} (μg/mL)	
				MCF-7 cell lines	RAW 64.7 cell lines
A	0.2	11.34	1147	0.31	4.37
B	0.3	12.19	1601	0.54	4.89
C	0.4	13.70	2873	0.71	5.04

Against MCF-7, the IC_{50} values of CuNPs were 0.31, 0.54 and 0.71 μg/mL for sample A, B and C, respectively. Whereas against RAW 264.7, IC_{50} values of CuNPs were 4.37, 4.89 and 5.04 μg/mL for samples A, B and C, respectively. IC_{50} values of all the tested CuNPs were in the range of 0.3-0.7 μg/mL for MCF-7 and 4-5 μg/mL for RAW 264.7. Irrespective of nanoparticle yield, IC_{50} values of CuNPs (Sample A, B, C) were much lower for MCF-7 as compared to RAW 264.7 suggesting CuNPs possess greater

cytotoxicity against MCF-7 breast cancer cells. Further, over all change in IC_{50} values *viz-a-viz* tested concentration range (0-100 μg/mL) was minimal, suggesting that the scale-up of CuNPs per batch yield did not significantly alter the cytotoxicity of nanoparticles. This indicates that the scale-up protocols presented in this work do not impact negatively on the bio-activities of CuNPs.

5.4 Colorimetric Cell Viability Assay: Live and Dead Cells Staining

To differentiate between live and dead cells, colorimetric cell viability assay was done. Cultures were stained with neutral red and trypan blue [Sumit et al., 2018]. For staining, both cell lines (MCF-7 and RAW 264.7) were seeded at the cell density of 1×10^4/well in 96-well plates and cells were allowed to adhere for 24 h at 37 ºC in 5% CO_2 humidified atmosphere. After incubation, the growth media was replaced with the aliquots of fresh growth media containing the desired concentration of CuNPs. Four concentrations of each CuNPs (sample A, B and C) that corresponds to 25 %, 50 %, 75 % and 100 % cell inhibition in MTT assay were chosen for colorimetric cell viability assay. Plates were then incubated for another 24 h in the same culture conditions. After incubation, old media from each well was removed and cells were washed twice with PBS. For cell staining, 100 μL of neutral red (200 μg/mL in DMEM) was added to each well and incubated for another 4 h at 37 ºC in 5% CO_2 humidified atmosphere. After incubation for 4 h, cells were washed with PBS and stained with 40 μL of trypan blue (0.4 % w/v). Plates were again incubated for another 15 mins. Each well was then washed with PBS.

To understand the effect of CuNPs on the cellular morphology of MCF-7 breast cancer cell lines and RAW 264.7 macrophage cell lines, optical microscopy was performed after staining. Optical micrographs of MCF-7 and RAW 264.7 cell lines obtained after cell staining were shown in Fig. 5.2 and Fig. 5.3, respectively. Neutral red dye was picked by live cells, which appear red in micrographs, while the trypan blue was picked by the dead cells and they appear blue in the micrographs. All cells in micrographs of controls (0% CuNPs) appear red as in the absence of CuNPs, no cell inhibition was expected. Further, no changes in the size and morphology of cells were observed in controls.

Cells treated with lower concentration of CuNPs show fewer changes in the cell morphology as compared to cells treated with higher concentrations in both cell lines (Fig. 5.2 and Fig. 5.3). The MCF-7 controls (cells without CuNPs treatment) show typical epithelial polygonal shape with high density of cell layers growing in compact (Fig. 5.2). Whereas, MCF-7 cells treated with CuNPs show irregular or round shape cells or cells with shrinkage having low density of cell layers, which were grown loose [Khan et al., 2018; Clarance et al., 2020]. The RAW 264.7 controls (cells without CuNPs treatment) show small cells in round shape grown as monolayer (Fig. 5.3).

Whereas, RAW 264.7 cells treated with CuNPs elongates into polygonal or irregular shape with low density. As shown in Fig. 5.3, some treated cells also show dendrite like morphologies [Loan et al., 2019; Zhang et al., 2019]. As seen in Fig. 5.2 and Fig. 5.3, the CuNPs treated cells of both the cell lines lose their morphological integrity. This was evident from rupture of cell membrane, cell shrinkage, conversion to irregular shape and fragmentation of cells.

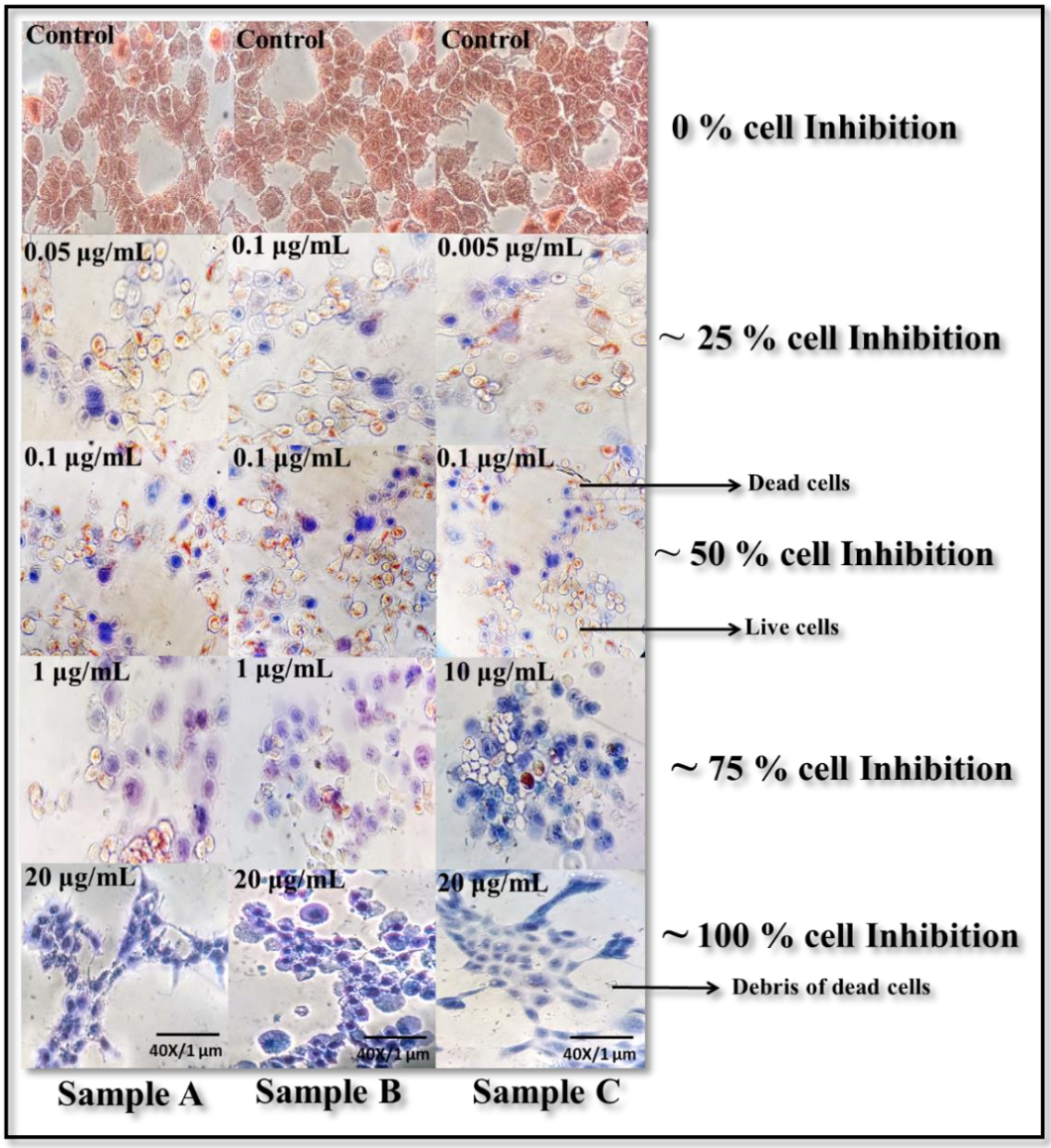

Figure 5.2 Optical microscopic images (20 X) of live and dead MCF-7 cells treated with CuNPs [Sample A (yield 0.2 g; particle size 11.34 nm), sample B (yield 0.3 g; particle size 12.19 nm) and sample C (yield 0.4 g; particle size 13.7 nm)]. The staining was done after 24 h treatment of cells with CuNPs. Red color represents staining of live cells and blue color represents staining of dead cells after 24 h incubation. Control represents microscopic images of MCF-7 cells not treated with CuNPs.

Decreasing number of cells stained with neutral red and increasing number of cells stained with trypan blue was observed in the micrographs with increasing concentration of CuNPs. The presence of large cellular debris observed in the micrographs formed due to the apoptotic cell death. At CuNPs concentration corresponding to 100 % cell inhibition, no surviving cells were observed (Fig. 5.2: 20 µg/mL and Fig. 5.3: 30 µg/mL). This was also in good agreement with the observations of MTT assays (Fig. 5.1). Further, live and dead staining also confirms that the morphological and cytotoxic effects of CuNPs on MCF-7 and RAW 264.7 cell lines were identical and independent of nanoparticles per batch yield.

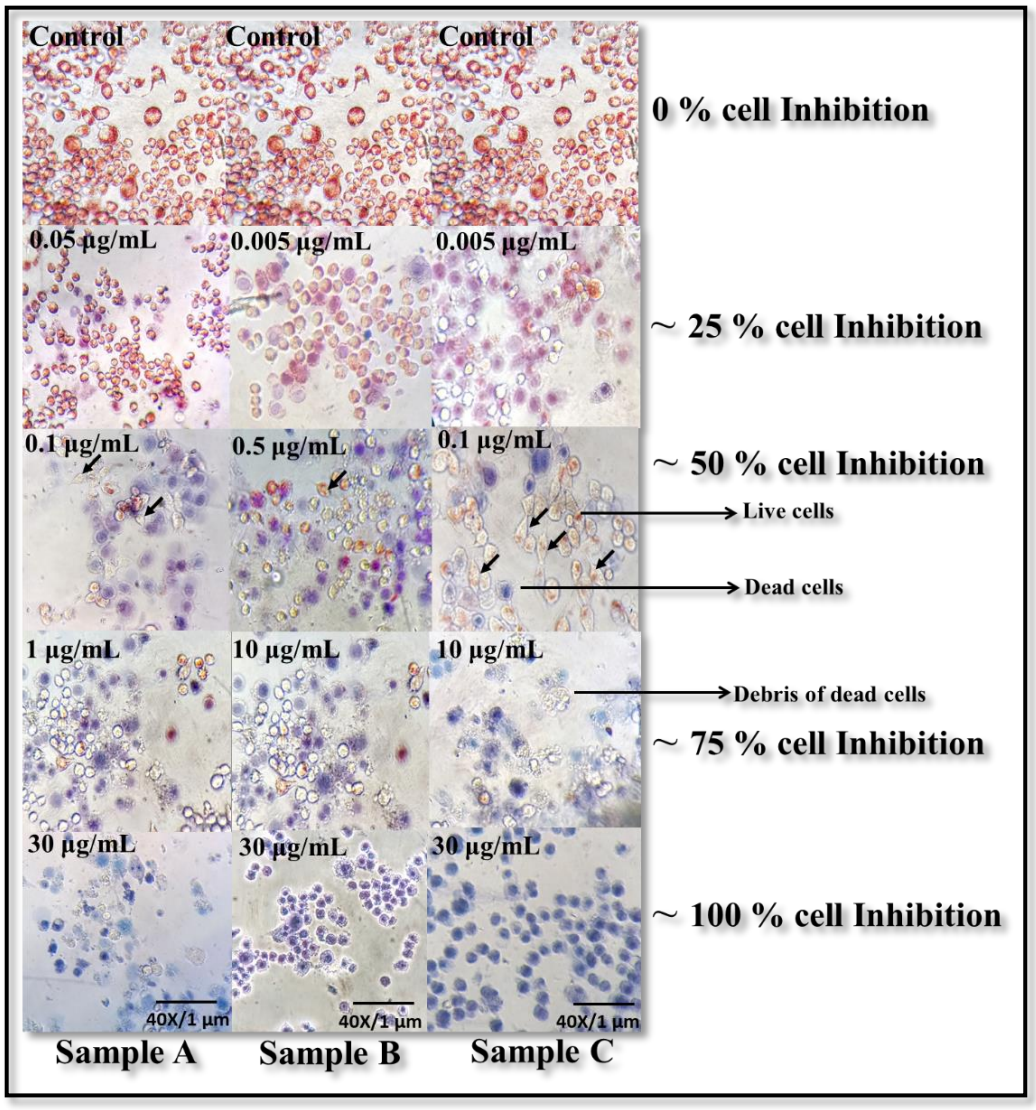

Figure 5.3 Optical microscopic images (20 X) of live and dead RAW 264.7 cells treated with CuNPs [Sample A (yield 0.2 g; particle size 11.34 nm), sample B (yield 0.3 g; particle size 12.19 nm) and sample C (yield 0.4 g; particle size 13.7 nm)]. The staining was done after 24 h treatment of cells with CuNPs. The arrows represent the formation of dendritic like bodies after treatment with CuNPs. Red color represents staining of live cells and blue color represents staining of dead cells after 24 h incubation. Control represents microscopic images of RAW 264.7 cells not treated with CuNPs.

5.5 Reactive Oxygen species (ROS) assay

Interaction of nanoparticles with cells can produce ROS that result into oxidative stress which can cause external or internal cell damage [Jeong et al., 2011]. ROS can affect various cell functions by interfering with cellular components such as lipids and proteins, causing DNA fragmentation which lead to the cell death by apoptotic or necrosis pathways [Jeong et al., 2011; Li et al., 2012]. ROS assay was used to understand the process of cell death in CuNPs treated MCF-7 and RAW 264.7 cell lines.

Intracellular reactive oxygen species (ROS) generation in cell lines after treating them with CuNPs was measured with the help of fluorescent dye DCFH-DA (dichloro-dihydro-fluorescein diacetate) [Hong and Joseph, 1999]. DCFH-DA has no fluorescence and passively enters into the cell through plasma membrane, where it is converted to DCFH by intracellular esterase. DCFH as such cannot pass through the cell membrane and gets oxidized by cellular ROS to highly fluorescent derivative DCF (2', 7'-dichlorofluorescein) whose fluorescence intensity is directly proportional to the ROS generated intracellularly [Yanjie et al., 2014].

ROS generation in CuNPs treated MCF-7 and RAW 264.7 cells lines were measured by two methods: fluorometric quantitative assay and cell imaging by fluorescence microscopy [Maqusood et al., 2016]. From both these measurements, ROS generation in MCF-7 and RAW 264.7 was estimated both quantitatively and qualitatively. For quantitative fluorometric assay, MCF-7 and RAW 264.7 cells lines at a cell density of 2.5×10^4 cell/well were seeded in 6-well plates and incubated for 24 h at 37 ºC in 5% CO_2 humidified atmosphere. These cells were then treated with CuNPs. Tests concentrations of CuNPs along with details of volumes used were provided in Table 5.2. Plates were incubated for 24 h at same culture conditions. Hydrogen peroxide (0.1 mM) was used as a positive control [Maqusood et al., 2016]. 10 mM stock solution of DCFHDA was prepared in DMSO and further diluted in DMEM (without FBS) to yield a working solution of 100 μM DCFHDA [Gaharwar et al., 2017]. After incubation, the supernatant from each well was discarded. Following this, cells were washed with PBS. 1 mL of working solution of DCFHDA was added in each well and cells were incubated at 37 ºC for 30 mins in dark. After incubation, cells were lysed by using trypsin-EDTA solution and then centrifuged at 2000 rpm for 10 mins. Controls (media + cell) were also treated with the same amount of DCFH-DA under identical conditions. 1 mL supernatant from each well was used for the fluorescence intensity measurement at 520 nm.

Fluorescence intensity of CuNPs treated cells was shown in Fig. 5.4. Fluorescence intensity of control (media + cells) was set at 100 % and fluorescence intensity of CuNPs treated cells was presented as relative intensity (%) of control.

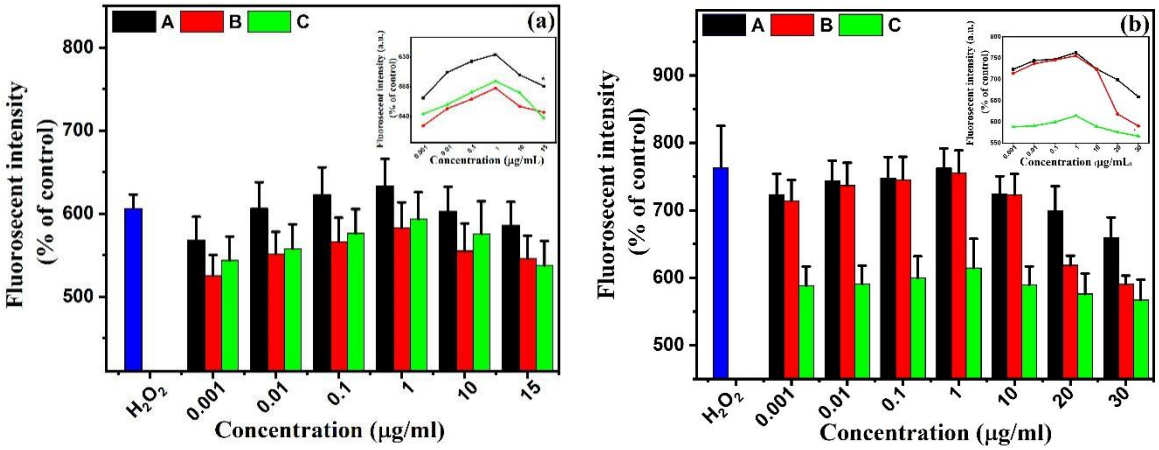

Figure 5.4. Intracellular ROS generation (measured in terms of fluorescence intensity of DCF) in (a) MCF-7 and (b) RAW 264.7 cell lines treated with CuNPs [Sample A (yield 0.2 g; particle size 11.34 nm), sample B (yield 0.3 g; particle size 12.19 nm) and sample C (yield 0.4 g; particle size 13.7 nm)]. Untreated cells were negative control and hydrogen peroxide (0.1 mM) treated cells were positive control. Intensity values were expressed as % of negative control which was adjusted to 100 %. Each data point was expressed as mean ± standard deviation of three experiments. Statistical data at all tested concentrations were not significant different at $p < 0.05$ as indicated by t-tests.

Oxidative stress generated by intracellular ROS and measured in term of fluorescence intensity of DCFH in CuNPs treated MCF-7 and RAW 264.7 exhibits weak concentration dependence. In both the cell lines the fluorescence intensity increases with the increase in the CuNPs concentration. Irrespective of the CuNPs per batch yield or their hydrodynamic size, ROS level in cell lines increases with increase in CuNPs concentration. It peaks around CuNPs concentration, which was its IC_{50} (Table 5.2). Beyond this concentration (> 1 μg/mL), the fluorescence intensity was quenched in both the cell lines. This might be because of drastic decrease in the % of surviving cells, which was observed in MTT assay (Fig. 5.1). Similar trend of ROS dependence on nanoparticle concentration was previously reported by Yanjie et al., 2014 in HepG2 cells treated with AuNCs. Concentration dependence of observed ROS of all three samples in both MCF-7 and RAW 264.7 were statistically insignificant as indicated by t-tests ($p < 0.005$). However, there was a marked difference in the ROS production of Sample A as compared to sample B and C in MCF-7. In RAW 264.7, there was a marked difference in the ROS production of Sample C as compared to sample A and B. Hence, viz-a-viz to nanoparticle size, ROS production of sample A and Sample C was statistically different in MCF-7 and RAW 264.7, respectively. This might be because of difference in preferential binding sites in two cell lines [Zhang et al., 2016].

Fluorescence microscopy on CuNPs treated MCF-7 and RAW 264.7 cells was also performed after incubating them for 30 min in dark. Effect of oxidative stress on the cell morphology of MCF-7 and RAW 264.7 cells were shown in Fig. 5.5 and Fig. 5.6, respectively.

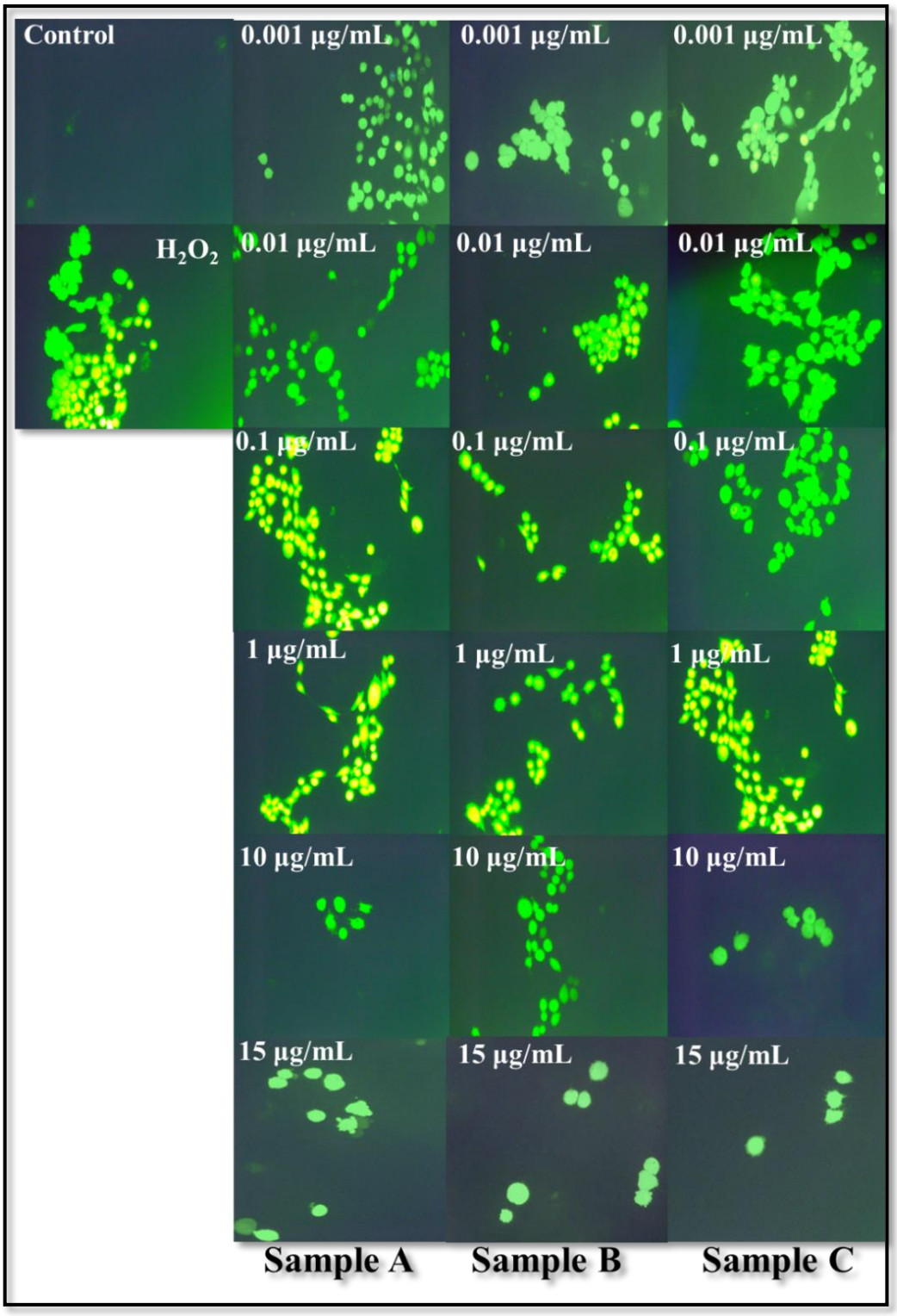

Figure 5.5 Fluorescent microscopic images of MCF-7 human breast cancer cell lines after treatment with CuNPs [Sample A (yield 0.2 g; particle size 11.34 nm), sample B (yield 0.3 g; particle size 12.19 nm) and sample C (yield 0.4 g; particle size 13.7 nm)]. Concentration of CuNPs was varied from 0 – 15 µg/mL. The untreated cells were negative control (without CuNPs) and hydrogen peroxide treated cells were the positive control.

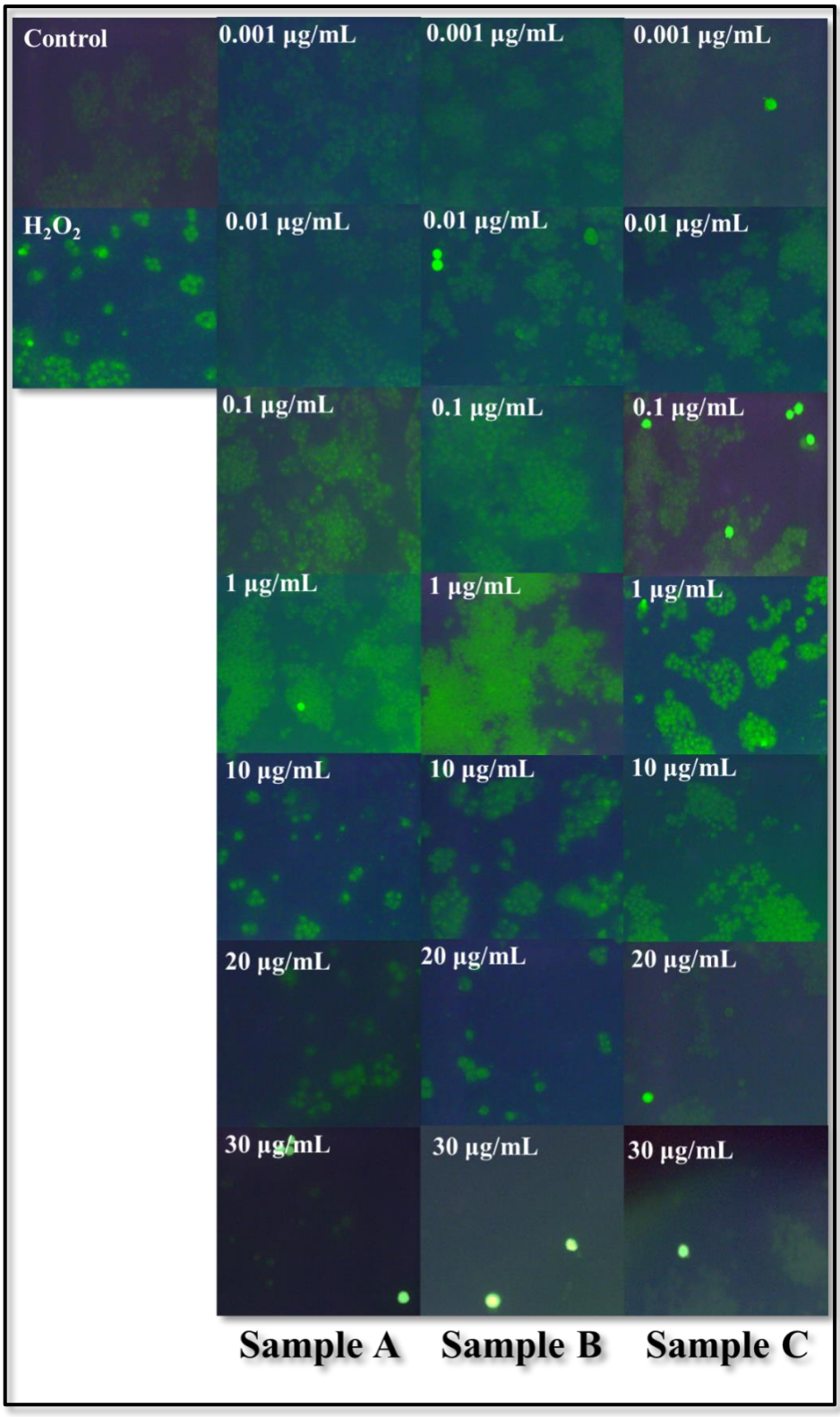

Figure 5.6 Fluorescent microscopic images of RAW 264.7 macrophage cell lines after treatment with CuNPs [Sample A (yield 0.2 g; particle size 11.34 nm), sample B (yield 0.3 g; particle size 12.19 nm) and sample C (yield 0.4 g; particle size 13.7 nm)]. Concentration of CuNPs was varied from 0 – 30 µg/mL. Untreated cells were negative control (without CuNPs) and hydrogen peroxide treated cells were the positive control.

In both the Figures, fluorescence intensity of cells increases with increase in CuNPs concentration till 1 μg/mL. Beyond this concentration, the florescence intensity was visibly quenched. This observation was in good agreement with the fluorometric quantitative assay (Fig. 5.4). Oxidative stress generated by ROS was higher in CuNPs treated cells having smaller hydrodynamic size (sample A) in both the cell lines. This is in good agreement with the existing literature [Mendoza et al., 2014; Zhang et al., 2018]. However, at tested concentration (0.001 μg/mL-30 μg/mL) with different size nanoparticles (sample A -11.34 nm, sample B-12.19 nm and sample C-13.7 nm), fluorescence intensity did not change significantly in both cell lines, indicating that cells were under similar oxidative stress level due to the ROS generation. Persistent of similar cellular stress may enhance other pathways of cell damage such as rupturing of cell membrane, shrinkage and fragmentation of cells causing the observed cytotoxicity of CuNPs in MCF-7 and RAW 264.7 (Fig. 5.2 and Fig. 5.3).

5.6 Conclusion

MTT, colorimetric, and ROS assays along with optical and fluorescence microscopy confirmed the strong dose-dependent cytotoxicity of as-synthesized CuNPs against MCF-7 human breast cancer cell line and RAW 264.7 macrophage cell lines. No significant difference was observed in the cytotoxicity of CuNPs of samples A (0.2 g), B (0.3 g), and C (0.4 g) having hydrodynamic size of 11-14 nm. This suggests that the cytotoxicity of the CuNPs was independent of nanoparticle yield and it only depends on nanoparticle dose. Oxidative stress produced by generation of extracellular ROS in the cells treated with CuNPs might have damaged membrane lipids causing cell shrinkage and fragmentation leading to the cell death. Further investigation is required to pinpoint the exact mechanism of cytotoxicity of CuNPs in MCF-7 human breast cancer cell line and RAW 264.7 macrophage cell lines. This study confirms that increase in CuNPs yield from 0.2 to 0.4 g has no negative correlation with their cytotoxic response. The ability to scale up the nanoparticle yield with strong dose-dependent cytotoxicity makes CuNPs potential candidate for the development of anticancer drugs.

CHAPTER 6

Summary

Colloidal copper nanoparticles (CuNPs) with moderate yield were synthesized by chemical reduction method. CuNPs were prepared by reducing copper (II) chloride with a combination of strong ($NaBH_4$) and weak (L-ascorbic acid) reducing agents in the presence of a capping agent (PVP). Synthesis protocols (copper precursors, reaction temperature and reaction time) were optimized by monitoring surface plasmon resonance (SPR), hydrodynamic particle size and per batch yield of CuNPs. $CuCl_2$ as copper precursor, reaction time of 5 min and reaction temperature of 80 °C were the optimized parameter. With these parameters, CuNPs with moderate per batch yield (0.2 g), small hydrodynamic particle size (38 ± 0.52 nm) and stable SPR (571.5 ± 10 nm) were prepared.

Under optimized synthesis conditions, per batch yield of CuNPs were further scaled-up from 0.2 g (sample A) to 0.4 g (sample C). No major impact of process scale-up on physical and plasmonic properties of CuNPs were observed. Irrespective of per batch yield, synthesized CuNPs exhibited a single SPR band, which was centred at 568 nm. Presence of single SPR band in the UV-visible spectra of as-synthesized CuNPs indicated that small spherical nanoparticles were formed, which was further confirmed by transmission electron microscopy and photon correlation spectroscopy (PCS). A monomodal hydrodynamic particle size distribution was observed in the PCS study, which has further confirmed the formation of symmetric (spherical) nanoparticles. As-synthesized CuNPs exhibited small hydrodynamic particle size (11-14 nm), which was in good correlation with their physical size (9.88 - 11.49 nm) obtained from TEM. As evident from the zeta potential (-44 ±2 mV) of as-synthesized colloids, irrespective of per batch yield, CuNPs exhibited good colloidal stability.

Effects of aging on the colloidal stability of CuNPs (sample A, B and C) against oxidation and aggregation were evaluated in terms of changes in their hydrodynamic particle size and its influence on the plasmon resonance band (λ_{SPR} and A_{max}). With aging a gradual increase in the hydrodynamic size of CuNPs was observed, which had resulted in gradual red shift of SPR band, indicating a possible aggregation of nanoparticles. Irrespective of per batch yield, CuNPs colloids were stable for ≈ 180 days.

In vitro antibacterial activities of CuNPs (sample A, B and C) were evaluated by MIC (minimum inhibitory concentration), MBC (minimum bactericidal concentration), cytoplasmic leakage and ROS (reactive oxygen species) assays on two pathogenic [(*Escherichia coli* (MTCC No. 739), *Proteus vulgaris* (MTCC No. 426)] and two soil bacteria [*Bacillus subtilis* (MTCC No. 441), *Pseudomonas fluorescens* (MTCC No. 1749)]. Both MIC and MBC depicted bacteriolytic actions of CuNPs in concentration

dependent manner.

Irrespective of nanoparticle yield or their hydrodynamic size, CuNPs (sample A, B, C) exhibited strong antibacterial activities against pathogenic (*E. coli, P. vulgaris*) and soil (*B. subtilis, P. fluorescence*) bacteria indicating that scale-up of nanoparticle yield has not adversely affected the biochemical activities of CuNPs. Concentration dependent cytoplasmic leakage of sugars and proteins and oxidative stress induced by reactive oxygen species (ROS) produced by CuNPs-bacteria interactions were also observed. As evident from MIC, MBC, cytoplasmic leakage and ROS assays, antibacterial activities of CuNPs decreases with increase in their hydrodynamic particle size (sample A $\rightarrow$ C).

CuNPs can easily penetrate the cell walls in Gram-negative strains and because of this, antibacterial activities of CuNPs were more pronounced in Gram-negative soil bacteria (*P. fluorescens*). CuNPs induce oxidative stress causes cell apoptosis by DNA, nucleic acid and protein oxidation, or thorough loss of cell membrane integrity and intracellular respiratory failure. CuNPs also exhibited strong synergistic effects on antibacterial activities of conventional antibiotics (tetracycline, streptomycin, kanamycin and ampicillin). CuNPs – antibiotic synergy was highest against Gram-positive, *B. subtilis*, which was otherwise protected by thick and rigid peptidoglycan layer. Thus, combination of CuNPs with conventional antibiotics could prove to be more lethal as compared to nanoparticles or antibiotics in isolation.

Dose-dependent cytotoxicity of CuNPs (sample A, B and C) were also evaluated against two clinically important cell lines (MCF-7 human breast cancer cell line and RAW 264.7 macrophage cell line) by MTT (3-(4,5-dimethylthiazol-2-yl)-2,5-diphenyltetrazolium bromide) assay, colorimetric cell viability assay and ROS (reactive oxygen species) assay. CuNPs induced morphological changes in MCF-7 and RAW 264.7 cell lines. CuNPs treated cells show ruptured cells with nuclear fragmentation indicated by the presence of large cellular debris, which were formed because of apoptotic cell death. IC_{50} values of CuNPs were independent of per batch yield. No significant difference was observed in the cytotoxicity of CuNPs (sample A, B and C). This suggests that the cytotoxicity of the CuNPs was independent of nanoparticle yield and only depends on its dose. This confirms that increase in CuNPs yield from 0.2 g to 0.4 g has no negative correlation with their cytotoxicity. The ability to scale-up the nanoparticle yield with strong dose-dependent cytotoxicity makes CuNPs a potential candidate for the development of antineoplastic drugs.

Future Scope of Work

As-synthesized CuNPs can find potential applications in pharmaceutical and health-care industries. Commercial applications of these nanostructures and their formulations with conventional antibiotics further requires development of large scale synthesis protocols, which could yield air stable CuNPs with reproducible physical, plasmonic and

biochemical properties. CuNPs prepared in the present study were stable against oxidation and aggregation for 180 days, beyond which they loses their colloidal stability and plasmonic properties. Shelf life of CuNPs needs to be further improved.

Multiple reports on antibacterial and cytotoxic activities of CuNPs suggests that before commercial utilization of these nanoparticles, they have to pass through clinical trials in accordance with the regulatory standards set by different agencies like food and drug administration (FDA) and health ministry. These standards define permissible dosage and exposure limits. For nanomaterial-based antibiotics, such standards are not available. An extension of *in vitro* cytotoxicity study of CuNPs on other important clinical cell lines needs to be carried out followed by a detailed toxicity analysis *in vivo* as per clinical standards of regulatory agencies before concluding feasibility of antineoplastic drugs. A detailed *in vitro* study needs to be conducted to understand the mechanisms responsible for antibacterial and cytotoxic activities of CuNPs. Pathogenic microorganisms, which are developing resistance to conventional antibiotics through mutations as well as genetic recombination are unlikely to develop similar resistance against CuNPs. However, this claim needs to be ascertained by testing CuNPs and CuNPs-antibiotics cocktails against pathogenic strains resistant to multiple antibiotics.

Nanoparticles are now explored in large number of technical, engineering and medical products and eventually leach out and bioaccumulate causing severe damage or alteration to terrestrial ecosystem. A detailed systematic study needs to be carried out to ascertain impacts of nanoparticles on soil and aquatic ecosystem. Leaching of nanoparticles could alter soil properties like pH, cation exchange capacity, porosity, organic matter content and availability of plant nutrients. They also impact soil enzyme activities, microbial communities and biogeochemical nutrient cycling. *In-situ* studies needs to be conducted to gauge the overall impact of nanoparticles on soil health and soil micro flora, which will eventually define permissible levels of nanoparticles in air, soil and water bodies.

References

- A Alshareef, K Laird and RBM Cross, 2017, Acta Metallurgica Sinica (English Letters), 30, 29.
- A Alum, A Alboloushi and M Abbaszadegan, 2018, Journal of Environmental Science and Health, Part A, 53, 643.
- A Avalos, AI Haza, D Mateo and P Morales, 2014, Journal of Applied Toxicology, 4, 413.
- A Azam, AS Ahmed, M Oves, MS Khan, SS Habib and A Memic, 2012, International Journal of Nanomedicine, 7, 6003.
- A Dhanalakshmi, A Palanimurugan and B Natarajan, 2018, Materials Science and Engineering C, 90, 95.
- A Khan, A Rashid, R Younas and R Ching, 2016, International Nano Letters, 6, 21.
- A Maqusood, JV Akhtar JV, AA Hisham and AWS Alshamsan, 2016, Colloids and Surface B: Biointerfaces, 142, 46.
- A Mendoza, JA Torres-Hernandez, JG Ault, JH Pedersen-Lane, D Gao and DA Lawrence, 2014, Cell Stress and Chaperones, 19, 777.
- A Nel, T Xia, L MaEdler and N Li, 2006, Science, 311, 622.
- A Olad, M Alipour and R Nosrati, 2017, Bulletin of Materials Science, 40, 1013.
- A Orell, CA Navarro, R Arancibia, JC Mobarec, and CA Jerez, 2010, Biotechnology Advances, 28, 839.
- A Sharma, AK Goyal and G Rath, 2017, Journal of Drug Targeting, 26, 617.
- A Tokeer, AW Irshad, M Nikhat, A Jahangeer and MS Abdullah, 2013, Colloids and Surfaces B: Biointerfaces, 107**,** 227.
- A Yuqab, N Malkani, A Shabbir, AS Ditta, F Tanvir, S Ali, M Naz, SAR Kazmi and R Ullah, 2020, Current Microbiology, 77, 2287.
- ABS Sastry, RBK Aamanchi, CRL Prasad and BS Murthy, 2013, Environmental Chemistry Letters, 11, 183.
- AD Karthik and K Geetha, 2013, Journal of Applied Pharmaceutical Science, 3, 16.
- AJ Bone, BP Colman, AP Gondikas, KM Newton, KH Harrold, RM Cory, JM Unrine, SJ Klaine, CW Matson and RT Di Giulio, 2012, Environmental Science Technology, 46, 6925.
- AK Chatterjee, R Chakraborty and T Basu, 2014, Nanotechnology, 25, 135101.
- AK Chatterjee, RK Sarkar, AP Chattopadhyay, P Aich, R Chakraborty and T Basu, 2012, Journal of Nanotechnology, 23, 085103.
- AM Allahverdiyev, KK Volodymyrivna, ES Abamor, M Bagirova and M Rafailovich, 2011, Expert Review of Anti-Infective Therapy, 9, 1035.

- B Aslam, W Wang, MI Arshad, M Khurshid, S Muzammil, MH Rasool, MA Nisar, RF Alvi, MA Aslam, MV Qamar, MKF Salamat and Z Baloch, 2018, Infection and drug Resistance, 11, 1645.
- B Bagchi, S Dey, S Bhandary, S Das, A Bhattacharya, R Basu and P Nandy, 2012, Materials Science and Engineering C, 32, 1897.
- B Janic, F Liu, KR Bobbitt, SL Brown, IJ Chetty, G Mao, B Movsas and N Wen, 2018, Journal of Nanomedicine and Nanotechnology, 9, 1.
- B Spellberg and DN Gilbert, 2014, Clinical Infectious Disease, 59, 71.
- B Spellberg, A Srinivasan and HF Chambers, 2016, Journal of American Medical Association, 315, 1229.
- BM Prabhu, SF Ali, RC Murdock, SM Hussain and M Srivatsan, 2010, Nanotoxicology, 4,150-160.
- BP Colman, CL Arnaout, S Anciaux, CK Gunsch, MF Hochella, B Kim, GV Lowry, BM McGill, BC Reinsch, CJ Richardson, JM Unrine, JP Wright, L Yin and ES, Bernhardt, 2013, PLoS One, 8, e57189.
- BP Sekhon, 2010, Journal of Pharmaceutical Education and Research, 1, 1.
- BS Sooch, MK Mann and M Sharma, 2020, Journal of Cluster science, https://doi.org/10.1007/s/10876-020-01878-5.
- C Carlson, SM Hussain, AM Schrand, LK Braydich-Stolle, KL Hess, RL Jones and JJ Schlage, 2008, Journal of Physical Chemistry B, 112, 13608.
- C Khurana, AK Vala, N Andhariya, OP Pandey and B Chudasama, 2014, Journal of Biomedical Materials Research A, 102A, 3361.
- C Khurana, AK Vala, N Andhariya, OP Pandey and B Chudasama, 2014, Environmental science processes and impacts, 16, 2191.
- C Khurana, N Andhariya, OP Pandey and B Chudasama, 2013, RSC Advances, 3, 1127.
- C Khurana, P Sharma, OP Pandey and B Chudasama, 2016, Journal of Materials Science and Technology, 32, 524.
- CL Ventola, 2015, Pharmacy and Therapeutics, 40, 277.
- Coronavirus Outbreak. Available at: https://www.worldometers.info/coronavirus/. Accessed 26 April 2020.
- CW Wu, BP Mosher and TF Zeng, 2006, Journal of Nanoparticle Research, 8, 965.
- D Aditi, M Subhankar, C Sourav, M Dipankar, C Dipankar, R Anupam, D Subhjit, GC Braja and R Somenath, 2019, Journal of Saudi Chemical Society, 23 222.
- D Laha, A Pramanik, J Maity, A Mukherjee, P Pramanik, A Laskar and P Karmakar, 2014, Biochemistry and Biophysics Acta, 1840, 1.
- D Laha, A Pramanik, S Chattopadhyay, SK Dash, S Roy, P Pramanik and P Karmakar, 2015, RSC Advances, **5**, 68169.
- D Manayasree, MP Kiran and R Kumar, 2017, International Journal of Applied Pharmaceutics, 9, 71.

- D Nayak, S Ashe, PR Rauta, M Kumari and B Nayak, 2016, Materials Science and Engineering C, 58, 44.
- D Oleszak and PH Shingu, 1996, Journal of Applied Physics, 79, 2975.
- D Pissuwana, T Niddomea and MB Cortiec, 2011, Journal of Control Release, 149, 65.
- D Sahu, GM Kanan and R Vijayaraghavan, 2014, Journal of Toxicology and Environmental Health, Part A, 77, 177.
- DE Bloom and D Cadarette, 2019, Frontiers in Immunology, 10, 549.
- DG Diana, AK Perla, P Sanjiv, RD Antonio, PL Paulina and GR Santiaqo, 2019, Pharmaceutics, 11, 30.
- DS Sukar and RM Albadran, 2015, European Journal of Experimental Biology, 3, 354.
- E Etebu and I Arikekpar, 2016, International Journal of Applied Microbiology and Biotechnology Research, 4, 90.
- E Laseni, F Navi, R Lasemi and N Lasemi, 2016, A Textbook of Advanced Oral and Maxillofacial Surgery, 3.
- ES Azam and WA EI-Said, 2014, Bioorganic Chemistry, 57, 5.
- F Chen, Z Shi, KG Neoh and ET Kang, 2009, Biotechnology and Bioengineering, 104, 30.
- F Faedmaleki, FH Shirazi, AA Salarian, HA Ashtiani and H Rastegar, 2014, Iranian Journal of Pharmaceutical Research, 13, 235.
- F González-Candelas, I Comas, JL Martínez, JC Galán, F Baquero, 2017, Ed.; Elsevier: London, UK, 257.
- F Mirajani, A Ghassempur, A Aliahmadi and MA Esmaeili, 2011, Microbiological Research, 62, 542.
- F Rispoli, A Angelov, D Badia, A Kumar, S Seal and V Shah, 2010, Journal of Hazardous Materials, 180, 212.
- FA Khan, S Akhtar, SA Almofty, D Alomhazad and M Alomeri, 2018, Biomolecules, 8, 1-13.
- Fellahi, RK Sarma, MR Das, R Saikia, L Marcon, Y Coffinier, T Hadjersi, M Maamache and R Boukherroub, 2013, Nanotechnology, 13. 495101.
- G Kapoor, S Saigal and A Elongavan, 2017, Journal of Anesthesiology Clinical Pharmacology, 33, 300.
- G Mary, SK Baypai and N Chand, 2009, Journal of Applied Polymer Science, 113, 757.
- G Miller, 1959, Analytical Chemistry, 31, 426.
- G Shobha, S Sagar, KS Shashidhara, V Mahadimane and S Ananda, 2019, Research Journal of Biotechnology, 14, 105.
- GAM Castanon, NN Martinez, FM Gutierrez, JRM Mendoza and F Ruiz, 2008, Journal of Nanoparticle Research, 10, 1343.

- GD Saratale, RG Saratale, D Kim, DY Kim and HS Shin, 2020, Nanomaterials, 10, 1457.
- GDB 2015 Diseases and Injury Incidence and Prevalence Collaborates, The Lancet, 388, 1459.
- GN Kumar, SD Pandey, S Mallick, SK Ghosh, P Pramanik and AS Ghosh, 2020, Indian Journal of Biochemistry and Biophysics, 57, 151.
- GV Vimbela, SM Ngo, C Fraze, L Yang and D Stout, 2017, International journal of nanomedicine, 12, 3941.
- H Khaid, S Shamaila and N Zafar, 2015, Science International, 27, 3085.
- H Libalova, PM Costa, M Olsson, L Farcal, S Ortelli, M Blosi, J Topinka, AL Costa and B Fadeel, 2017, Chemosphere, 196, 482.
- H Sadeghi-Aliabadi, M Minaiyan and A Dabestan, 2010, Research in Pharmaceutical Sciences, 5, 127-133.
- H Tang, M Xu, XR Zhou, X Zhang, L Zhao, G Ye, F Shi, C Lv and Y Li, 2018, Material Science and Engineering C, 93, 649.
- HA Alhadlaq, MJ Akhtar and M Ahamed, 2015, Cell Biology, 55, 1.
- HA Hemeg, 2017, International Journal of nanomedicine, 12, 8211.
- Hackett DW. Hepatitis A outbreak reaches 10,582 cases during 2018. *Precision Vaccines*, 31 December (2018).
- Hemeg HA, Nanomaterials for alternative antibacterial therapy, International Journal of Nanomedicine, 2017, 12, 8211.
- I Chopra, 2007, Journal of Antimicrobial Chemotherapy, 59, 578.
- I Sondi and BS Sondi, 2004, Journal of Colloid and Interface Science, 275, 177.
- International Association for Medical Assistance for Travelers. United States of America recommended vaccinations: Hepatitis A iamat.org/country/united-states-of-america/risk/hepatitis-a (Accessed on January 3 2019).
- J Ahmad, HA Alhadlaq, AWS Alshamsan, MA Siddiqui, Q Saquib, ST Khan, R Wahab, AA Al-Khedhairy, J Musarrat, MJ Akhar and M Ahamed, 2015, Journal of Applied Toxicology, 36, 1284-1293.
- J Davies and D Davies, 2010, Microbiology and Molecular Biology Reviews, 74, 417.
- J Kreuter, 2007, Indian Journal of Pharmacology, 331, 1.
- J Park, D-H Lim, H-J Lim, T Kwon, J-S Choi, S Jeong, IH Choi and J Cheon, 2011, Chemical Communications, 47, 4382.
- J Rousk, K Ackermann, SF Curling and DL Jones, 2012, PLoS One, 7, e34197.
- J Whitworth, 2018, Food Safety News. 4 September.
- J Xiong, Y Wang, Q Xue and X Wu, 2011, Green Chemistry, 13, 900.
- J Zhang, J Liu, Q Peng, X Wang and Y Li, 2006, Chemistry of Materials, 18, 867.
- J Zhang, N Liu, C Sun, D Sun and Y Wang, 2019, RSC Advances, 9, 17988.

- JA Haggstrom, KJ Klabunde and GL Marchin, 2010, Nanoscale, 2, 399.
- JK Sumit, P Ranjana, P Sandeep and NP Tejo, 2018, Food and Function, 9, 1998.
- JLC Hauman, K Sato, S Kurtia, T Matsumoto and B Jayadevan, 2011, Journal of Materials Chemistry, 21, 7062.
- JM Arg¨uello, D Raimunda, and T Padilla-Benavides, 2013, Cellular and Infection Microbiology, 3, 1.
- JM Blair, MA Webber, AJ Baylay, DO Ogbolu and LJ Piddock, 2014, Nature Review Microbiology, 13, 42.
- JM Firdhouse and P Lalitha, 2015, Progress in Biomaterials, 4, 113.
- JP Ruparelia, AK Chatterjee, SP Duttagupta and S Mukherji, 2008, Acta Biomaterialia 4, 707.
- JR Morones, JL Elechiguerra, A Camacho, K Holit, JB Kouri, JT Ramirez and MJ Yacaman, 2005, Journal of Nanotechnology, 16, 2346.
- JW Betts, M Hornsey and RM La Ragione, 2018, Advances in Microbial Physiology, 73, 123.
- K Chaloupka, Y Malam and AM Seifalian, 2010, Trends in Biotechnology, 28, 580.
- K Ebrahimi, S Shiravand and H Mahmoudvand, 2017, Marmara Pharmaceutical Journal, 21, 866.
- K Giannousi, K Lafazanis, J Arvanitidis, A Pantazaki and CD Samara, 2014, Journal of Inorganic Chemistry, 133, 24.
- KK Hegde, R Goswami, SJ Sarma, VD Veeranki, SK Brar and RY Surampalli, 2015, American Society of Civil Engineers, 1, 357.
- K Kalishwaralal, S BarathManiKanth, SR Pandian, V Deepak and S Gurunathan, 2010, Colloids Surfaces B Biointerfaces, 79, 340.
- K Mandava, K Kadimcharla, NR Kessara, NF Sumayya, B Parthyusha and UR Batchu, 2017, Indian Journal of Pharmaceutical Sciences, 24, 136.
- K Molbak, 2004, Journal of Veterinary Medical B Infectious Disease Public Health, 51, 364.
- K Nomiya, A Yoshizawa, K Tsukagoshi, NC Kasuga, S Hirakawa and J Watanabe, 2004, Journal of Inorganic Biochemistry, 98, 46.
- Kon K and Rai M, 2013, Journal of Comparative Clinical Pathology, 2, 160.
- KY Yoon, J Hoon Byeon, JH Park and J Hwang, 2007, Science of Total Environment, 373, 572.
- L Li, J Sun, X Li, Y Zhang, Z Wang, J Dai and Q Wang, 2012, Biomaterials, 33, 1714.
- L Wang, H Chen and S Lonqquan, 2017, International Journal of Nanomedicine, 12, 1227.
- L Zhang, L Wu, Y SiiD and K Shu, 2018, PLoS One, 13, e0209020.

- LA Figueroa, RA Morales-Luckie, RJ Scougall-Vilchis and OF Olea-Mejia, 204, Progess in Natural Science and Materials International, 24, 321.
- LA Tomayo, PA Zapata, FM Rabagliati, MI Azocar, LA Munoz, X Zhou, GE Thompson and MA Paez, 2015, Journal of Materials Science: Materials in Medicine, 26, 129.
- LIU Qing-Ming, Z De-Bi, Yu-ya Yamamoto, K Kuruda and O Masazumi, 2012, Transactions of Nonferrous Metals Society of China, 22, 2991.
- M Azizi, G Hedayatollah, Y Fatemeh, D Fariba and A Hojjat A, 2017, PLoS One, e0188639.
- M Banoee, S Seif, ZE Nazari, PJ Fesharaki, HR Shahverdi, A Moballegh, KM Moghaddam and AR Shahverdi, 2010, Journal of Biomedical Materials Research Part B Applied Biomaterials, 93, 557.
- M Hessleng, J Feiertag and K Hoenes, 2017, Bioscience Biotechnology Research Communication, 10, 3.
- M Hu, J Chen, ZY Li, A Leslie, GV Hartland, L Xingde, M Mannel and X Younam, 2006, Chemical Society Reviews, 35, 1084.
- M Li, K Xiang, G Luo, D Gong, Q Shen and L Zhang, 2013, Chinese Journal of Chemistry, 31, 1285.
- M Raffi, S Mehrwan, TM Bhatti, JI Akhtar, A Hameed, W Yanwar and MM Ul-Hasan, 2010, Annals of Microbiology, 60, 75.
- MA Ansani, HM Khan, AA Khan, A Malik, A Sultan, M Shaid, F Shujatullah and A Azam, 2011, Biology and Medicine, 3, 141.
- MA Fayaz, K Balaji, M Girilal, R Yadav, PT Kalaichelvan and R Venketesan, 2010, Nanomedicine: Nanotechnology, Biology and Medicine, 6, 103.
- MA Franco-Molina, E Mendoza-Gamboa, CA Sierra-Rivera, RA Goamez-Flores, P Zapata-Benavides, P Castillo-Tello, JM Alcocer-Ganzalaz, DF Miranda-Hernandez, RS Tamez-Tuerra and C Rodrigenz-Padilla, 2010, Journal of Experimental Clinical Cancer Research, 29, 148.
- MA Kohanski, DJ Dwyer and JJ Collins, 2010, Nature Reviews, 8, 423.
- MI Samanovic, C Ding, D J Thiele, and KH Darwin, 2012, Cell Host and Microbe, 11, 106.
- MS Aguilar, R Esparza and G Rosas, 2019, Transactions of Nonferrous Metals Society of China, 7, 1510.
- MS Naisari, Z Fereshteh and F Davar, 2009, Polyhedron, 28, 126.
- MS Usman, NA Irabim, K Shameli, N Zainuddin and WMW Yunus, 2012, Molecules, 17, 14928.
- MV Berridge and AS Tan, 1993, Archives of Biochemistry and Biophysics, 303, 474–482.
- N Cioffi, L Torsi, N Ditaranto, T Giuseppina, G Lina, S Luigia, BZ Teresa, DA Maria, PZ Giorgio and T Enrico, 2005, Chemistry of Materials, 17, 5255.

- N Jayarambabu, A Allam, TV Rao and RR Kumar, 2019, Materials Letters, 259, 126813.
- N Singh, B Dahiya, VS Radhakrishana, T Pasand and PK Mehta, 2018, International Journal of Nanomedicine, 13, 8523.
- NJ Maximino, MP Alvarez, RS Avila, CA Avila-Orta, EJ Razalado, AM Bello, PG Morones and GC Pliego, 2018, Journal of Nanomaterials, Article ID 9512768.
- NJ Pendleton, SP Gorman and BF Gilmore, 2013, Expert Review of Anti-Infective Therapy, 11, 297.
- NN Martinez, MFS Orozco, GA Martinez-Castanon, FT Mendez and F Ruiz, 2019, International journal of Molecular sciences, 20, 2808.
- OH Lowry, NJ Rosebrough, AL Farr and RJ Randall, 1951, Journal of Biological Chemistry, 193, 265.
- P Clarance, B Lenakar, J Sales, A Kherson, P Agarsitan, JC Tack, MM Alkulaifi, HA Al-shwaiman, AM Elgorban, A Syaed and HJ Kim, 2020, Saudi Journal of Biological Sciences, 27, 706-712.
- P Edwin Das, IA Abu Yousef, AF Majalawieh, A Narasimhan and P Poltronieri, 2020, Molecules, 25, 555.
- P Gajjar, B Pettee, DW Briti, W Huang, WP Johnson and AJ Anderson, 2009, Journal of Biological Engineering, 3, 1.
- P Habibovic and JE Barralet, 2011, Acta Biomaterialia, 7, 3013.
- P Kanninan, C Johans, J Merta and K Kontturi, 2008, Journal of Colloid Interface Science, 318, 88.
- P Kaur and B Chudasama, 2014, RSC Advances, 4, 36006-36011.
- P Kaur, AG Nene, D Sharma, PR Somani and HS Tuli, 2019, Bio-Materials and Technology, 1, 33.
- P Li, J Li, C Wu, Q Wu and J Li, 2005, Nanotechnology 16, 1912.
- P Padiyara, H Inoue and M Sprenger, 2018, Infectious Disease: Research and Treatment, 11, 1.
- P Pulkkinen, J Shan, K Leppanen, A Kansakoshi, A Laiho, J Mikael and T Heikki, 2009, ACS Applied Materials and Interfaces, 1, 519.
- P Sharma, D Goyal and B Chudasama, 2019, Micro and Nano Letters, 14, 1388.
- P Singh, H Singh, S Ahn, V Castro-Aceituno, Z Jimenez, SY Simu, YJ Kim and DC Yang, 2017, Artificial Cells, Nanomedicine and Biotechnology, 45, 1415.
- PK Khanna, P More, J Jawalkar, Y Patil and NK Rao, 2009, Journal of Nanoparticle Research, 11, 793.
- PR Jayes, KC Arup, PD Siddhartha and M Suparna, 2008, Acta Biomaterials, 4, 707.
- PS Harikumar and A Aravind, 2016, International Journal of Sciences, 5, 83.
- QI Rahman, A Ali, N Ahmed, MB Lohani, SK Mehta and M Muddassir, 2020, Journal of Nanoscience and Nanotechnology, 20, 7716.

- QL Feng, J Wu, GQ Chen, FZ Cui, TN Kim and JO Kim, 2002, Journal of Biomedical Materials Research, 52, 662.
- QM Liu, T Yasunami, K Kuruda and M Okido, 2012, Transactions of Nonferrous Metals Society of China 22, 2198.
- R Anitha, KV Ramesh, TN Ravishankar, KH Sudheer Kumar and T Ramakrishnappa, 2018, Journal of Science: Advanced Materials and Devices, 3, 440.
- R Chakraborty and T Basu, 2017, Nanotechnology, 28, 105101.
- R Hassanien, DZ Husein and MF Al-Hakkani, 2018, Heliyon, 4, e01077.
- R Kumari, AK Saini, A Kumar and VR Saini, 2020, Journal of Biological Inorganic Chemistry, 25, 23.
- R Sankar, R Maheswari, S Karthik, KS Shivashangari and V Ravikumar, 2014, Materials Science and Engineering: C, 44, 234.
- R Saranya and M Mubarak Ali, 2017, Journal of Chemical and Pharmaceutical Sciences, Special Issue 1, 1.
- R Zia, M Raiz, N Farooq, A Qamar and S Aujum, 2018, Materials Research Express, 5, 075012.
- RA Soomro, STH Sherazi, SN Memon, MR Shah, NH Kalwar, KR Hallam and A Shah, 2014, Advanced Materials Letters, 5, 191.
- RV Kumar, Y Mastai, Y Diamant and A Gedanken, 2011, Journals of Materials Chemistry A, 11, 1209.
- RY Pelgrift and AJ Friedman, 2013, Advanced Drug Delivery Review, 65, 1803.
- S Chouhan, K Sharma and S Guleria, 2017, Medicines, 4, 58.
- S Jain, A Jain and V Devra, 2014, Journal of Science and Engineering Research, 5, 973.
- S Kumar and BR Singh, 2013, Advances in Animal and Veterinary Sciences, 1, 7.
- S Lanone, F Rogerieux, J Geys, A Dupon, E Maillot-Marechal, J Baczkowsi, G Lactoix G and P Hoet, 2009, Particle and Fibre Toxicology, 14, 1.
- S Magdassi, M Grouchko and A Kamyshny, 2010, Materials, 3, 4626.
- S Nair, A Sasidharan, RVV Divya, M Deepthy, S Nair, K Manzoor and S Raina, 2009, Journal of Materials Science Materials in Medicine, 20, 235.
- S Rajesh, V Dharanishanthi and AV Kanna, 2014, Journal of Experimental Nanoscience, 10, 1143.
- S Shaikha, N Nazam, SMD Rizvi, K Ahmad, MH Baig, EJ Lee and I Choi, 2019, International Journal of Molecular sciences, 20, 2468.
- S Shankar and JW Rhim, 2014, Materials Letters, 132, 307.
- S Shiv and R Jong-Whan, 2014, Materials Letters, 132, 307.
- S Tardito and L Marchio, 2009, Current in Medicine Chemistry, 16, 1325.

- S Triboulet, C Aude-Garcia, M Carrie, H Diemer, F Proamer, AL Habert, M Chevallet, V Collin-Faure, JM Strub, D Hanau, A Dorsselaer, N Herlin-Boime and T Rabilloud, 2013, The American Society for Biochemistry and Molecular Biology, 12, 3108.
- S Vinopal, T Ruml, and P Kotrba, 2007, International Biodeterioration & Biodegradation, 60, 96.
- S Vivek, L Neha, H Vikas and B Manoj, 2017, Indian Journal of Biochemistry and Biophysics, 54, 135.
- S Yerukala and V Sagar, 2018, International Journal of Current Microbiology and Applied Sciences, 7, 1607.
- SA Deckers, S Loo, M Mayne-L'hermite, N Herlin-Boime, N Henguy, C Reynud, B Gouget and M Carriere, 2009, Journal of Environment Science and Technology, 43, 84231.
- SA Mohameed, 2020, Heliyon, 6, 03123.
- SD Bucchianico, MR Fabbrizi, SK Misra, E Valsami-Jones, D Berhanu, P Reip, E Bergamaschi and L Migliore, 2013, Mutagenesis, 1.
- Selvarani M, 2010, International Journal of Pharmacy and Pharmaceutical Science, 10, 83.
- SH Kim, HS Lee, DS Ryu, RS Choi and DS Lee, 2011, Korean Journal of Microbiology and Biotechnology, 39, 77.
- SH Wu and DH Chen, 2004, Journal of Colloid Interface Science, 273, 65.
- SI Concha-Guerrero, EMS Brito, HA Piñón-Castillo, SH Tarango-Rivero, AC César, A Luna-Velasco, R Duran and E Orrantia-Borunda, 2014, Journal of Nanomaterials, 9, 1.
- SJ Yu, YG Yin and JF Liu, 2013, Environment Science Process Impact, 15, 78.
- SS Birla, VV Tiwari, AK Gade, AP Ingle, AP Yadav and MK Rai, 2009, Letters of Applied Microbiology, 48, 173.
- SU Muhameed, ZEE Modamed, S Kamyer, Z Norhazlin, S Mahamed and I Nor Azoma, 2013, International journal of Nanomedicine, 8, 4467.
- SY Xie, ZJ Ma, CF Wang, SC Lin, ZY Jiang, RB Huang and LS Zheng, 2004, Journal of Solid State Chemistry, 177, 3743.
- SZH Naqui, U Kiran, MI Ali, A Jamal, A Hameed, S Ahmed and N Ali, 2013, International Journal of Nanomedicine, 8, 3187.
- T Kruk, K Szczepanowicz, J Stefanska, RP Socha and P Warszynski, 2015, Colloids and Surfaces B: Biointerfaces, 128, 17.
- TJ Humphrey, F Jorgensen, JA Frost, H Wadda, G Domingue NC Elviss, DJ Griggs and LJ Piddock, 2005, Antimicrobial Agents of Chemotherapy, 49, 690.
- TMD Dang, TTT Le, EB Fribourg and MC Dang, 2011, Advances in Nature Sciences: Nanoscience and Nanotechnology, 2, 105009.
- TMD Dang, TTT Le, EB Fribourg and MC Dhang, 2011, Advances in Nature Sciences: Nanoscience and Nanotechnology, 2, 025004.

- TP Van Boeckel, C Brower, M Gilbert, BT Grenfell, SA Levin, TP Robinson, A Teillent and R Laxminnarayan, 2015, Proceedings of the National Academy of Sciences, 112, 5649.
- TS Lobana, M Kaushal, R Bala, L Nim, K Paul, DS Arora, A Bhatia, S Arora and JP Jasinski, 2020, Journal of inorganic Biochemistry, 212, 111205.
- TT Loan, LT Do and H Yoo H, 2019, Journal of Nanoscience and Nanotechnology, 19, 709.
- U Bogdanovic, V Lazic, V Vodnik, M Budimir, Z Markovic and S Dimitrijevic, 2014, Materials Letters, 182, 75.
- US Gaharwar, R Meena and P Rajamani, 2017, Journal of Applied Toxicology, 37, 1232.
- V Bastos, IF Duarte, C Santos and H Oliveria, 2017, Journal of Nanoparticle Research 9, 163.
- V Modem, B Manoj, S Nallapeta and A Kumar, 2017, Annals of Microbiology, 3, 255.
- V Tiwari, N Mishra, K Gdani, PS Solanki, NA Shah and M Tiwari, 2018, Frontiers in Microbiology, 9, 1.
- V Vellora, T Padil and M Cernik, 2013, International Journal of Nanomedicine 8, 889.
- W Hong and JA Joseph, 1999, Free Radical Biology and Medicine, 27, 612-616.
- W Shao, S Wang, J Wu, M Huang, H Liu and H Min, 2016, RSC Advances, 6, 65879.
- W Yu, H Xie, L Chen, Y Li and C Zhang, 2009, Nanoscale Research Letters 4, 465.
- World Health Organization. 2019, Outbreak update – Cholera in Yemen, 20 December2018.emro.who.int/pandemic-epidemic-diseases/cholera/outbreak-update-cholera-in-yemen-20-december-2018.html (Accessed on January 3 2019).
- Wright GD, 2010, BMC Biology, 8, 123.
- X Cheng, X Zhang, H Yin, A Wang and Y Xu, 2006, Applied Surface Science, 253, 2727.
- X Li, Q Ma, T Liu, Z Dhong and W Fan, 2020, RSC Advances, 10, 5058.
- XF Zhang, W Shen and S Gurunathum, 2016, International Journals of Molecular Sciences, 17, 1603.
- Y Wei, X Huaqing, C Lifei, L Yang and Z Chen, 2009, Nanoscale Research Letters, 4, 465.
- Y Yanjie, N Jing, H Jianwen, Y Bianfei, Z Tong, X Shung, L Shauangyu and Z Haixia, 2014, International Journal of Nanomedicine, 9, 5441.
- YG Yuan, QL Peng and S Gurunathum, 2017, International Journal of Molecular Sciences, 18, 569.
- YH Hsueh, WJ Ke, CT Hsieh, KS Lin, DY Tzou and CL Chiang, 2015, PLoS One, 10, 1.

- YN Slavin, J Asnis, UO Hafeli and H Bach, 2017, Journal of Nanobiotechnology, 15, 65.
- YS Jeong, WK Oh, S Kim and J Jang, 2011, Biomaterials, 32, 7217.
- Z Chen, H Meng, G Xing, C Chen, Y Zhao, GG Jia, T Wang, H Yuan, C Ye, Z Zhao, F Chai, C Zhu, X Fang, B Ma and L Wan, 2006, Toxicology Letters, 163, 109.
- Z Liu and Y Bando, 2003, Advanced Materials, 15, 303.
- Z Qiu-Li, Y Zhi-mou, D Bing-jun, L Xin-Zhi L and GT Ying-Jaun, 2010, Transactions of Nonferrous Metals Society of China, 20, 240.

Role of hydrodynamic size in colloidal and optical stability of plasmonic Copper nanoparticles

Purnima Sharma[1,2], *Dinesh Goyal*[1], *Bhupendra Chudasama*[2] ✉

[1]*Department of Biotechnology, Thapar Institute of Engineering and Technology, Patiala 147 004, India*
[2]*School of Physics and Materials Science, Thapar Institute of Engineering and Technology, Patiala 147 004, India*
✉ *E-mail: bnchudasama@gmail.com*

Published in Micro & Nano Letters; Received on 14th March 2019; Revised on 26th June 2019; Accepted on 26th September 2019

Metallic nanoparticles (NPs) exhibit interesting plasmonic characteristics that depend on their size, shape and dielectric medium. Any change in these parameters can lead to significant alternation in plasmonic behaviour of NPs. Plasmonic nanostructures are prepared by wet chemical approaches, which produce NPs with a moderate yield. Amongst plasmonic class of NPs, gold and silver are widely explored in sensors because of their strong plasmon excitation. Copper NPs (CNPs) are gaining increasing attention in plasmonic sensors because of its economic advantages over silver and gold. However, major limitations of these nanostructures are their low yield and poor colloidal stability. In this Letter, authors report scale up of CNPs yield by 100% and studied their colloidal stability in terms of changes in hydrodynamic size and its influence on surface plasmon resonance (SPR). It has been observed that SPR of CNPs is independent of their yield. A gradual decrease in SPR is observed with ageing. This can be attributed to the aggregation-induced microstructural changes in the dispersion. CNPs irrespective of their yield are stable up to 180 days beyond which they lose their colloidal stability and plasmonic properties. Loss of colloidal and plasmonic characteristics of CNPs can be attributed to enhanced hydrodynamic size.

1. Introduction: Metal nanoparticles (NPs) have attracted a lot of attention in past few years due to their unique plasmonic properties [1]. Amongst metals, copper (Cu) because of its antiseptic properties assumes immense importance in biology and medicine since ancient time [2]. Copper NPs (CNPs) show strong antibacterial, antifungal and antifouling characteristics [3, 4]. Apart from these, CNPs have been used in collagen cross-linking and bone formation as well [5]. They are also the potential candidates to replace gold- and silver-based nanostructures in plasmonic sensors.

CNPs are synthesised by variety of chemical methods that include chemical reduction [6–10], microemulsion [11], sonochemical [12], electrochemical [10], thermal reduction [13, 14], pulse laser ablation [15, 16], vacuum vapour deposition [17] and green synthesis [18]. Colloidal stability of NPs synthesised by these routes is an important aspect and has a significant influence on the performance of plasmonic nanostructures. Among these synthesis routes, chemical reduction method is widely explored and most versatile. It is simple, economical and quick approach for NP synthesis. In chemical reduction method, it is possible to control the particle size and shape of CNPs. There are several reports of CNPs synthesis by chemical reduction method. Khaid *et al.* [19] synthesised CNPs by chemical reduction method using ascorbic acid as antioxidant and sodium borohydride ($NaBH_4$) as a reducing agent and polyvinylpyrrolidone (PVP) as capping agent by adjusting the pH of solution. Synthesised CNPs possess Cu (Cu^0) and cuprous oxide (Cu^{1+}) phases. Wu and Chen [20] synthesised metallic CNPs by reduction of cupric chloride with hydrazine using cetyltrimethylammonium bromide (CTAB) as capping agent in inert atmosphere. It is observed that CTAB prevents aggregation of as-synthesised CNPs. Kanninen *et al.* [21] studied the effect of ligand exchange on the stability of CNPs prepared with different capping agents. They have concluded that oleic acid capped NPs showed better stability than the thiols capped NPs.

Dang *et al.* [22] studied the effect of colloidal medium on the stability of CNPs. As-synthesised CNPs were dispersed in water and ethylene glycol. Their stability was evaluated by spectroscopic techniques. CNPs are stable up to 60 days in ethylene glycol, while it precipitates in water after 22 days, indicating CNPs possess better colloidal stability in ethylene glycol. Dang *et al.* [23] have also studied the colloidal stability of CNPs as a function of reduction time. Maximum stability of 5 days was observed for polyethylene glycol capped CNPs when prepared with a reduction time of 60 min. The surface plasmon resonance (SPR) and oxidation resistance of CNPs show strong dependence on reaction time, pH and relative ratio of surfactant to Cu salt. Li *et al.* [24] have developed a chemical reduction method for the synthesis of uncapped CNPs which are stable for several months. They have also demonstrated that the size and size distribution of CNPs can be controlled by altering the order of addition of chemical reagents in the synthesis. Xiong *et al.* [25] have synthesised 2 nm size CNPs by using L-ascorbic acid as reducing and capping agent. These NPs are stable up to 60 days in aqueous medium and suitable for biomedical applications due to their non-toxic and environmentally friendly reaction medium. Jain *et al.* [26] have studied the effect of reactant concentration and reaction temperature on the morphology, particles sizes and agglomeration of as-synthesised CNPs. Colloids were stable up to 2 months and did not sediment. This Letter also concludes that initial concentration of reactants and reaction temperature has remarkable effect on the particle size and agglomeration of the CNPs.

Although significant work has been done to study the colloidal stability of CNPs, very little information is available on the effect of scale up of NP yield on the colloidal stability of CNPs. Furthermore, the correlation between the colloidal stability and plasmonic properties of CNPs is also not well-understood in the literature. The present work aims to scale up the yield of CNPs (from 200 to 400 mg) without compromising their physical and plasmonic characteristics.

In this Letter, we report the effect of ageing on the colloidal stability of CNPs and its correlation with NPs yield. CNPs were synthesised by chemical reduction method using reducing agents ($NaBH_4$), antioxidant agent (ascorbic acid), stabilisers and capping agent PVP. As-synthesised CNPs were characterised by ultraviolet–visible (UV–vis) spectroscopy, dynamic light scattering (DLS) and transmission electron microscopy (TEM). Colloidal and plasmonic stability of CNPs was evaluated by monitoring the hydrodynamic size (D_H) through DLS and SPR band through UV–vis spectroscopy as a function of time. Stability of the colloids has also been estimated from these studies.

doi: 10.1049/mnl.2019.0145

2. Material and methods

2.1. Materials: Copper chloride, $NaBH_4$ and PVP (PVP 10,000) were purchased from Sigma-Aldrich. L-ascorbic acid was procured from Merck, India. All chemicals were used as received without any further purification. Aqueous solutions were prepared in Milli-Q water (ρ=18.2 MΩ).

2.2. Synthesis of CNPs: Aqueous colloidal dispersions of CNPs were prepared by chemical reduction method [27]. In brief, 5 mM PVP (MW: 10,000) was dissolved in 25 ml warm distilled water under constant magnetic stirring. The requisite quantity of aqueous solution of Cu chloride (1.11 mM) was added into PVP solution and heated at 80°C under constant magnetic stirring. On addition of Cu chloride, the colour of solution changes from yellow to green. To this, 10 mM aqueous solution of $NaBH_4$ was added dropwise. This changes the solution's colour from green to black. An aqueous solution of ascorbic acid (10 mM) was added to this black solution and allowed to react at 80°C for 5 min. The colour of the colloid changes from black to red indicating the reduction of Cu chloride that leads to formation of CNPs [27]. After this, it was cooled to room temperature. Colloidal dispersion was centrifuged at 6000 rpm for 10 min to remove clusters of CNPs if any. The supernal containing colloidal dispersion of CNPs was stored at room temperature. Nanoparticle yield for this reaction was 0.2 g. By following the identical protocols, colloidal dispersions of CNPs having NP yield of 0.3 and 0.4 g were also prepared.

2.3. Characterisation of as-synthesised CNPs: As-synthesised CNPs were characterised by UV–vis absorbance spectroscopy, DLS and TEM. UV–vis absorption spectra of CNPs were recorded in the spectral range of 300–700 nm at room temperature on Shimadzu UV-2600 spectrophotometer. Measurements of hydrodynamic particle size and its distribution were performed by the DLS technique. Measurements were carried out on Brookhaven 90Plus particle size analyser. The scattering angle was fixed at 90°. TEM measurements were carried out on Philips CM200 electron microscope operated at 200 kV. Samples for TEM microscopy were prepared by placing a drop of colloidal CNPs on a carbon-coated Cu grid with a mesh size of 200. The aqueous colloid was dried overnight under vacuum. Changes in the plasmonic characteristics [i.e. position of the plasmon resonance band (λ_{SPR}) and its intensity (A_{max})], and hydrodynamic size (D_H) of CNPs were tracked over an extended period of 180 days to determine the extent of aggregation in the dispersion and its effect on the colloidal stability and plasmonic properties of CNPs.

3. Results and discussion: As-synthesised CNPs prepared for 0.2 g (sample A), 0.3 g (sample B) and 0.4 g (sample C) yield were characterised by UV–vis spectroscopy, DLS and TEM. The UV–vis absorption spectra of as-synthesised dispersions of CNPs are shown in Fig. 1. A single plasmon resonance band centred at 570–580 nm is observed in the UV–vis spectra of each of the three CNPs dispersions. As can be seen in Fig. 1, irrespective of the CNPs yield, their plasmon bands are similar. This identical plasmonic characteristic of CNPs in the three tested samples indicates the successful scale up of NPs' yield from 0.2 to 0.4 g without any significant deviation in their physical and plasmonic properties. Position of SPR band centred around 570–580 nm is also the characteristic signature of formation of CNPs in Cu^0 state [28]. If CNPs changes their ionic state, a significant blue shift is expected in their plasmon band position [29]. If Cu^0 oxidises to Cu^{2+} (CuO), a plasmon band from 570 to 580 is expected to blue shift to 370 nm, and if Cu^0 oxidises to Cu^{1+} (Cu_2O), the plasmon band is expected to shift to 450 nm [30]. The absence of any additional plasmon absorption bands around 370 and 450 nm indicates that as-synthesised CNPs are primarily in its native metallic Cu^0 state.

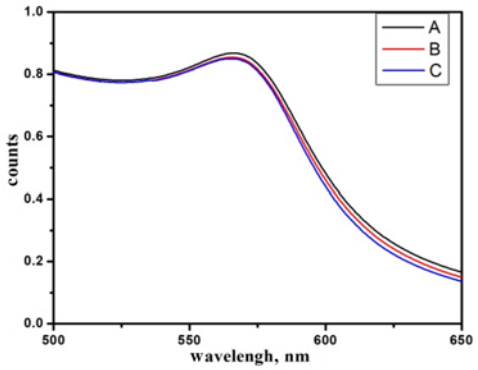

Fig. 1 *UV–vis absorption spectra of as-synthesised CNPs (A: 0.2 g, B: 0.3 g and C: 0.4 g yields)*

Position of plasmon resonance bands (λ_{SPR}) of as-synthesised CNPs along with their absorption maximum (A_{max}) is summarised in Table 1 for CNPs' dispersions having yields of 0.2 g (sample – A), 0.3 g (sample – B) and 0.4 g (sample – C). The presence of single plasmon resonance band in each spectrum with identical band positions is an indication of the presence of symmetric (spherical) NPs in colloid having similar particle sizes.

Hydrodynamic particle size distribution histograms of as-synthesised CNPs are shown in Fig. 2.

Single size distribution is observed in each histogram. This indicates that NPs are spherical. This observation is in good agreement with the previous assessment of shape of NPs from plasmon

Table 1 Plasmonic and physical characteristics of as-synthesised CNPs

Parameters	Sample A	Sample B	Sample C
yield, g	0.20	0.30	0.40
λ_{SPR}, nm	576.50	572.00	577.50
A_{max}	0.39	0.60	0.74
D_H, nm	13.70	11.30	12.10
polydispersity (σ)	0.32	0.30	0.29
particle size, nm	22.8	22.00	23.70

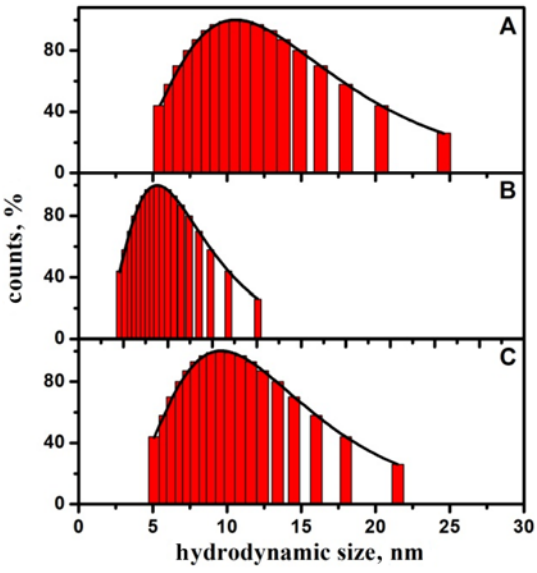

Fig. 2 *Hydrodynamic particle size distributions of as-synthesised CNPs (A: 0.2 g, B: 0.3 g and C: 0.4 g yields)*

resonance bands observed in Fig. 1 [31]. Each histogram in Fig. 2 is fitted with log-normal particles size distribution function [32]

$$P(D) = \frac{1}{(D\sigma\sqrt{2\pi})} \exp\left[-\frac{(\ln(/DD_o))^2}{2\sigma^2}\right]$$

where σ is the standard deviation, D is the hydrodynamic particle diameter and $\ln D_o$ is the mean of $\ln D$.

The mean hydrodynamic size (D_H) and polydispersity index (σ) thus obtained from the fits are reported in Table 1. The mean hydrodynamic sizes as obtained from the fits for samples A, B and C are identical and ranges between 11 and 14 nm. Their polydispersity (σ) which is a measure of particle size distribution is also similar and ranges between 0.29 and 0.32. Comparable hydrodynamic sizes and polydispersity indexes of all the three dispersions indicate that as-synthesised CNPs have identical physical characteristics.

TEM images of CNPs are shown in Fig. 3 along with their size distribution histograms.

Each histogram is fitted with log-normal particles size distribution function. Mean particle sizes obtained from these histograms are also reported in Table 1. In each TEM, micrographs aggregated NPs with near-spherical morphology can be visualised, which is predicted earlier from UV–vis spectroscopy (Fig. 1) and DLS experiments (Fig. 2). The mean particle size as obtained from the log-normal fit of the particle size distribution histograms ranges between 22 and 24 nm, which is nearly doubled as compared with hydrodynamic particle size (D_H) obtained from DLS. This may be because of heavy clustering of NPs in TEM micrographs, which is making it very difficult to distinguish boundaries of individual NPs.

The colloidal stabilities of as-synthesised CNPs were monitored at periodic intervals of 20 days in terms of SPR peak position by UV–vis spectroscopy and hydrodynamic particle size (D_H) with DLS. The UV–vis spectra of colloids were recorded at periodic intervals over 200 days. The position of SPR bands (λ_{SPR}) and its absorption maximum (A_{max}) as a function of ageing time is shown in Figs. 4 and 5, respectively. A gradual red shift was

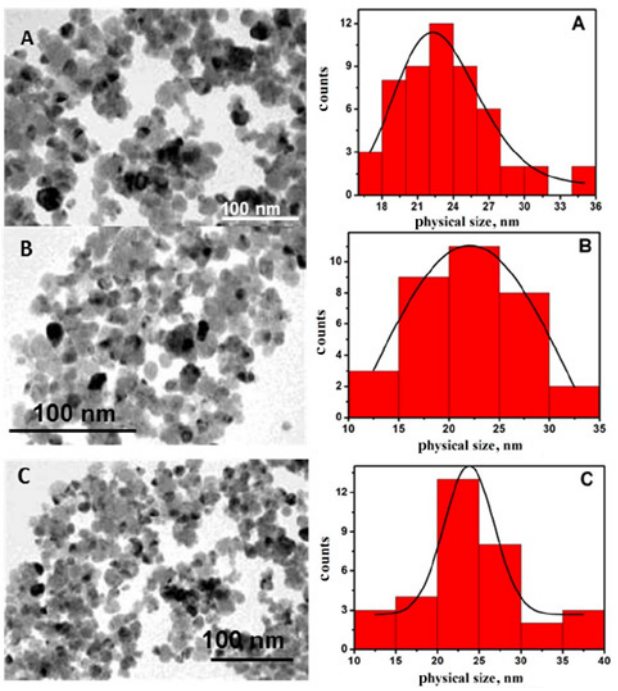

Fig. 3 *TEM micrographs and corresponding size distribution histograms of as-synthesised CNPs (A: 0.2 g, B: 0.3 g and C: 0.4 g yields)*

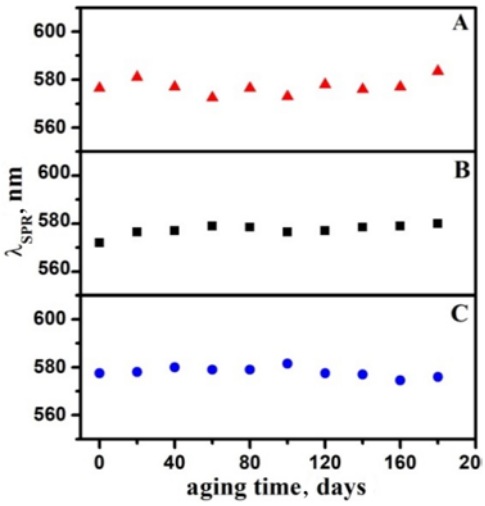

Fig. 4 *Effect of ageing on the position of SPR band (λ_{SPR}) of CNPs (A: 0.2 g, B: 0.3 g and C: 0.4 g yields)*

observed in the SPR peak position with ageing indicating a possible aggregation or Ostwald ripening of NPs [25]. The mean positions of λ_{SPR} of samples A, B and C are 577.1, 577.4 and 578 nm, respectively. An overall change in the λ_{SPR} position of CNPs is <2% over an ageing period of 180 days. This indicates that irrespective of the yield of NPs, all dispersions show impressive colloidal stability. A gradual decrease in A_{max} of CNPs was observed while ageing (Fig. 5). This might be due to the aggregation of NPs increasing the hydrodynamic particle size of the colloids.

To verify this hypothesis, hydrodynamic particle size (D_H) and the size distribution of CNPs were also observed at periodic intervals of 20–180 days. Each histogram was fitted with log-normal particle size distribution function. From these fits, the mean hydrodynamic sizes of CNPs were determined. Irrespective of the yield of CNPs and time of ageing, each CNPs dispersion show a monomodal particle size distribution indicating that the dispersion contains symmetrical (spherical) NPs. The plot of mean hydrodynamic size of CNPs as a function of ageing time is shown in Fig. 6. Each curve in Fig. 6 is fitted with the following expression:

$$D_H(t) = D_{H0} \exp(t/t)$$

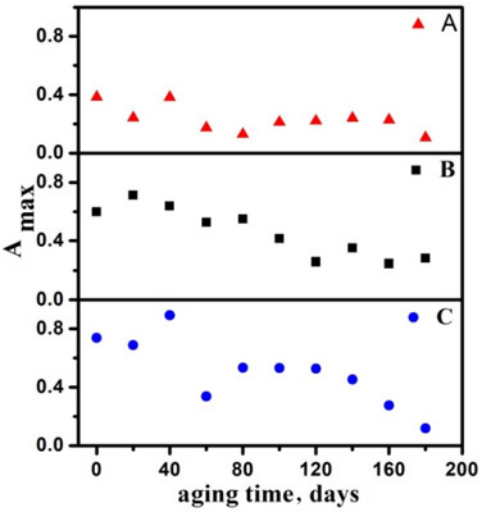

Fig. 5 *Effect of ageing on the absorption maximum (A_{max}) of SPR band of CNPs (A: 0.2 g, B: 0.3 g and C: 0.4 g yields)*

doi: 10.1049/mnl.2019.0145

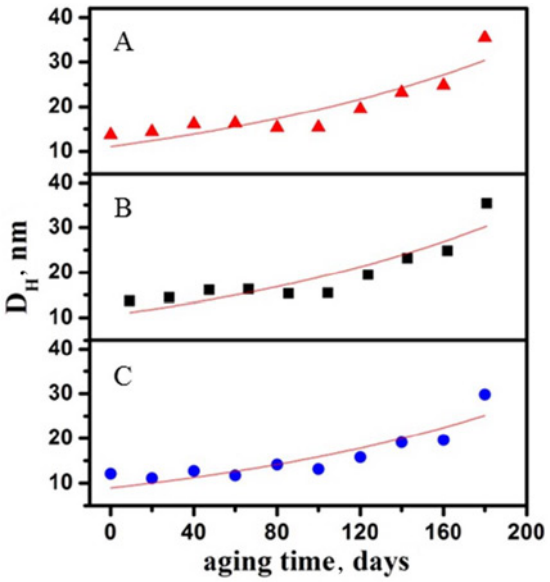

Fig. 6 *Effect of ageing on the hydrodynamic particle sizes of CNPs (A: 0.2 g, B: 0.3 g and C: 0.4 g yields)*

where $D_H(t)$ is the hydrodynamic particle size of the colloids measured after the ageing for time t, D_{H0} is the hydrodynamic particle size at $t = 0$ day and τ represents the shelf life of the colloid. From these fits, the shelf lives of samples A, B and C are determined which are 179, 179 and 174 days, respectively.

As evident from Fig. 6, irrespective of the NP yield (i.e. samples A/B/C), their hydrodynamic particle size increases with ageing. This might be because of the cluster formation in the dispersion caused by desorption of the protective layer of surfactant from the NPs' surface [27]. This gradual increase in the hydrodynamic size with ageing is in good agreement of previous observations of blue shift in SPR peak position and decrease in A_{max} in UV–vis spectroscopy. With ageing, clustering of NPs take place in the dispersion, which results in gradual decrease in the colloidal stability of CNPs. This also led to the decay in the plasmonic performance (A_{max}) of NPs. Colloids lose their dispersion stability beyond 180 days. This decrease in the colloidal stability of CNPs might be due to desorption of the protective layer of surfactant (ascorbic acid) from the surface of CNPs [27].

4. Conclusion: Irrespective of the yield of the CNPs, their hydrodynamic particle size and polydispersity indices are comparable, which indicates that as-synthesised CNPs have identical physical characteristics. With ageing, CNPs lose their colloidal stability and plasmonic properties. Irrespective of the yield or concentration of NPs, dispersions lose their colloidal stability with ageing. Their shelf life is of the order of 180 days. This Letter concludes that effect of ageing on the shelf life of CNPs is independent of NPs' yield and depends only on the surface desorption of surfactant(s).

5. Acknowledgment: Authors are thankful to DST, New Delhi for the FIST – I (SR/FST/PSI-176/2012) programme.

6 References

[1] Emory S.R., Nie S.J.: 'Screening and enrichment of metal nanoparticles with novel optical properties', *Phys. Chem. B*, 1998, **102**, (3), pp. 493–497
[2] Kruk T., Szczepanowicz K., Stefanska J., *ET AL.*: 'Synthesis and antimicrobial activity of monodisperse copper nanoparticles', *Colloids Surf. B, Biointerfaces*, 2015, **128**, pp. 17–22
[3] Cioff I.N., Torsi L., Ditaranto N., *ET AL.*: 'Copper nanoparticles/polymer composites with antifungal and bacteriostatic properties', *Chem. Mater.*, 2005, **17**, (21), pp. 5255–5262
[4] Ibrahim N.A, Abo-Shosha H., Gaffar M.A., *ET AL.*: 'Antimicrobial properties of ester-cross-linked cellulose-containing fabrics post-treated with metal salts', *Polym. Plast. Technol. Eng.*, 2006, **45**, (6), pp. 719–727
[5] Tapeiro H., Townsend D.M., Tew K.D.: 'Trace elements in human physiology and pathology. Copper', *Biomed. Pharmacother.*, 2003, **57**, (9), pp. 386–398
[6] Cheng X., Zhang H., Yin A., *ET AL.*: 'Modifier effects on chemical reduction synthesis of nanostructured copper', *Appl. Surf. Sci.*, 2006, **253**, (5), pp. 2727–2732
[7] Pulkkinen P., Shan J., Leppanen K., *ET AL.*: 'Poly (ethyleneimine) and tetraethylenepentamines as protecting agent for metallic copper nanoparticles', *Appl. Mater. Interfaces*, 2009, **1**, (2), pp. 519–525
[8] Zheng Q.L., Yang Z.M., Ding B.J., *ET AL.*: 'Preparation of copper nanoparticles by chemical reduction method using potassium borohydride', *Trans. Nonferrous Metals Soc.*, 2010, **20**, (1), pp. 240–244
[9] Khanna P.K., More P., Jawalkar J., *ET AL.*: 'Synthesis of hydrophilic copper nanoparticles: effect of reaction temperature', *J. Nanoparticle Res.*, 2009, **11**, (4), pp. 793–799
[10] Wei Y., Huaqing X., Lifei C., *ET AL.*: 'Synthesis and characterization of monodispersed copper colloids in polar solvents', *Nanoscale Res. Lett.*, 2009, **4**, (5), pp. 465–470
[11] Lisiecki I., Pileni M.P.: 'Synthesis of copper metallic clusters using reverse micelles as microreactors', *J. Am. Chem. Soc.*, 1997, **115**, (10), pp. 3387–3897
[12] Kumar R.V., Mastai Y., Diamant Y., *ET AL.*: 'Sonochemical synthesis of amorphous Cu and nanocrystalline Cu_2O embedded in a polyaniline matrix', *J. Mater. Chem.*, 2001, **11**, (4), pp. 1209–1213
[13] Dhas N.A., Raj C.P., Gedanken A.: 'Synthesis, characterization and properties of metallic copper nanoparticles', *Chem. Mater.*, 1998, **10**, (5), pp. 1446–1452
[14] Naisari M.S., Fereshteh Z., Davar F.: 'Synthesis of oleylamine capped copper nanocrystal via thermal reduction of new precursor', *Polyhedron*, 2009, **28**, (1), pp. 126–130
[15] Yeh M.S., Yang Y.S, Lee Y.P., *ET AL.*: 'Formation and characterization of Cu colloids from CuO powder by laser irradiation in 2-propanol', *J. Phys. Chem. B*, 1999, **103**, (33), pp. 6851–6857
[16] Maurizio M.M., Cristina G., Emilia G.: 'Surface-enhanced Raman scattering from copper nanoparticles obtained by Laser ablation', *J. Phys. Chem. B*, 2011, **115**, (12), pp. 5021–5027
[17] Liu Z., Bando Y.: 'A novel method for preparing copper nanorods and nanowires', *Adv. Mater.*, 2003, **15**, (4), pp. 303–305
[18] Sastry A.B.S., Aamanchi R.B.K., Prasad C.R.L., *ET AL.*: 'Large-scale green synthesis of Cu nanoparticles', *Environ. Chem. Lett.*, 2013, **11**, (2), pp. 183–187
[19] Khaid H., Shamaila S., Zafar N.: 'Synthesis of copper nanoparticles by chemical reduction method', *Sci. Int.*, 2015, **27**, (4), pp. 3085–3088
[20] Wu S.H., Chen D.H.: 'Synthesis of high concentration of Cu nanoparticles in aqueous CTAB solution', *J. Colloid Interface Sci.*, 2004, **273**, (1), pp. 165–169
[21] Kanninen P., Johans C., Merta J., *ET AL.*: 'Influence of ligand structure on the stability and oxidation of copper nanoparticles', *J. Colloid Interface Sci.*, 2008, **318**, (1), pp. 88–95
[22] Dang T.M.D., Le T.T.T., Fribourg E.B., *ET AL.*: 'The influence of solvents and surfactants on the preparation of copper nanoparticles by a chemical reduction method', *Adv. Nat. Sci. Nanosci. Nanotechnol.*, 2011, **2**, (1), pp. 025004–025011
[23] Dang T.M.D., Le T.T.T., Fribourg E.B., *ET AL.*: 'Synthesis and optical properties of copper nanoparticles prepared by chemical reduction method', *Adv. Nat. Sci. Nanosci. Nanotechnol.*, 2011, **2**, (1), pp. 105009–105015
[24] Li M., Xiang K., Luo G., *ET AL.*: 'Preparation of monodispersed copper nanoparticles by an environmentally friendly chemical reduction', *Chin. J. Chem.*, 2013, **31**, (10), pp. 1285–1289
[25] Xiong J., Wang Y., Xue Q., *ET AL.*: 'Synthesis of highly stable dispersions of nanosized copper nanoparticles using L-ascorbic acid', *Green Chem.*, 2011, **13**, (8), pp. 900–904
[26] Jain S., Jain A., Devra V.: 'Experimental investigation on the synthesis of copper nanoparticles by chemical reduction method', *Int. J. Sci. Eng. Res.*, 2014, **5**, (11), pp. 973–978
[27] Khurana C., Sharma P., Pandey O.P., *ET AL.*: 'Synergistic effect of metal nanoparticles on the antimicrobial activities of antibiotics against biorecycling microbes', *J. Mater. Sci. Technol.*, 2016, **32**, (6), pp. 524–532
[28] Guajardo-Pacheco M.J., Morales-Sanchaz J.E., Hernanadez J.G., *ET AL.*: 'Synthesis of copper nanoparticles using soybean as a chelant agent', *Mater. Lett.*, 2010, **64**, (12), pp. 1361–1364

[29] Hauman J.L.C., Sato K., Kurtia S., *ET AL.*: 'Copper nanoparticles synthesis by hydroxyl ion-assisted alcohol reduction for conducting links', *J. Mater. Chem.*, 2011, **21**, (20), pp. 7062–7069
[30] Hu M., Chen J., Li Z.Y., *ET AL.*: 'Gold nanostructures: engineering their plasmonic properties for biomedical properties', *Chem. Soc. Rev.*, 2006, **35**, (11), pp. 1084–1094
[31] Pal S., Tak Y.K., Song J.M.: 'Does antibacterial activity of silver nanoparticles depends on the shape of nanoparticles? A study of Gram-negative Bacteria *Escherichia coli*', *Appl. Environ. Microbiol.*, 2007, **73**, (6), pp. 1712–1720
[32] Khurana C., Vala A.K., Andhariya N., *ET AL.*: 'Antibacterial activity of silver: the role of hydrodynamic particle size at nanoscale', *J. Biomed. Mater. Res. A*, 2014, **102**, (10), pp. 3361–3368

doi: 10.1049/mnl.2019.0145

J Nanopart Res (2020) 22:244
https://doi.org/10.1007/s11051-020-04976-7

RESEARCH PAPER

ROS-induced cytotoxicity of colloidal copper nanoparticles in MCF-7 human breast cancer cell line: an in vitro study

Purnima Sharma · Dinesh Goyal · Manoj Baranwal · Bhupendra Chudasama

Received: 19 February 2020 / Accepted: 5 August 2020

Abstract Copper is known for its bactericidal properties since ancient time. Development of copper nanoparticle (CNP) based antimicrobial products has generated interest in studying their toxicological properties. In this article, we have investigated the ROS (reactive oxygen species)–induced cytotoxicity of colloidal CNPs on MCF-7 human breast cancer cells. To understand the dependence of nanoparticle's anticancer potential on their per batch yield, three identical sets of CNPs with similar physical properties with hydrodynamic size (11–14 nm) were prepared by chemical reduction method with per batch yield of 0.2 g, 0.3 g, and 0.4 g. Dose-dependent toxicity of as-synthesized (i.e., without any post preparation treatment) CNPs was evaluated by MTT (3-(4,5-dimethylthiazol-2-yl)-2,5-diphenyltetrazolium bromide) colorimetric assay for CNP concentrations of 0.001–100 μg/mL. Strong dose-dependent toxicity was observed in all CNPs batches, which was because of the mitochondrial damage in MCF-7. Cytotoxicity in MCF-7 exposed to CNPs was observed due to rupture of cell membrane and shrinkage as well as oxidative stress induced by reactive oxygen species (ROS). IC_{50} values of CNPs were independent of per batch yield of CNPs. This confirms that increase in CNPs yield from 0.2 to 0.4 g has no negative correlation with their cytotoxic response. The ability to scale up the nanoparticle yield with strong dose-dependent cytotoxicity makes CNPs potential candidate for the development of anticancer drugs.

Keywords Colloidal copper nanoparticles · MCF-7 · cytotoxicity · MTT assay · Reactive oxygen species · Health effects

This article is part of the topical collection: Nanoparticles in Biotechnology and Medicine

Xiaoshan (Sean) Zhu, University of Nevada, Guest Editor

Electronic supplementary material The online version of this article (https://doi.org/10.1007/s11051-020-04976-7) contains supplementary material, which is available to authorized users.

P. Sharma · D. Goyal · M. Baranwal
Department of Biotechnology, Thapar Institute of Engineering and Technology, Patiala 147004, India

P. Sharma · B. Chudasama
School of Physics and Materials Science, Thapar Institute of Engineering and Technology, Patiala 147004, India

B. Chudasama (✉)
Thapar-VT Center of Excellence in Emerging Materials (CEEMS), Thapar Institute of Engineering and Technology, Patiala 147004, India
e-mail: bnchudasama@gmail.com

Introduction

Cancer is one of the leading causes of death worldwide. Among different types of cancer, breast cancer is the most invasive and difficult to treat by conventional therapeutic methods. In USA alone, 1.7 million breast cancer cases were reported in 2018 (Janic et al. 2018). In Indian population particularly in the age group of 20–30, multifold increase in the aggressive cases of breast

Published online: 12 August 2020

cancer has been reported (Firdhouse and Lalitha 2015). Therefore, it is necessary to look for alternative cost-effective treatment of breast cancer with lesser side-effects (Janic et al. 2018; Firdhouse and Lalitha 2015).

Metals like copper and silver are known for their disinfectant characteristics and are widely used in home remedies to contain foodborne microbial contamination. Recent developments in nanotechnology have offered opportunities to develop, detect, and modulate biological processes that occur at nanometer scale (Kawaski and Player 2005). Metallic nanoparticles are now being used in health care as antimicrobial agents and imaging platforms and as a carrier in targeted drug delivery (Rizvi and Saleh 2018; Chandra et al. 2011) as well as bioremediation (Wang et al. 2018). Copper is an essential trace element that plays a vital role in metabolic and physiological processes (Azizi et al. 2017). It inhibits the formation of proteasome of a protein complex whose photolytic activity is essential for cellular processes (Zhang et al. 2017). CNPs have impressive binding and conjugation ability with proteins and enzymes that could cause necrosis in malignant tumors causing breast cancer (Saranya and Zali. 2017) and hence can be explored as antineoplastic agent. Among metallic nanoparticles, copper nanoparticles (CNPs) in medicinal products have also been approved for human usage by US environmental protection agency (Azizi et al. 2017).

Prabhu et al. (2010) studied the effect of size (40 nm, 60 nm, and 80 nm) and concentration (10–100 μm) on the toxicity of CNPs on the dorsal root ganglion neurons of rat. They reported strong size- and concentration-dependent toxicity of CNPs. Tang et al. (2018) studied the effects of nanoparticle size (30 nm, 50 nm, 80 nm, and 100 nm) on the toxicity of CNPs. They observed highest toxicity for CNPs with particle size 80 nm. Chen et al. (2006) found that CNPs (23.5 nm) induced greater toxicological effects and pathological injuries to the kidney, liver, and spleen of mice as compared with bulk copper. Song et al. (2014) evaluated the species-specific toxicity of CNPs on two mammalian cell lines (H4IIE and HepG2) and two piscine cell lines (PLHC-1 and RTH-149) with four different sizes of nanoparticles. They reported that CNPs follow multiple pathways in inducing the cell apoptosis in these species with increasing toxicity with a decrease in nanoparticle size. Chakroborty and Basu (2017) also demonstrated cytotoxic potency of CNPs on human skin cancer cell line (A-375) and observed that CNPs exhibits size-dependent anticancer properties through apoptotic pathways.

Despite multiple attempts; evaluating the cytotoxicity of CNPs remains ambiguous in cancerous tissues as it is strongly dependent on the physical properties of nanoparticles. No attempts have so far been made to understand the effect of per batch yield of CNPs on their cytotoxicity. In the present work, to understand the effect of per batch yield on the ROS-induced cytotoxicity of nanoparticles, three identical sets of CNPs with similar physical properties and hydrodynamic size (11–14 nm) were prepared by chemical reduction method with nanoparticle yield 0.2 g, 0.3 g, and 0.4 g and their dose-dependent cytotoxicity was evaluated on MCF-7 human breast cancer cells by MTT and intracellular ROS assays.

Materials and methods

Chemicals

Dulbecco's modified eagle's medium (DMEM), 2.5 μg/mL amphotericin B (antifungal), antibiotic solution 100X (100 IU/mL penicillin and 100 μg/mL streptomycin), fetal bovine serum (FBS), phosphate buffer saline (PBS 1X), trypsin-EDTA and 2, 5-diphenyltetrazoliumbromide (MTT) salt, 2, 7-dichlorofluorescin diacetate (DCFH-DA) dye, neutral red and trypan blue were purchased from Himedia. Doxorubicin hydrochloride was obtained from Khandelwal Ltd, India. Copper chloride ($CuCl_2{\cdot}2H_2O$), sodium borohydride ($NaBH_4$), polyvinylpyrrolidone (PVP; MW = 10,000), and dimethyl sulfoxide (DMSO) were procured from Sigma-Aldrich and L-ascorbic acid from Merck India. All aqueous solutions were prepared in sterilized Milli-Q ultrapure water (R = 18.2 MΩ).

Synthesis of colloidal copper nanoparticles

Three sets of colloidal CNPs with target yield 0.2 g (sample A), 0.3 g (sample B), and 0.4 g (sample C) were prepared by chemical reduction method as per the protocols developed previously (Khurana et al. 2016). In short, 5 mM PVP (polyvinylpyrrolidone) was dissolved in 25 mL warm distilled water under constant magnetic stirring. To this, requisite quantity of aqueous solution of copper chloride was added and heated to 80 °C under constant magnetic stirring. Ten millimolar ice-cooled aqueous solution of $NaBH_4$ was then added drop-wise. Followed by the addition of $NaBH_4$, 10 mM ascorbic acid was also added under constant magnetic

stirring at 80 °C. Reaction was allowed to proceed further for 5 min. Color of the solution changes from black to dark red indicating the reduction of Cu^{2+} to Cu^0, which spontaneously aggregates to form colloidal CNPs (Khurana et al. 2016). This colloidal dispersion of CNPs was cooled to room temperature and centrifuged at 6000 rpm for 10 min to remove clusters of CNPs, if any. Supernatant of colloidal CNPs was preserved at room temperature in air tight container for further analysis.

Characterization of colloidal CNPs

Colloidal CNPs were characterized by UV-visible absorbance spectroscopy, photon correction spectroscopy, and inductively coupled plasma atomic emission spectroscopy (ICP-AES, Prodigy). UV-visible absorption spectra of CNPs were recorded at 25 °C in the spectral range of 300–700 nm at room temperature on Shimadzu 2600 UV-visible spectrophotometer. Hydrodynamic particle size and size distribution of CNPs were determined by photon correction spectroscopy on Brookhaven 90 plus particle size analyzer at 25 °C. Concentration of copper in CNPs colloids was determined by ICP analysis. Measurements were performed on Leeman Lab prodigy ICP-AES spectrophotometer. Samples for ICP analysis were prepared by digesting CNP colloids with concentrated nitric acid at 90 °C. Each sample was diluted adequately before the measurement. Microplate reader (Tecan Infinite, Austria) was used to measure spectral response of cell cultures/nanoparticles in 96-well plate. Fluorescence intensity was measured at 520 nm ($\lambda_{ex} = 485$ nm) on Carry Eclipse fluorescence spectrophotometer to estimate the amount of reactive oxygen species (ROS) generated in MCF-7 when treated with CNPs. Optical and fluorescence microscopy of treated cells was performed on Nikon eclipse TS100 optical microscope and Dewinter trinocular fluorescence microscope, respectively.

Cell culture and nanoparticle exposure

MCF-7 cell line was procured from National Center for Cell Culture (NCCS), Pune, India, and was cultured in DMEM growth media supplemented with 10% FBS, 2.5 μg/mL amphotericin, and 1% antibiotic solution (100 IU/mL penicillin and 100 μg/mL streptomycin). It was maintained at 37 °C under 5% CO_2 humidified atmosphere. At a confluence of 80–90%, cells were washed with 1X phosphate buffer saline (PBS) and then trypsinized. Suspensions of suitable cell density were prepared after the cell counting. Cells were allowed to adhere to wells of plates for 24 h before the addition of CNPs. Colloidal CNPs were diluted in DMEM to have their final concentrations as 0.001, 0.005, 0.01, 0.05, 0.1, 0.5, 1, 10, 15, 20, 25, 30, and 100 μg/mL. Wells containing cells without nanoparticles were treated as negative control. The OD of each treated well was corrected by deducing the corresponding absorbance from wells containing media and nanoparticles alone.

MTT assay

MTT (3-(4,5-dimethylthiazol-2-yl)-2,5-diphenyltetrazolium bromide) assay is a colorimetric assay which was based on the reduction of tetrazolium salt to formazone: a blue-colored compound by mitochondrial dehydrogenases of viable cells (Ahmad et al. 2016). The insoluble formazone formed in this assay was solubilized in DMSO. To evaluate the cytotoxicity of CNPs, MCF-7 at cell density of 1×10^4 was seeded in a 96-well plate. It was allowed to grow for 24 h at 37 °C in 5% CO_2 humidified atmosphere. After overnight incubation, the used media was replaced with the aliquots of fresh growth media containing CNPs from samples A, B, and C in adequate concentrations (0–100 μg/mL) (Table S1). Doxorubicin hydrochloride (DOX) was also used as positive control (Kwan et al. 2016, Kumari et al. 2020). Plates were then incubated for 24 h again. After that 20 μL MTT (5 mg/mL in PBS) was added in each well and incubated for 4 h at culture conditions. Supernatant (150 μL) was removed from each well, and 100 μL DMSO was added to dissolve the formazone crystals. The OD of each well was recorded at 570 nm on microplate reader. Experiments were carried out in triplicate. The % cell inhibition was calculated by using the following equation (Vivek et al. 2017):

$$\text{Cell growth inhibition } (\%) = \frac{(A-B)}{A} \times 100$$

Here *A* represents mean differential OD of negative control (wells with untreated cells (media and MCF-7 cells without any CNPs)) and blank (wells with media and CNPs without MCF-7 cells) measured after treating them with MTT assay as per the protocols described in the "Materials and methods section." *B* represents mean differential OD of wells with and without cells having

CNPs (in equal concentrations), which was measured after treating them with MTT assays.

Staining of live and dead cells of MCF-7

To differentiate between live and dead cells, cultures were stained with neutral red and trypan blue (Sumit et al. 2018). For this, MCF-7 were seeded at the cell density of 1×10^4/well in 96-well tissue culture plates and allowed to adhere for 24 h at 37 °C in 5% CO_2 humidified atmosphere. After overnight incubation, the old media was replaced with the aliquots of fresh growth media containing the desired concentration of CNPs of samples A, B, and C. Four concentrations of CNPs that correspond to 25%, 50%, 75%, and 100% cell inhibition in MTT assay have been chosen for each CNP sample. They were incubated for 24 h at 37 °C in 5% CO_2 humidified atmosphere in triplicate. After incubation, media from each well was removed and cells were washed twice with PBS. One hundred microliters of neutral red (200 μg/mL in DMEM) was added to each well and incubated for another 4 h at 37 °C in 5% CO_2 humidified atmosphere. After incubation for 4 h, cells were washed with PBS. It was then stained with 40 μL trypan blue (0.4% w/v). Plates were then incubated for another 15 min in culture conditions. Each well was again washed with PBS. After washing, 100 μL PBS was added in each well. Optical microscopy was performed to differentiate between the live and dead cells.

Cellular reactive oxygen species assay

The intracellular ROS generation in cell lines after treating them with CNPs was measured with the help of a fluorescent dye DCFHDA (dichloro-dihydro-fluorescein diacetate) (Hong and Joseph 1999). Fluorogenic substrate DCF (2′, 7′-dichlorofluorescein) was formed due to the oxidation of DCFHDA (dichloro-dihydro-fluorescein diacetate) by the reactive oxygen species (ROS). There was a direct relationship between the level of intracellular ROS generated and fluorescence intensity of DCF (Saranya and Zali 2017). The ROS levels in CNPs treated MCF-7 were measured by two methods: fluorometric quantitative assay and cell imaging by fluorescence microscopy (Maqusood et al. 2016). For fluorometric quantitative assay, 2.5×10^4 cells/well in 6-well plates were seeded and incubated for 24 h at 37 °C in 5% CO_2 humidified atmosphere. These cells were then treated with CNPs (of samples A, B, and C) having concentrations 0.001, 0.01, 0.1, 1, 10, and 15 μg/mL in triplicate (Table S1). They were incubated for 24 h at culture conditions. Hydrogen peroxide (0.1 mM) was used as a positive control (Kwan et al. 2016; Maqusood et al. 2016 and Kumari et al. 2020). DCFHDA stock solution of 10 mM was prepared in DMSO and further diluted in DMEM (without FBS) to yield a working solution of 100 μM (Gaharwar et al. 2017). After the exposure time of 24 h, the supernatant from each well was discarded and cells were washed with PBS. Cells were then incubated with 1 mL of working solution of DCFHDA at 37 °C for 30 min in dark (Maqusood et al. 2016). Control (media and MCF-7 without CNPs) was also treated with the same volume of DCFHDA under identical conditions. Cells were lysed by adding trypsin-EDTA solution and centrifuged at 2000 rpm for 10 min. One milliliter of supernatant was used for fluorescence measurement (Kheirollahi et al. 2014). Fluorescence microscopy of treated MCF-7 cells was also performed after their incubation for 30 min in dark.

Statistical analysis

Data were expressed as mean ± standard deviation of three independent experiments. Statistical analysis was carried out by using analysis of variance, and the means were compared by t tests having $p < 0.05$ as limit of significance (Vivek et al. 2017).

Results

Synthesis and characterization of CNPs

Three sets of colloidal CNPs with per batch yield of 0.2 g (sample A), 0.3 g (sample B), and 0.4 g (sample C) of 50 mL stock were prepared by chemical reduction method. As-synthesized CNPs were characterized by UV-visible spectroscopy, photon correction spectroscopy, and inductively coupled plasma atomic emission spectroscopy. UV-visible absorption spectra (Fig. 1) of samples A, B, and C showed single plasmon resonance band centered around 550–600 nm in all samples irrespective of their yield which indicates formation of spherical nanoparticles with single Cu^0 phase (Guajardo-Pacheco et al. 2010). By increasing $CuCl_2$, the concentration of nanoparticles increased which leads to higher peak in UV absorption spectra (C > B > A) as shown in Fig. 1. The hydrodynamic particle size distribution histograms of CNPs are shown in Fig. 2. For all the three samples, irrespective of their per batch yield, a

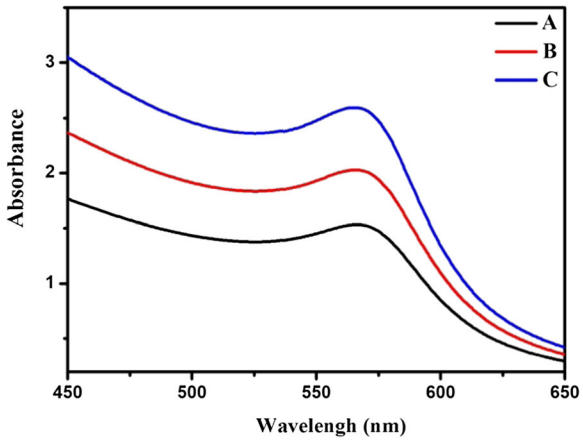

Fig. 1 UV visible absorption spectra of as-synthesized CNPs (sample A (yield 0.2 g; particle size 11.34 nm), sample B (yield 0.3 g; particle size 12.19 nm), and sample C (yield 0.4 g; particle size 13.7 nm))

monomodal hydrodynamic particle size distribution was observed that agrees well with the observed single plasmon resonance band in their UV-visible spectra (Khurana et al. 2014). Each histogram was fitted with lognormal particle size distribution (Khurana et al. 2014).

$$P\,(D) = \frac{1}{\left(D\sigma\sqrt{2\pi}\right)} \exp\left[-\frac{\left(\ln\left(\frac{D}{Do}\right)\right)^2}{2\sigma^2}\right]$$

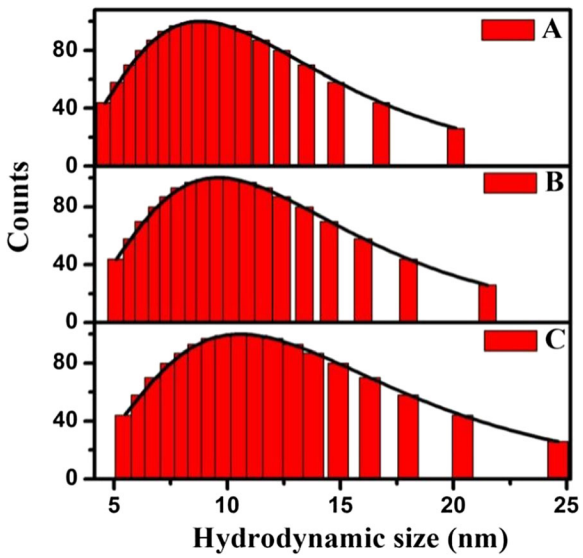

Fig. 2 Hydrodynamic particle size distribution histograms of CNPs (sample A (yield 0.2 g; particle size 11.34 nm), sample B (yield 0.3 g; particle size 12.19 nm), and sample C (yield 0.4 g; particle size 13.7 nm)). Each histogram was fitted with lognormal particle size distribution function

where σ is the standard deviation, *D* is the hydrodynamic particle diameter, and ln *D*o is the mean of ln D.

The mean hydrodynamic size (*D*) and polydispersity index (σ) as determined from these fits are reported in Table 1. The mean hydrodynamic size of samples A, B, and C was 11.34 nm, 12.19 nm, and 13.7 nm, respectively. Polydispersity (σ) of CNPs was between 0.32 and 0.36. This confirms that all the three as-synthesized CNP colloids possess nanoparticles, which were polydispersity. In a recent study by Qing et al. (2018), biosynthesis of CNPs possessing particle size 10–16 nm was reported. CNP concentration of Cu in CNP colloids was determined by ICP-AES measurements (Table 1). As the yield increased from 0.2 to 0.4 g, Cu concentration in CNP colloids increases from 1147 to 2873 μg/mL. These CNP concentrations were in good agreement with the per batch yield of CNPs.

Cytotoxic assays

MTT assay

To study the dose-dependent cytotoxic effect of CNPs, MTT assay was performed on MCF-7. In this experiment, doxorubicin (DOX) was used as a positive control. It was a sensitive method for the determination of cell integrity and inhibition of cell proliferation (Alhadlaq et al. 2015; Avalos et al. 2014). MTT was a mitochondrial toxicity assay that depends on mitochondrial respiration, which occurs outside the mitochondrial inner membrane and involves NADH- and NADPH-dependent mechanism that eventually triggers the cell inhibition (Berridge and Tan 1993).

Dose-dependent toxicity of CNPs was evaluated for all the three CNP samples with hydrodynamic size 11–14 nm in a broad concentration range of 0.001–100 μg/mL (Fig. 3). All experiments were repeated three times, with three replicates in each, and the data was expressed as the mean of nine values. At $p < 0.05$, the data are significantly different at all tested concentrations (0.001–100 μg/mL) in cytotoxicity assay. MCF-7 cells were exposed to nanoparticles for 24 h, then washed and incubated with MTT reagent for 4 h and allowed to recover. Irrespective of nanoparticle per batch yield, they show strong concentration-dependent cell cytotoxicity on MCF-7. In each tested sample, the percentage cell inhibition increased with increase in CNP concentration. At lower concentration (< 0.005 μg/mL), the inhibition was < 50%, and at higher concentrations (>

Table 1 Nanoparticle yield, hydrodynamic size, polydispersity, Cu concentration in colloids, and IC_{50} values of as-synthesized CNPs

Sample	Yield (g)	Hydrodynamic size (nm)	Polydispersity (σ)	Cu concentration (μg/mL)	IC_{50} (μg/mL)
A	0.2	11.34	0.32	1147	0.31
B	0.3	12.19	0.35	1601	0.54
C	0.4	13.7	0.36	2873	0.71

0.005 μg/mL), the % cell inhibition increased exponentially. Cell viability measured by MTT assay for sample B (yield 0.3 g) at 0.001, 0.01, 0.05, and 0.1 μg/mL of CNP was 28.74 ± 2.17%, 36.96 ± 1.34, 38.99 ± 2.14%, and 50.87 ± 4.37%, respectively. Similarly, cell viability for sample C (yield 0.4 g) at 0.01, 0.1, 0.5, and 1 μg/mL was 39.47 ± 7.4%, 52.66 ± 2.06%, 54.28 ± 0.74%, and 57.53 ± 1.82%, respectively. In multiple repetitions it was observed that the cell viability was mainly affected by the concentration of CNP.

Cell viability drops to 0% (inhibition = 100%), when CNP concentration was ≥ 20 μg/mL. IC_{50} at which cell inhibition is 50% is an important pharmacological measure used to determine the effectiveness of the toxicity of nanoparticles. MTT assay revealed IC_{50} values of test samples as 0.3, 0.5, and 0.7 μg/mL for samples A, B, and C respectively (Table 1). The change in IC_{50} values viz-a-viz tested concentration range (0–100 μg/mL) was minimal, suggesting that the scale-up of CNPs yield does not significantly alter their bio-activities.

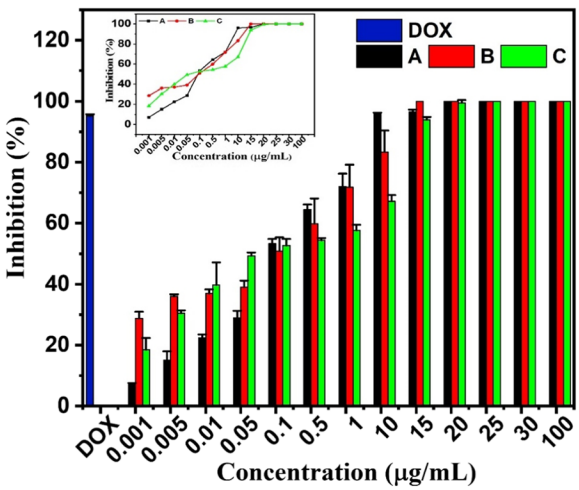

Fig. 3 Dose-dependent cytotoxicity determined by MTT assay of CNPs (sample A (yield 0.2 g; particle size 11.34 nm), sample B (yield 0.3 g; particle size 12.19 nm), and sample C (yield 0.4 g; particle size 13.7 nm)) on MCF-7 human breast cancer cell. Doxorubicin (Dox) (12 μg/mL) was used as positive control. Data was expressed as mean ± standard deviation of three sets of three independent experiments. Statistical data were significantly different at $p < 0.05$ as indicated by t tests. 20 μL of MTT was used in each experiment. Cells were incubated for 4 h after their treatment with MTT. The OD of each well was recorded at 570 nm on microplate reader from which % inhibition was calculated

Staining of live and dead cells of MCF-7

To understand the effect of CNPs on the cell morphology of MCF-7, optical microscopy was done after neutral red and trypan blue staining which differentiates between the live and the dead cells (Sumit et al. 2018). The neutral red dye was picked up only by the living cells that appear red while the trypan blue was picked by the dead cells, which appear blue. Cell staining at different concentrations of CNP causing inhibition (0, 25, 50, 75, and 100%) in MTT assay revealed that the cell size and morphology of control (polygonal) were intact as compared with CNP-treated cells which were round or irregularly shaped. Cells exposed to low concentration of CNPs showed less changes in cell morphology as compared with cells treated with higher concentration of CNPs (Fig. 4). Cell viability (%) also decreased with the increase in concentration of CNPs as revealed by decreasing number of cells stained with neutral red. At CNP concentration showing 100% inhibition, no surviving cells were observed (Fig. 4: 20 μg/mL), which is in good agreement with higher concentrations of each sample (Fig. 3). Exposure of cells to CNP causes rupture of cell membranes, and shrinkage and fragmentation of cells as revealed by microscopic observation of cell debris (Fig. 4).

Cellular reactive oxygen species assay

Interaction of nanoparticles with cells can produce reactive oxygen species (ROS) that results into oxidative stress that can cause external or internal cell damage (Nel et al. 2006). Several biological functions were involved in ROS generation both in normal and stressed condition of cells. ROS triggers growth in normal conditions and leads to the cell death if stressed (Hu et al.,

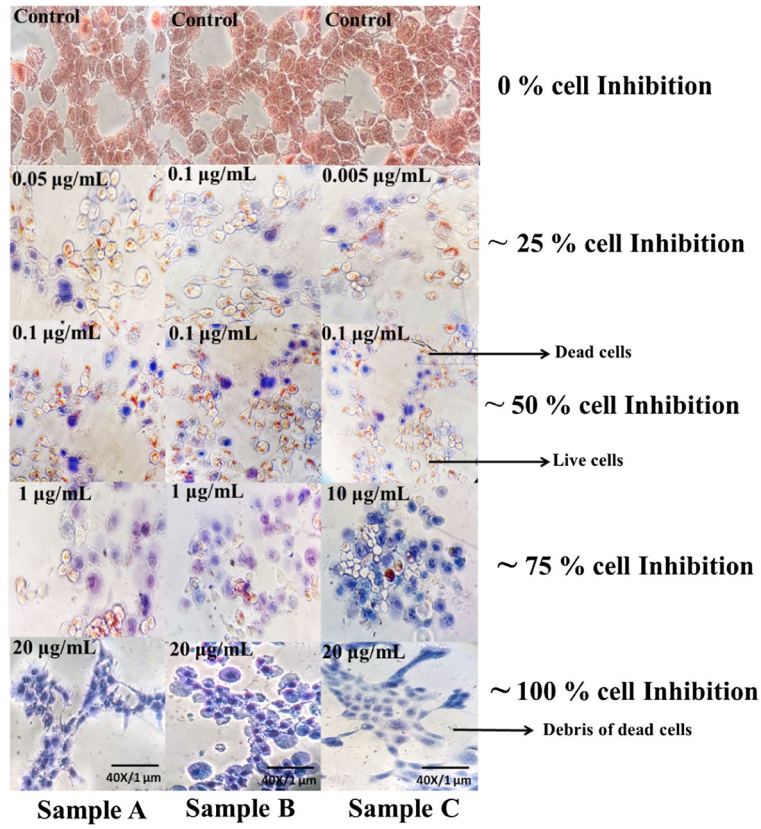

Fig. 4 Optical microscopic images (× 20) of live and dead MCF-7 cells treated with CNPs (sample A (yield 0.2 g; particle size 11.34 nm), sample B (yield 0.3 g; particle size 12.19 nm), and sample C (yield 0.4 g; particle size 13.7 nm)). The staining was done after 24-h treatment of cells with CNPs. Red color represents staining of live cells and blue color represents staining of dead cells after 24-h incubation. Control represents microscopic images of MCF-7 cells not treated with doxorubicin

2009). ROS can affect cell various functions by interfering with cellular components such as lipids and proteins and causing DNA fragmentation that results in decrease in cell proliferation, which ultimately leads to cell death by either apoptosis or necrosis (Li et al. 2012; Jeong et al. 2011). DCFH-DA has no fluorescence and passively enters into the cell through plasma membrane, where it is converted to DCFH by intracellular esterase. DCFH as such cannot pass through the cell membrane and gets oxidized by cellular ROS to highly fluorescent derivative DCF whose fluorescence intensity is directly proportional to the ROS generated intracellularly (Yanjie et al. 2014). In a similar study, ROS generation in the presence of scavengers like FE-EDTA (ethylenediaminetetraacetic acid), sodium oxalate, Cr (VI), isopropanol and TEMPOL (4-hydroxy2,2,6,6-tetramethylpiperdinyloxy) leading to decoloration of MO (methyl orange) by VS_4/CP (vanadium tetrasulfide carbon powder) nanocomposites was observed in an extracellular reaction by Cai et al. (2017).

In the present study, ROS assay was used to understand the process of cell death in MCF-7 treated with CNPs. ROS generation was determined by fluorometric quantitative assay. Hydrogen peroxide (0.1 mM) was used as positive control. The fluorescence intensity of MCF-7 negative control (without treatment of CNPs) was set at 100%. Fluorescence intensity of treated samples was presented as relative intensity (%) of negative control, which was set at 100% (Yanjie et al. 2014). ROS generation in MCF-7 cells treated with CNPs (0.001, 0.01, 0.1, 1, 10, and 15 µg/mL) can be observed in terms of increase in the fluorescence intensity (Fig. 5). Concentration dependence of observed ROS of all three samples was statistically insignificant. However, there was a marked difference in the ROS production of sample A as compared with samples B and C. Hence, viz-a-viz to nanoparticle size, ROS production of sample A having smaller size was statistically different from sample B and sample C. Effect of oxidative stress on the cell morphology of MCF-7 was also observed in fluorescence microscopy (Fig. 6). At all CNP concentrations below < 1 µg/mL, a gradual increase in the fluorescence intensity and hence ROS generation was observed, whereas at CNP concentration > 1 µg/mL, the fluorescence intensity was quenched.

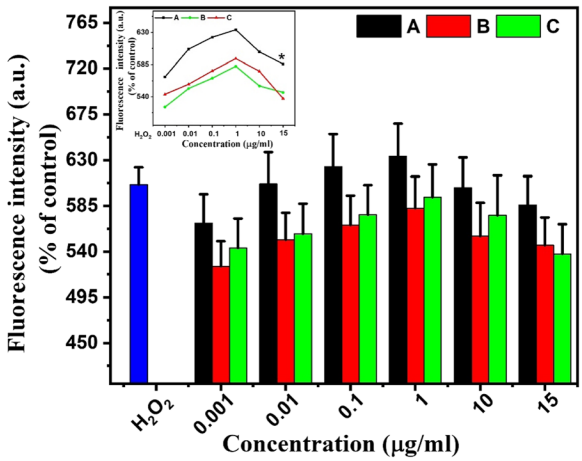

Fig. 5 Intracellular ROS generation (measured in terms of fluorescence intensity of DCF) in MCF-7 human breast cancer cell line treated with CNPs (sample A (yield 0.2 g; particle size 11.34 nm), sample B (yield 0.3 g; particle size 12.19 nm), and sample C (yield 0.4 g; particle size 13.7 nm)). Intracellular ROS was measured after incubating the cells for 24 h following CNP treatment. The untreated cells are negative control (without CNPs) and hydrogen peroxide–treated cells are positive control. Intensity values were expressed as % of negative control which was adjusted to 100%. H_2O_2 (0.1 mM) was treated as positive control. Data was expressed as mean ± standard deviation of three experiments. Statistical data at all tested concentrations were not significantly different at $p < 0.05$ as indicated by t tests. The asterisk (inset graph) indicated that sample A having smaller size was statistically different from samples B and sample C

Discussions

Three sets of colloidal CNPs with per batch yield of 0.2 g (sample A), 0.3 g (sample B), and 0.4 g (sample C) with hydrodynamic size of 11–14 nm were prepared by chemical reduction method and were characterized by UV-visible absorption spectroscopy, photon correlation spectroscopy, and inductively coupled plasma atomic emission spectroscopy. Identical plasmon resonance band (Fig. 1), small size variations (11–14 nm), and size distribution (Fig. 2) indicated that as-synthesized CNPs have identical physical characteristics and scale-up of nanoparticle yield has no significant impact on their physical characteristics.

CNPs show strong dose-dependent cell cytotoxicity on MCF-7 in MTT assay, irrespective of their per batch yield. At lower concentrations (< 0.1 μg/mL), smaller sized (sample A) nanoparticles were unable to provide required copper and because of which their toxicity was lower as compared with the larger sized nanoparticles (sample C). With increase in CNP concentration (0.1 to 15 μg/mL), the density of nanoparticles in smaller sized CNPs (sample A: 11.3 nm) was more as compared with that in larger sized CNPs (sample C: 13 nm) (Fig. 3). At these concentrations, small size nanoparticles due to higher surface area to volume ratio might be responsible for greater cytotoxicity (Prabhu et al. 2010). They reported that smaller size nanoparticles (i.e., 40 nm and 60 nm) are more toxic than the larger size (80 nm) nanoparticles at higher concentration (from 40 to 100 μM) of CNPs. They have observed strong size and concentration dependence of toxicity of CNPs (Prabhu et al. (2010). Similarly Tang et al. (2018) observed highest toxicity for CNPs with particle size 80 nm. Initially with the increase in particle size, toxicity of CNPs increases up to 80 nm followed by a drop in the toxicity at 100 nm. However, they could not explain such unusual size dependence of observed toxicity.

Cell inhibition was increased with increase in CNP concentration as observed in samples A, B, and C, which was in accordance with as reported by Azizi et al. (2017). No significant toxicity at lower concentrations was observed, since copper is an essential trace element involved in several metabolic pathways and at higher concentrations it inhibits cell proliferation resulting into higher toxicity by interfering with catalytic activities, structural integrity, and regulatory functions of the cells (Azizi et al. 2017).

IC_{50} values of all the tested CNPs were in the range of 0.3–0.7 μg/mL. The change in IC_{50} values (from 0.3 to 0.7 μg/mL) viz-a-viz to the change in tested concentration (0–100 μg/mL) was minimal and hence can be concluded that the scale-up of CNPs yield does not significantly alter their bio-activities. Lanone et al. (2009) has reported similar IC_{50} (1.17 μg/mL) value of CNPs on human skin cancer cell A-375.

CNPs cause cell cytotoxicity and lead to morphological changes in MCF-7 cells. The control cells (without CNP treatment) show typical epithelial polygonal shape with high density of cell layers growing in compact form (Fig. 4), whereas MCF-7 cells treated with CNPs show irregular or round shape cells or cells with shrinkage and low density in less or no compact layers (Clarance et al. 2020). Treated cells showed ruptured cells with nuclear fragmentation as indicated by the presence of large cellular debris formed due to the apoptotic cell death by nanoparticles. Similar observations were previously reported by Khan et al. (2018) and Clarance et al. (2020). Subcellular damage by membrane mineralization, lipid peroxidation, collapsed membrane potential, and intracellular damage including DNA degradation by nanoparticles has also been

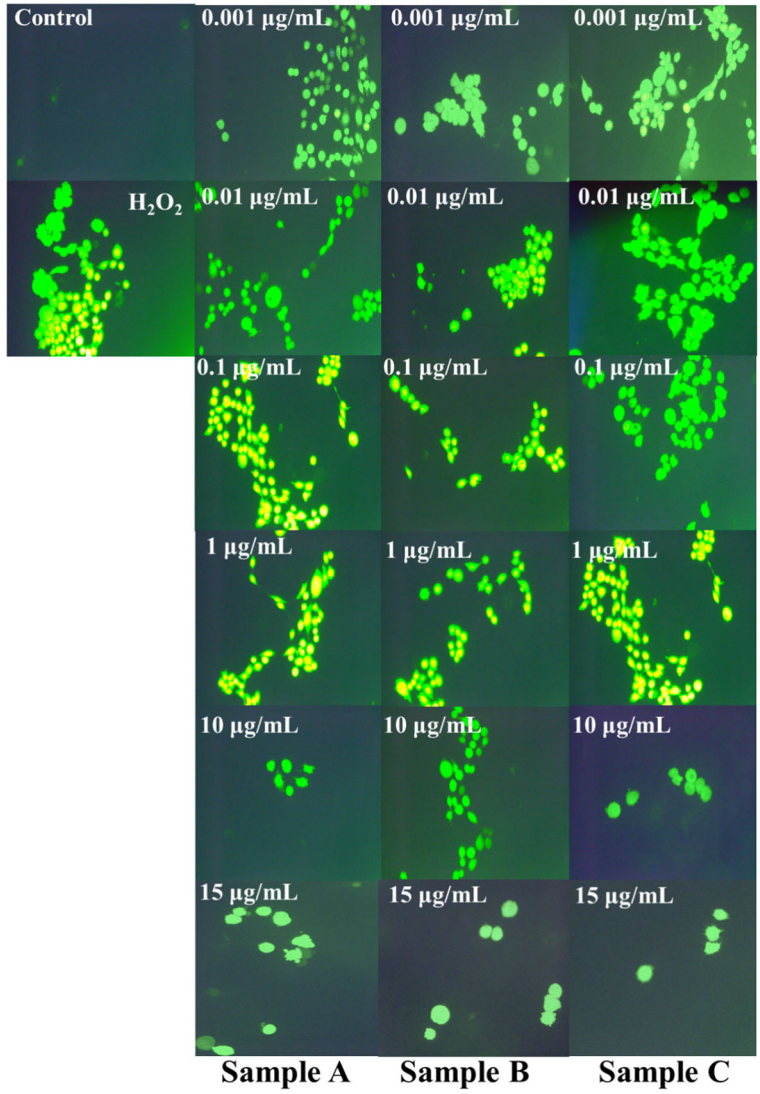

Fig. 6 Fluorescent microscopic images of MCF-7 human breast cancer cell after treatment with CNPs (sample A (yield 0.2 g; particle size 11.34 nm), sample B (yield 0.3 g; particle size 12.19 nm), and sample C (yield 0.4 g; particle size 13.7 nm)). Intracellular generated ROS was measured after incubating the cells for 24 h following CNP treatment. The untreated cells were negative control (without CNPs) and hydrogen peroxide–treated cells were the positive control

reported (Zhang et al. 2018). It is imperative to study the cytotoxicity of CNPs on normal cells before concluding the feasibility of CNPs as chemotherapeutic agent; however, in the present study and as per earlier reports (Ahmad et al. 2016), the cytotoxicity of CNPs has generally been evaluated under in vitro conditions on cancer cell line.

Oxidative stress generated through ROS in MCF-7 cells induced by CNPs (0.001, 0.01, 0.1, 1, 10, and 15 µg/mL) was observed by fluorescence intensity and microscopy. Below 1 µg/mL of CNPs there was gradual increase in the fluorescence intensity as ROS generation increased in each sample. But at higher CNP concentration (> 1 µg/mL), the fluorescence intensity was quenched, which might be because of decrease in viable cells (Fig. 3). Similar observation was previously reported in AuNC-treated HepG2 cells by Yanjie et al. (2014). At tested concentration (0.001–15 µg/mL) with different sized nanoparticles (sample A—11.34 nm; sample B—12.19 nm; and sample C—13.7 nm), fluorescence intensity did not change significantly, which indicates that cells were under similar stress level due to the ROS generation. Persistent cellular stress may enhance other pathways of cell damage such as rupturing of cell membranes, shrinkage, and fragmentation (Fig. 4).

Conclusions

MTT, colorimetric, and ROS assays along with optical and fluorescence microscopic images confirmed the

strong ROS-induced dose-dependent cytotoxicity of as-synthesized CNPs against MCF-7 human breast cancer cell. No significant difference was observed in the cytotoxicity of CNPs of samples A (0.2 g), B (0.3 g), and C (0.4 g) having hydrodynamic size of 11–14 nm. This suggests that the cytotoxicity of the CNPs was independent of nanoparticle yield and it only depends on its dose. Oxidative stress produced by extracellular ROS generation in the MCF-7 cells treated with CNPs might damage membrane lipids causing cell shrinkage and fragmentation leading to cell death. The results suggest that copper nanoparticles can be a potential candidate for the development of antineoplastic drugs.

Acknowledgments The authors are thankful to DST, New Delhi, for the FIST - I (SR/FST/PSI-176/2012) program.

Author contributions All the authors have contributed equally in this manuscript.

Compliance with ethical standards

Conflict of interest The authors declare that they have no conflict of interest.

References

Ahmad J, Alhadlaq HA, Alshamsan AWS, Siddiqui MA, Saquib Q, Khan ST, Wahab R, Al-Khedhairy AA, Musarrat J, Akhar MJ, Ahamed M (2016) Differential cytotoxicity of copper ferrite nanoparticles in different human cells. J App. Toxicol 36:1284–1293

Alhadlaq HA, Akhtar MJ, Ahamed M (2015) Zinc ferrite nanoparticles- induced cytotoxicity and oxidative stress in different human cells. Cell Biosc 5:1–11

Avalos A, Haza AI, Mateo D, Morales P (2014) Cytotoxicity and ROS production of manufactured silver nanoparticles of different size in heptoma and leukemia cells. J Appl Toxicol 34:413–423

Azizi M, Hedayatollah G, Fatemeh Y, Fariba D, Hojjat A (2017) Cytotoxic effect of albumin coated copper nanoparticles on human breast cancer cells of MDA-MB 231. PLoS One 12: e0188639

Berridge MV, Tan AS (1993) Characterization of the cellular reduction of 3-(4,5-dimethylthiazol-2-yl)-2,5-diphenyltetrazolium bromide (MTT): subcellular localization, substrate dependence, and involvement of mitochondrial electron transport in MTT reduction. Ach Biochem Biophys 303: 474–482

Cai R, Zhang B, Shi J, Li M, He Z (2017) Rapid photocatalytic decolorization of methyl orange under visible light using VS4/carbon powder nanocomposites. ACS Sustain Chem Eng 5:7690–7699

Chakraborty R, Basu T (2017) Metallic copper nanoparticles induce apoptosis in Human skin melanoma A-375 cell line. Nanotechnology 28:105101

Chandra S, Das P, Bag S, Laha D, Parmanik P (2011) Synthesis, functionalization and bioimaging applications of highly fluorescent carbon nanoparticles. Nanoscale 3:1533–1540

Chen Z, Meng H, Xing G, Chen C, Zhao Y, Jia G, Wang T, Yuan H, Ye C, Zhao F, Chai Z, Zhu C, Fang X, Ma B, Wan L (2006) Acute toxicological effects of copper nanoparticles in vivo. Toxicol Lett 163:109–120

Clarance P, Lenakar B, Sales J, Kherson A, Agarstian P, Tack JC, Alkhulaifi MM, Al- shwaiman HA, Elgorban AM, Syed A, Kim HJ (2020) Green synthesis and characterization of gold nanoparticles using endophytic fungi *Fusarium solani* and its in-vitro anticancer and biomedical applications. Saudi J Biol Sci 27:706–712

Firdhouse JM, Lalitha P (2015) Apoptotic efficacy of biogenic silver nanoparticles on human breast cancer MCF-7 cell lines. Prog Biomater 4:113–121

Gaharwar US, Meena R, Rajamani P (2017) Iron oxide nanoparticles induced cytotoxicity, oxidative stress and DNA damage in lymphocytes. J Appl Toxicol 37:1232–1244

Guajardo-Pacheco MJ, Morales-sanchaz JE, Hernanadez JG, Ruiz F (2010) Synthesis of copper nanoparticles using soybean as a chelant agent. Mater Lett 64:1361–1364

Hong W, Joseph JA (1999) Quantifying cellular oxidative stress by dichlorofluorscein assay using microplate reader. Free Radic Biol Med 27:612–616

Hu R, Yong KT, Roy I, Ding H, He S, Prasad PN (2009) Metallic nanostructures as localized plasmon resonance enhanced scattering probes for multiplex dark-field targeted imaging of cancer cells. J Phys Chem C 113:2676–2684

Janic B, Liu F, Bobbitt KR, Brown SL, Chetty IJ, Mao G, Movsas B, Wen N (2018) Cellular uptake and radio-sensitization effect of small gold nanoparticles in MCF-7 breast cancer cells. J Nanomed Nanotechnol 9:1–13

Jeong YS, Oh WK, Kim S, Jang J (2011) Cellular uptake, cytotoxicity, and ROS generation with silica/conducting polymer core/shell nanospheres. Biomaterials 32:7217–7225

Kawaski ES, Player A (2005) Nanotechnology, nanomedicine and the development of new, effective therapies for cancer. Nanomedicine 1:101–109

Khan FA, Akhtar S, Almofty SA, Almohazed D, Alomeri M (2018) FMSP-nanoparticles induced cell death on human breast adenocarcinoma cell line (MCF-7 Cells): morphometric analysis. Biomolecules 8:1–13

Kheirollahi A, Pordeli M, Safavi M, Mashkouri S, Naimi-Jamal MR, Ardestani SK (2014) Cytotoxic and apoptotic effects of synthetic benzochromene derivatives on human cancer cell lines. Naunyn Schmiedeberg's Arch Pharmacol 387:1199–1208

Khurana C, Vala AK, Andhariya N, Pandey OP, Chudasama B (2014) Antibacterial activity of silver: the role of hydrodynamic particle size at Nanoscale. J Biomed Mater Res part A 102:3361–3368

Khurana C, Sharma P, Pandey OP, Chudasama B (2016) Synergistic effect of metal nanoparticles on the antimicrobial

activities of antibiotics against biorecycling microbes. J Mater Sci Technol 32:524–532

Kumari R, Saini AK, Kumar A, Saini VR (2020) Apoptosis induction in lung and prostate cancer cells through silver nanoparticles synthesized from *Pinus roxburghii* bioactive fraction. JBIC 25:23–37

Kwan YP, Saito T, Ibrahim D, Saleh Al-Hassan FM, Oon CE, Chen Y, Jothy SL, Kanwar JR, Sasidharan S (2016) Evaluation of the cytotoxicity, cell-cycle arrest, and apoptotic induction by *Euphorbia hirta* in MCF-7 breast cancer cells. Pharm Biol 54:1223–1236

Lanone S, Francoise R, Jorina G, Aurelie D, Emmanuelle MM, Jorge B, Ghislaine L, Peter H (2009) Comparative toxicity of 24 manufactured nanoparticles in human alveolar epithelial and macrophage cell lines. Part Fiber Toxicol 6:1–12

Li L, Sun J, Li X, Zhang Y, Wang Z, Wang C, Dai J, Wang Q (2012) Controllable synthesis of monodispersed silver nanoparticles as standards for quantitative assessment of their cytotoxicity. Biomaterials 33:1714–1721

Maqusood A, Akhtar JV, Hisham AA, Aws A (2016) Copper ferrite nanoparticles- induced cytotoxicity and oxidative stress in human breast cancer MCF-7 cells. Colloids Surf B: Biointerfaces 142:46–54

Nel A, Xia T, MaEdler L, Li N (2006) Toxic potential of materials at the nanolevel. Science 31:622–627

Prabhu BM, Ali SF, Murdock RC, Hussain SM, Srivatsan M (2010) Copper nanoparticles exert size and concentration dependent toxicity on somatosensory neurons of rat. Nanotoxicology 4:150–160

Qing L, Zhang B, Xing X, Zhao Y, Cai R, Wang W, Gu Q (2018) Biosynthesis of copper nanoparticles using *Shewanella coihica* PV-4 with antibacterial activity: novel approach and mechanisms investigations. J Hazard Mater 347:141–149

Rizvi SAA, Saleh AM (2018) Applications of nanoparticles system in drug delivery technology. SPJ 26:64–70

Saranya R, Zali MM (2017) Synthesis of colloidal copper nanoparticles and its cytotoxicity effects on MCF-7 breast cancer cell lines. JCHPS 1:1–5

Song L, Mona C, Maria FL, Martina GV, Marta F, Estefania C, Greet RS, Wellie JGM, Jose MN (2014) Species-specific toxicity of copper nanoparticles among mammalian and piscine cell lines. Nanotoxicology 8(4):383–393

Sumit JK, Ranjana P, Sandeep PK, Tejo NP (2018) Bioaceesible selenium sourced from Se-rich mustard cake facilities protection from TBHP induced cytotoxicity in melanoma cells. Food Funct 9:1998–2004

Tang H, Xu M, Zhou XR, Zhang X, Zhao L, Ye G, Shi F, Lv C, LI Y (2018) Acute toxicity and biodistribution of different sized copper nano-particles in rats after oral administration. Mater Sci Eng C Mater Biol Appl 93:649–663

Vivek S, Neha L, Vikas H, Manoj B (2017) *Amomum subulatum* seed extract exhibit antioxidant, cytotoxic and immune-suppressive effect. IJBB 54:135–139

Wang W, Zhanga B, Liua Q, Dub P, Liub W, Hec Z (2018) Biosynthesis of palladium nanoparticles using *Shewanella loihica* PV-4 for excellent catalytic reduction of chromium (VI). Environ Sci Nano 5:730–739

Yanjie Y, Jing N, Jianwen H, Bianfei Y, Tong Z, Shung X, Shauangyu L, Haixia Z (2014) Cytotoxicity of gold nanoclusters in human liver cancer cells. In J Nanomedicine 9:5441–5448

Zhang Z, Wang H, Maocani Y, Wang H, Zhang C (2017) Novel copper complexes as potential proteasome inhibitors for cancer treatment. Mol Med Rep 15:3–11

Zhang B, Zou S, Cai R, Li M, He Z (2018) Highly-efficient photocatalytic disinfection of *Escherichia coli* under visible light under carbon supported vanadium tetrasulfide nanocomposites. Appl catal B 224:383–393